Multilayer approach to brain connectivity in Alzheimer's disease

Jérémy Guillon

▶ **To cite this version:**

Jérémy Guillon. Multilayer approach to brain connectivity in Alzheimer's disease. Neuroscience. Pierre and Marie Curie University, 2018. English. NNT : . tel-01985286v1

HAL Id: tel-01985286

https://theses.hal.science/tel-01985286v1

Submitted on 17 Jan 2019 (v1), last revised 11 Jun 2020 (v2)

HAL is a multi-disciplinary open access archive for the deposit and dissemination of scientific research documents, whether they are published or not. The documents may come from teaching and research institutions in France or abroad, or from public or private research centers.

L'archive ouverte pluridisciplinaire **HAL**, est destinée au dépôt et à la diffusion de documents scientifiques de niveau recherche, publiés ou non, émanant des établissements d'enseignement et de recherche français ou étrangers, des laboratoires publics ou privés.

Multilayer Approach to Brain Connectivity

in Alzheimer's Disease

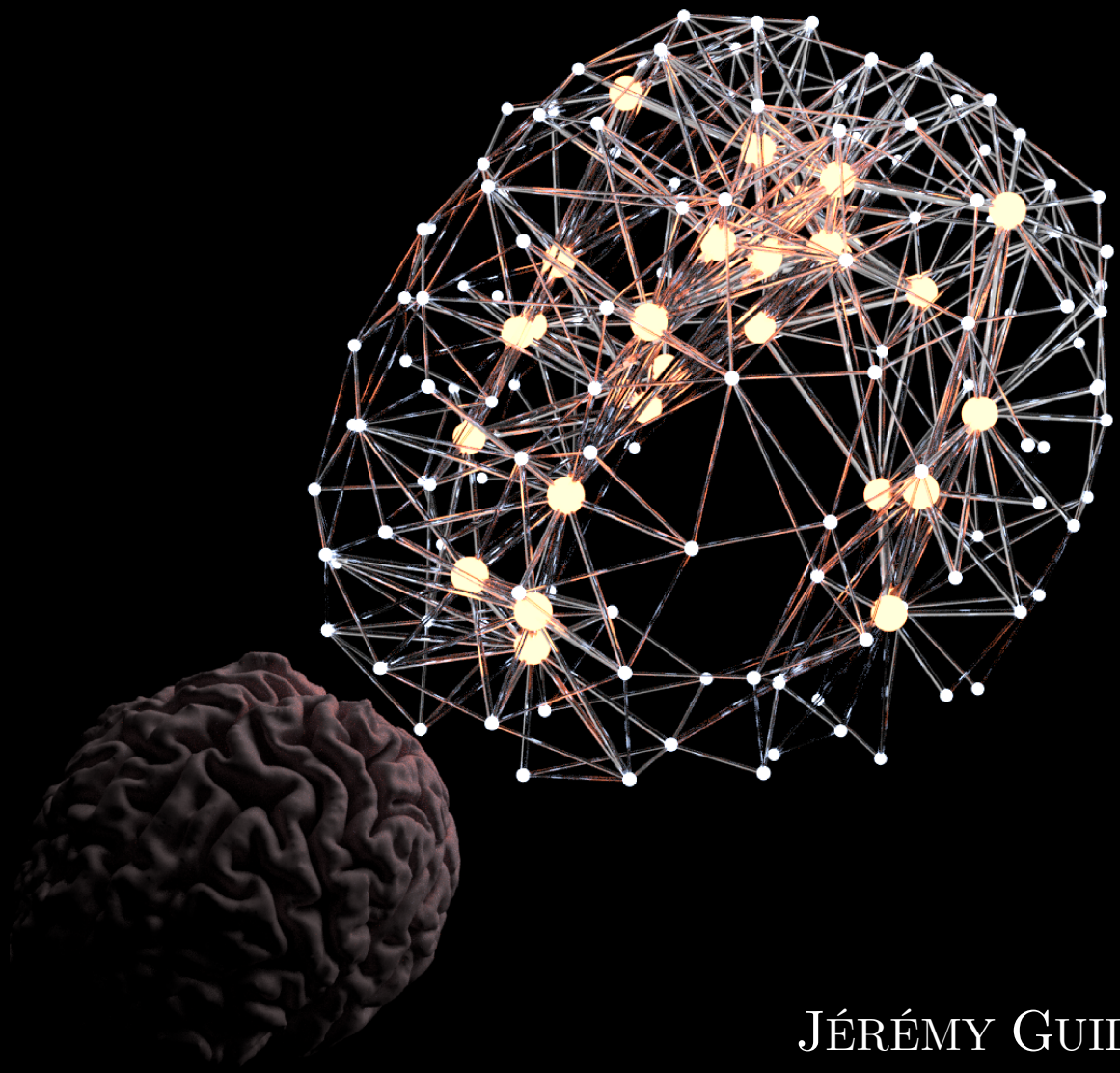

Jérémy Guillon

Under the supervision of Fabrizio De Vico Fallani

SORBONNE UNIVERSITÉ

CRÉATEURS DE FUTURS DEPUIS 1257

Sorbonne Université

École Doctorale d'Informatique, de Télécommunication et d'Électronique (EDITE)

ARAMIS LAB à l'Institut du Cerveau et de la Moelle épinière (ICM)

Approche multi-niveaux de la connectivité cérébrale dans la maladie d'Alzheimer

MULTI-LAYER APPROACH TO BRAIN CONNECTIVITY IN AZLHEIMER'S DISEASE

JEREMY GUILLON

Thèse de doctorat d'informatique

Dirigée par **Fabrizio De Vico Fallani**

Présentée et soutenue publiquement le *9 novembre 2018*

Devant un jury composé de :

- **M. Dimitri Van De Ville**, Professeur (rapporteur)
- **M. Alex Arenas**, Professeur (rapporteur)
- **Mme. Raffaella Lara Migliaccio**, Investigateur Principal
- **M. Alexandre Gramfort**, Directeur de Recherche
- **M. Fabrizio De Vico Fallani**, Investigateur Principal
- **M. Lionel Tabourier**, Maître de conférence

Table of contents

Remerciements

A MES ENCADRANTS.

J'aimerais avant tout remercier **Fabrizio**, encadrant de thèse pour qui il sera difficile de ne pas exagérer les éloges. Parfaitement équilibré ; ni trop présent ni trop absent ; ni trop compatissants ni trop exigeant, rassurant même pour respecter des deadlines impossibles... Perfectionniste à souhait, surtout lorsqu'il s'agit de figures d'articles, seules les couleurs pouvaient nous opposer !

Olivier, merci encore d'avoir fait suite à ma demande de stage dans l'équipe ARAMIS il y a maintenant 3 ans et demi, départ de cette aventure. Merci pour avoir été, avec **Stanley**, des chefs d'équipe exemplaires, toujours à l'écoute, toujours présents pour les pauses café avec des sujets de conversation toujours aussi passionnants, toujours prêts à entendre et écouter les critiques et les propositions.

AUX MEMBRES DE L'ECOLE DOCTORALE.

Je vous remercie d'avoir accepté ma candidature et de m'avoir donné l'opportunité de réaliser cette thèse.

À MESDAMES ET MESSIEURS LES MEMBRES DU JURY.

M. Dimitri Van de Ville, M. Alex Arenas, Mme. Rafaella Lara Migliaccio, M. Alexandre Gramfort, M. Lionel Tabourier, merci d'avoir accepté d'être membres du jury de ma thèse. Je suis très honoré de pouvoir présenter ces travaux devant vous et de pouvoir bénéficier de votre expertise.

A L'EQUIPE.

Merci à **ARAMIS LAB**, le meilleur labo du monde, et à tous ceux que je ne pourrai pas citer individuellement qui sont, ou ont été et resteront, membres de l'équipe ! Et désolé à ceux que je citerai accompagnés d'un qualificatif trop bref pour être juste.

Merci à mes premiers compagnons de galère : **Cata** pour tous ces moments incroyavles, **Jorge** pour avoir été là lors de la nuit la plus blanche de ma vie, **Hao** pour le doux son de ton beat box résonant dans les couloirs et **Alexandre R.** pour ta joie de vivre et ta motivation contagieuses !

A tous ceux des générations 3.0 et 4.0 : **Alex** le city boy, **Igor** le hipster, **Maxime** le grimpeur, **Manon** la veggie, DJ **Arnaud** le woodfloor expert et **Raphael** l'aventurier, surfer-rider et bon dernier !

Au club des filles italiennes : **SimoNA** pour ta bonne humeur permanente toujours accessible en un coup d'œil, tata **TitziaNA**, **Giulia BassignaNA**, et... **PascaliNA** !?

Merci aux anciens : papa **Pietro**, **J-B**, **Barbara**, Monsieur **Morin**, **Thomas** le Sharknado fan boy et **Michael** le fervent défenseur de la coolitude.

AUX AUTRES.

Papa, maman, Catcath' et Tessette la mi-fa, papa Franck, Eden & Elio sans qui je ne serais jamais arrivé jusque-là. **Nadine et la famille poneys** pour nous permettre de bien se ressourcer les week-ends, **Cécile et Coralie** pour m'avoir supporté, dans les deux sens du terme.

Scientific productions

Scientific publications

Published

Guillon, J., Y. Attal, O. Colliot, V. La Corte, B. Dubois, D. Schwartz, M. Chavez, and F. De Vico Fallani. "Loss of Brain Inter-Frequency Hubs in Alzheimer's Disease." Scientific Reports 7, no. 1 (September 7, 2017): 10879. https://doi.org/10.1038/s41598-017-07846-w.

Battiston, F., **J. Guillon**, M. Chavez, V. Latora, and F. De Vico Fallani. 2018. "Multiplex Core–Periphery Organization of the Human Connectome." Journal of The Royal Society Interface 15 (146): 20180514. https://doi.org/10.1098/rsif.2018.0514.

Samper-González, J., N. Burgos, S. Bottani, S. Fontanella, P. Lu, A. Marcoux, A. Routier, **J. Guillon**, M. Bacci, J. Wen, A. Bertrand, H. Bertin, M.-O. Habert, S. Durrleman, T. Evgeniou and O. Colliot. 2018. "Reproducible Evaluation of Classification Methods in Alzheimer's Disease: Framework and Application to MRI and PET Data." *NeuroImage* 183 (December): 504–21. https://doi.org/10.1016/j.neuroimage.2018.08.042.

Under submission

Guillon, J., V. La Corte, M. Thiebaut de Shotten, B. Dubois, O. Colliot, M. Chavez, and F. De Vico Fallani. 2018. "Disrupted core-periphery structure of multimodal brain networks in Alzheimer's Disease."

Routier, A., N. Burgos, **J. Guillon**, J. Samper-González, J. Wen, S. Bottani, A. Marcoux, M. Bacci, S. Fontanella, T. Jacquemont, P. Gori, A. Guyot, P. Lu, M. Diaz Melo, E. Thibeau-Sutre, T. Moreau, M. Teichmann, M.-O. Habert, S. Durrleman and O. Colliot. "Clinica: an open source software platform for reproducible clinical neuroscience studies."

Grants & Awards

Best Lightning Presentation Award. December 2017. *Complex Networks 2017 - 6th International Conference on Complex Networks and Their Applications.*

Travel Grant. April 2017. *NetSci 2017 - International School and Conference on Network Science.*

Bridge Grant. November 2016. *YRNCS - Young Researchers Network On Complex Systems.*

Travel Grant. May 2016. *XSYS - Toulouse Institute for Complex Systems Studies.*

PhD Fellowship. October 2015. *EDITE - Ecole Doctorale d'Informatique de Télécomunication et d'Electronique.*

Event organization

Brainhack Networks 2018

Brainhack networks was the *first international hackathon on brain networks*. In the now well-known series of ***Brainhack*** (http://www.brainhack.org), it took place at the Brain and Spine Institute (ICM) on the 9-10th of June 2018 in the context of the international conference ***NetSci 2018***, in Paris. More than 40 students, researchers, engineers, and renown experts of the field came from all around the world and took the opportunity to share their knowledge around 4 projects.

I took part in all the aspects of the organization of this event; the concept, the scientific content, the included social events, the animation, the food, the website and the whole communication.

Open-source software contributions

Clinica software

Clinica (http://clinica.run) is a software platform for clinical research studies involving patients with neurological and psychiatric diseases and the acquisition of multimodal data (neuroimaging, clinical and cognitive evaluations, genetics...), most often with longitudinal follow-up.

I participated in the main software architecture, "strategic" decisions, pipelines developments and the visual identity.

`nipype` python library

Nipype, an open-source, community-developed initiative under the umbrella of NiPy, is a Python project that provides a uniform interface to existing neuroimaging software and facilitates interaction between these packages within a single workflow.

I contributed in the development of wrappers for the SPM and MrTrix3 softwares.

Brainstorm software

Brainstorm (https://neuroimage.usc.edu/brainstorm/Introduction, Tadel et al. 2011) is a collaborative, open-source application dedicated to the analysis of brain recordings: MEG, EEG, fNIRS, ECoG, depth electrodes and animal electrophysiology.

I added the support of the Lausanne2008 parcellation as defined by Hagmann et al. (2008).

`easy_lausanne` command line tool

`easy_lausanne` (https://github.com/mattcieslak/easy_lausanne) is a stripped-down version of the connectome mapper, all it does is create the Lausanne2008 parcellations from an existing FreeSurfer directory and align them to a target volume (BOLD or B0) using `bbregister`.

So far, I simply fixed a bug but though it was worth advertising this piece of software that is still in early beta version.

Brain networks toolbox (BNT)

BNT (https://github.com/brain-network/bnt) is a simple repository containing all the scripts that contributed to paper publications in the field brain connectivity packaged as a MATLAB® toolbox. The goal is to make them accessible as quickly as possible to the public before, maybe, introduce them in bigger projects such as Brainstorm, MNE (https://martinos.org/mne/stable/index.html) or other softwares.

I created this repository from scratch, developed most of the scripts that it contains and adapted the rest of them from other contributors.

Communications

Oral presentations

- 15min talk + Poster, *NetSci 2018*, in Paris, France
- Lightning talk, *Complex Networks 2017*, in Lyon, France
- 15min talk, *Lipari School 2017*, in Lipari, Italy
- Lightning talk + Poster, *NetSci 2017*, in Indianapolis, USA
- Poster, *OHBM 2016*, in Geneva, Switzerland
- 15min talk, *XSYS 2016*, in Toulouse, France
- 15min talk, *IBERSINC 2016*, in Tarragona, Spain

Other

Selection of two scientific-artistic figures (including the one on the cover of this report) for the soon to be published *Atlas du Cerveau* by *Le Monde.*

Abbreviations

EEG	Electroencephalography
MEG	Magnetoencephalography
MRI	Magnetic Resonance Imaging
fMRI	Functional MRI
sMRI	Structural MRI
rsfMRI or rs-fMRI	Resting State Fmri
DTI	Diffusion Tensor Imaging
DWI, DW-MRI or dwMRI	Diffusion Weighted Imaging/MRI
AD	Alzheimer's Disease (Patient)
HC or NC	Healthy/Normal Control (Subject)
SC	Structural Connectivity
FC	Functional Connectivity
BOLD	Blood Oxygen-Level Dependent (Signal)
NMR	Nuclear Magnetic Resonance
T1	t_1 Time / T1-Weighted MRI
T2	t_2 Time / T2-Weighted MRI
WM	White Matter
GM	Gray Matter
CSF	Cerebrospinal Fluid
MD	Mean Diffusivity
ADC	Apparent Diffusion Coefficient

FA	Fractional Anisotropy
cFA	Colored FA
MSI	Magnetic Source Imaging
CBP	Connectivity-Based Parcellation
MICCAI	Medical Image Computing And Computer Assisted Intervention
ROI	Region Of Interest
AAL	Automated Anatomical Labeling
AVOI	Anatomical Volume Of Interest
HARDI	High Angular Resolution Diffusion-Weighted Imaging
FOD	Fiber Orientation Distribution
FACT	Fiber Assigned By Continuous Tracking
PET	Position Emission Tomography
OEF	Oxygen Extraction Fraction
Aβ	Amyloid-β

Introduction

The field of **complex networks** aims at studying non-trivial interactions between entities by mean of a mathematical object called **graph**. A graph is a set of elements, called **nodes**, and a set of links, called **edges**, linking together a subset of nodes by pairs. This representation of information can be applied in a wide range of domains, going from transportation with for example the complex network of airline routes (where the nodes represent the airports and the edges the direct flight routes between two airports) to sociology (friendship, professional relationship), biology (proteins interactions, epidemic spreading) and many more.

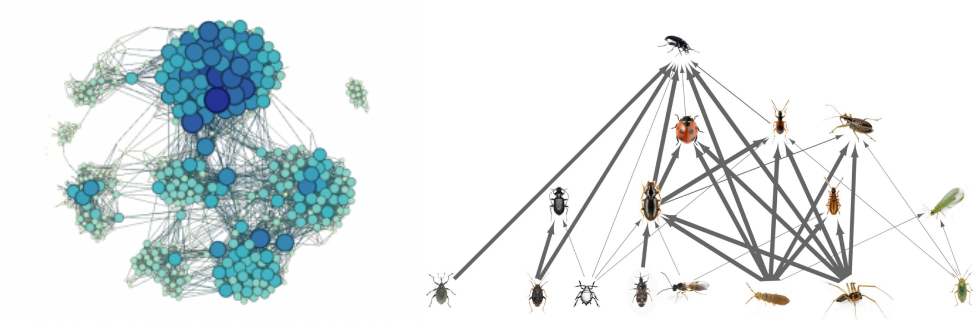

Illustration 1 Example of a Facebook friendship network (left) adapted from http://datasciencepost.com/en/visualize-your-facebook-network-with-gephi/, where each node represents a Facebook user, and each link a friendship connection; a food web (left) from (Bohan et al. 2017).

Complex networks have also found applications in neuroscience. Indeed, the brain exhibits patterns in the functional interactions of its parts or in their structure that are unique to individuals and that can be modelized using graph theory. Those models constitute what is called the **brain connectivity**. Brain connectivity can be of different type; one can have: *(i)* structural connectivity (SC); where links represent axons or neuronal fiber tracts or *(ii)* functional connectivity (FC) where links represent statistical dependencies between parts of the nervous systems. Those parts can be of different sizes leading to networks describing the brain connectivity at different scales. Depending on the spatial resolution of the physical measurements it is based

on, the "part" can be a single neuron (in that case the brain connectivity network is called a **connectome**[1]), an ensemble of neurons, or brain regions.

A neurodegenerative disease, such as **Parkinson's**, **Alzheimer's**, or **Huntington's disease**, causes the neurons, building blocks of the nervous system, to progressively degenerate or die. Neurons lose their structure and/or functions. That is why brain connectivity analysis is particularly suited to study this kind of diseases, their impact by comparing to healthy brains, or even their progression through time. It gives an understanding of the brain structure or function as a whole, and allows to *quantify* the effects of the disease on *different aspects*. In particular, this manuscript will focus on Alzheimer's disease's impact on brain connectivity. The knowledges about this disease are really poor; clinically it is characterized (in order of appearance) by short-term memory disorders, loss of language and motor skills, disorientation, confusion and long-term memory disorders; neuropathologically, by the accumulation of **tau protein** extracellular neurofibrillary tangles and of intracellular **amyloid-β (Aβ) protein** plaques. This is what causes neuronal loss and synaptic disruptions in specific cortical areas; and what made it being described as a *disconnection syndrome* (Buckner et al. 2005).

In the era of *big data*, more and more brain images, brain signals, cognitive tests scores, demographic or even physiological data can be acquired from a single patient in a reasonable amount of time. Understanding each one of this large quantity of data is a problem in itself but understanding them all together is another story. In the field of brain connectivity, this can be translated to the use of *multimodal, longitudinal, or high-resolution data*.

This thesis report will expose how multilayer complex networks framework applied to brain connectivity could help understanding Alzheimer's disease's impact and progression. I will try to provide the reader with the right amount of information, references and links to work with multimodal brain connectivity; from raw brain data to abstract graph models.

In the *first chapter*, I will go through the basics of brain connectivity, presenting the widely used brain imaging modalities and their associated (pre-)processing steps necessary to access to a functional or structural connectivity estimate. I will then, in a *second chapter*, present a few formalisms from graph theory that have been applied to model brain connectivity networks. How

[1] At the time of writing, only one connectome has been fully described and is the one of a 2mm worm called *Caenorhabditis elegans (White et al. 1986)*.

we manipulate them, what we can measure on them, and how these measures allowed us to learn about the brain and the impact that Alzheimer's disease has on it. The *third chapter* will be dedicated to the multilayer topology and its application to brain connectivity; a short review of the literature will help the reader to identify the context in which the studies that constitute the three following chapters were conducted. *Chapter 4* will illustrate a successful application of a specific type of multilayer topology called multiplex on a magnetoencephalography-based study of Alzheimer's disease. *Chapter 5* introduces a novel generalization of the concept of core-periphery structure in multiplex networks. And finally, *chapter 6* apply this newly defined core-periphery model to the first three-modalities multiplex networks and gives new insights on the impact of Alzheimer's disease on most important brain regions.

CHAPTER 1

Structural and functional brain connectivity

I Neuroimaging data

A Magnetic Resonance Imaging

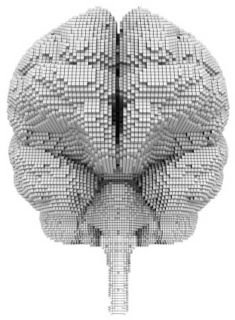

Illustration 2 Artistic representation of the voxels present in a human brain 3D scan.

Magnetic Resonance Imaging, abbreviated as MRI, is a medical imaging technique based on a physical phenomenon called nuclear magnetic resonance (NMR). By the mean of strong **magnetic fields** and **radio waves** pulses that excite atoms (mostly hydrogen) present in biological organisms, it is possible to measure some of their NMR properties and deduce the nature of the tissue they are in. The obtained signals can be localized by small unitary volumes (in the order of $1mm^3$) called a **voxel** (**Illustration 2**).

Repeating this operation for adjacent voxels allows to obtain a set of signals covering the entire desired volume. Finally, depending on the physical measure extracted from those signals and on the radio waves trains used to generate them, and on a lot of other physical conditions, a large variety of contrasts can emerge between the voxels allowing the creation of different 3D volumes (or scan) that are usually visualized by slices, i.e. 2D images.

Among the most used MRI techniques, one can present the following ones:

- ***T1- and T2-based MRI***: based on their respective **relaxation** time (denoted t_1 and t_2) needed by an excited atom to retrieve a stable state. These contrasts are the *core of almost every clinical MRI protocol* (Symms et al. 2004).
- ***fMRI***: functional MRI, based on the **blood-oxygen-level dependent** contrast (**BOLD**).
- ***DWI***: diffusion weighted imaging, based on the measure of the **Brownian motion** (random motion of water molecules).

i T1- and T2-weighted MRI

As mentioned above, these two contrasts are the basis of all MRI-based studies. T1 is mostly used to study normal anatomy while T2 is more appropriate to identify lesions.

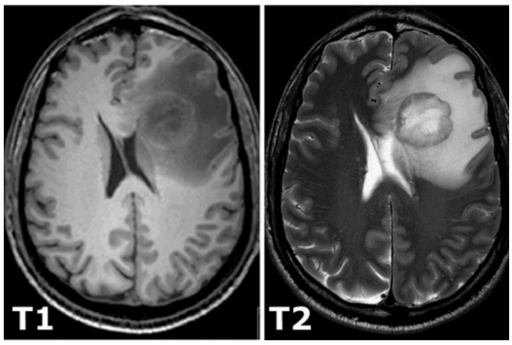

Illustration 3 Example of a brain tumor visualization on a T1- and T2-weighted MRI scans. Adapted from http://www.startradiology.com/the-basics/mri-technique/.

They are fast, thus reducing the risk of movement by the patient during the scan which makes them the least susceptible to image artifacts. And with a high spatial resolution, they allow to precisely *segment* the brain in to **white matter** (WM), **gray matter** (GM), and **cerebrospinal fluid** (CSF) (**Illustration 4**). A wide variety of automated segmentation techniques now exist (Liew and Yan 2006; de Boer et al. 2010) to deal with images data that are getting larger and larger[2] and for which it would take days for a trained anatomist to segment manually

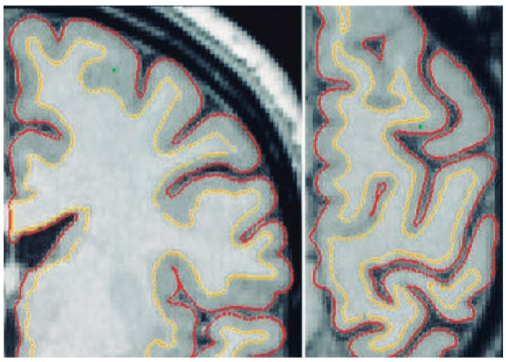

Illustration 4 Segmentation of the cortex. Gray/White matter (yellow) and pial (red) surfaces (Fischl and Dale 2000).

T1 images are also used to measure volumes of different brain parts, such as the hippocampus, or the global atrophy of the cortex by evaluating its thickness (**Illustration 4**). They give the reference 3D volume on which any further scans can be registered to.

ii fMRI

Functional MRI, as its name implies, gives information about the brain activity but *is not a direct measure of neural activation*. It is based on the BOLD contrast, first described in (Ogawa et al. 1990), that follows the blood oxygenation which itself reflects the demands in glucose, only source of energy of normal brain cells.

This contrast is *limited in spatial* - due to long range magnetic susceptibility - and *temporal resolution* due to the slow speed of the hemodynamic response. Also, the signal changes related

[2] 7T T1-weighted ultra-high resolution images can now weight more than 1 TB (Lüsebrink et al. 2017)

to cerebral activation are close to the noise level which led to numerous controversial results in the literature, especially when they are not corrected for multiple testing (Bennett, Wolford, and Miller 2009).

iii DWI

Diffusion represent the *random movements of molecules* (Brownian motion). In DWI, one study the *diffusion of water molecules*, largely present in the brain cells or in the CSF, by measuring its magnitude in a given direction with the appropriate MR sequences.

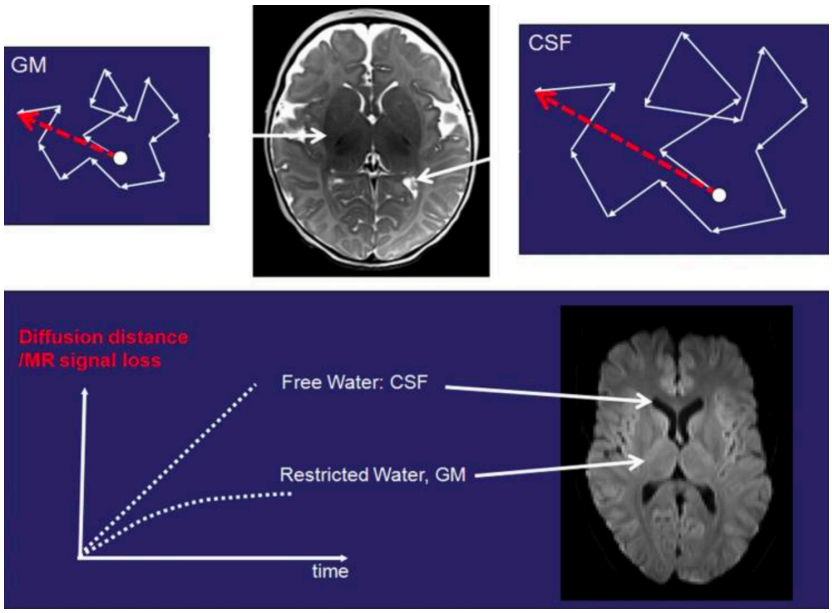

Figure 1.1 Graphical display of water molecules moving at different rates through the gray matter and cerebrospinal fluid (CSF). The effective distance that water molecules travel in gray matter is smaller than in CSF (represented by the magnitude of the red arrow). The difference in travelled diffusion distance versus time is displayed in the lower graph. The faster the molecules move, the more distance is travelled, the more signal loss will occur if diffusion gradients are applied. Consequently, the signal loss in the CSF is higher (hypointense) compared with the signal loss in the gray matter (hyperintense relative to the CSF). Extracted from (Huisman 2010).

Diffusion in brain tissues can be *isotropic*, such as in CSF or any other liquid in which the water can diffuse equally easily in each direction, or it can be *anisotropic*, such as in white matter that has an internal fibrous structure favoring diffusion of water in the direction of the main fibers (Huisman 2010). Therefore, the DWI contrast is dependent on the direction of the applied gradient.

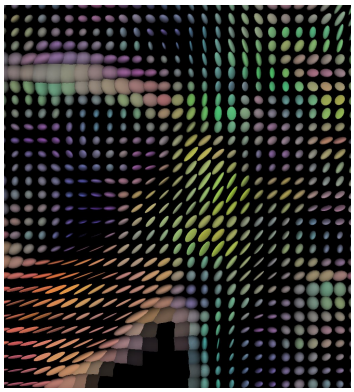

Illustration 5 Visualization of DTI data using ellipsoids.

By repeating the acquisition of DWI volumes for different gradient directions (three can be enough), one can build the diffusion profile (which is often summarized in a tensor and represented as an ellipsoid, see **Illustration 5**) at each voxel and thus deduce the main direction of propagation of the water molecules, it's called **diffusion tensor imaging** (DTI) (Peter J. Basser et al. 2000). From these, one can calculate various maps, such as:

- the **mean diffusivity** (MD), sometimes called **apparent diffusion coefficient** (ADC), it reflects the rotationally invariant magnitude of water diffusion within brain tissue (Clark et al. 2011);
- the **fractional anisotropy** (FA), a scalar between 0 and 1 which measures how asymmetric the diffusion inside a voxel is;
- the principal diffusion direction, usually referred to as **colored FA** (cFA) where the voxel hues are reflecting the main tensor orientation (usually with red indicating transverse, green indicating anterior–posterior, blue indicating superior–inferior; "RGB for xyz") and voxel brightness weighted by FA.

B EEG/MEG

Illustration 6 high resolution 256 electrodes EEG setup from http://dreamsessions.org/101artworks.html.

Electroencephalography (EEG) and ***magnetoencephalography*** (MEG) are monitoring methods used to respectively record brain electrical fields and brain magnetic fields. The EEG and MEG are very close methodologies, since the main sources of both kinds of signals are essentially the same, i.e., ionic currents generated by biochemical processes at the cellular level (Lopes da Silva 2013). While EEG consist in a set of electrodes to be placed in contact with the surface of the head and connected to a relatively small device, MEG is a large machine under which the subject has to place his head, inside a magnetically shielded room.

For an electric or magnetic signal to be recordable at a distance, a large enough assembly of neurons should activate in a coordinated way and be spatially organized. That is the case of a family of neurons called **pyramidal cells**. In order for electromagnetic fields to reach distant sensors, various tissues must be passed. The different layers, such as the

cerebrospinal fluid, skull, and skin, especially affect electric fields due to their different electrical conductivities but have less impact on the magnetic fields that are not distorted by scalp or skull for instance. However, the magnetic fields diminish as $1/r^3$ with the distance of r (Singh 2014).

EEG and MEG are subject to the problem of **source localization**. In many applications it is important to know from where the electromagnetic signal came from. The estimation of the sources from the scalp fields is called **inverse problem**. It is *ill-posed* and consequently, has an *infinite number of solutions* that need to be restrained by making assumptions on the nature of the sources. A large number of methods exist whose details go beyond the subject of this manuscript; for reviews on ***EEG/MEG source imaging*** (MSI) techniques, see (Michel et al. 2004; Grech et al. 2008; Becker et al. 2015).

Both modalities have their advantages and drawbacks. MEG is more sensitive in detecting currents that are tangential to the scalp whereas EEG is sensitive for both tangential and radial currents. This makes MEG detecting primarily the "fissural" cortex activities (i.e. activities present in the sulci). MEG is said to have a better spatial resolution with 3-4cm2 on scalp and 3-4mm when its signals are source-localized (Singh 2014). But it is also a lot more expensive than EEG, and has logistic constraints that could make difficult for research or clinical facilities to acquire it and/or run specific protocols.

Although the human brain produces activity in a wide range of frequencies (0.5 to 500 Hz), the most clinically relevant activities lie below 70 Hz (normal physiological or spontaneous waves) and the frequency bands are alpha (8 to 13 Hz), beta (13 to 30 Hz), theta (4 to 8 Hz), and delta (1 to 4 Hz). (Velmurugan, Sinha, and Satishchandra 2014)

II Structural and functional connectivity

A Concept and motivation

It has been shown that the human cerebral cortex is composed with distributed neural assemblies, densely *connected* and *interconnected* to form a large-scale cortical circuit or "web-like" structure (Varela et al. 2001; Boccaletti et al. 2006; Schnitzler and Gross 2005; Carter, Shulman, and Corbetta 2012). In that context, a *connection* is often said to be **structural or functional**.

The ***structural (or anatomical) connectivity*** (SC) corresponds to the physical connection between different brain sites. At a microscopic scale, those connections can correspond to synapses whereas at a more macroscopic level, when we study neural ensembles or cortex parcels, we observe white matter **fiber pathways or tracts** that are estimated using tractography algorithm based on DTI data (see section "Structural connectivity estimators" for more details). While this set of connections is quite stable at shorter time scales (seconds to minutes), it can be altered at longer time scales (hours and more) by a phenomenon called **plasticity** consisting in the strengthening/weakening of synapses or the remapping of cognitive functions to different cortical locations. These changes may be due to training (environmental *stimuli*), thoughts, emotions or injury.

The ***functional connectivity*** is a statistical concept defining how dependent spatially distant neurophysiological activities are. Due to the wide variety of neural activity recording methods and to the fact that, for most of these methods, activities recorded at one site may be influenced by its surrounding neighborhood (i.e. because of volume conduction), no unified definition of functional connectivity exist. For voxel-based modalities, such as fMRI or PET, the studied brain "sites" can be a single voxel or voxels aggregates, whereas sensor-based modalities, such as EEG or MEG, offer a choice between working directly with sensors or with reconstructed sources (De Vico Fallani et al. 2014).

In the framework of complex networks and to understand the systemic impact of wide spread neurodegenerative diseases such as AD, we build an interconnected representation of the brain based on those two concepts, a *whole brain* connectivity network or more concisely a brain network (Simpson and Laurienti 2016). In whole brain networks the connectivity is computed between all possible pairs of brain voxels, cortex parcels or white matter volumes that act as the nodes of the network. There are usually two families of scales at which functional or structural connectivity brain networks are computed: *voxel/vertex-level* or *region-level*. In the former, signals and images are kept in their thinner spatial resolution possible - the voxel in the case of MRI-based data, and the vertex or the sensor in EEG/MEG data. At this scale, the signals may be noisy or suffer from reconstruction algorithms limitations. Moreover, dealing with millions of time series might be computationally challenging. In the latter family of scales, time series or white matter tracts are aggregated in small brain regions following a **brain parcellation**.

B Brain parcellation

The choice of a parcellation is an important one, it will determine the number of nodes that the brain networks will be composed with, and thus the granularity of the brain connectivity profile. Grouping together cortex sub-parcels with opposite behaviors (functional or structural) into one single entity might generate, by average, a cancelation of its contribution in the whole network.

Brain parcellation is a real topic of research, as can attest the number of papers gathered in the past year by a single review by Craddock, Bellec, and Jbabdi (2018). This special issue reviews all the latest methods related to this domain going from cytoarchitecture-based manual parcellation to fully automated whole brain segmentation using deep learning. The importance of this aspect of brain connectivity is such that the well-known **MICCAI** international conference organized a challenge on this topic in 2013: MRBrainS (http://mrbrains13.isi.uu.nl/, Mendrik et al. 2015)

A large panel of brain parcellation methods exist, but the most commonly used in the field on brain networks can be divided in two categories; anatomy- or connectivity-based parcellation.

i Anatomy-based parcellation

Traditionally, anatomical brain atlases or templates are used to define **regions of interest** (ROIs), i.e. the nodes of the whole brain network. These atlases are derived from anatomical landmarks, cortex curvatures, or cytoarchitectonic[3] information. Then, the standard pipeline is the following: one or more subjects' anatomical images (usually T1) are manually parcellated, and registered onto the average brain in order to obtain a template brain. All new subject is then registered on this template which propagates its region labels onto the subject's brain in order to parcellate it (de Reus and van den Heuvel 2013).

[3] Architecture of neural cells

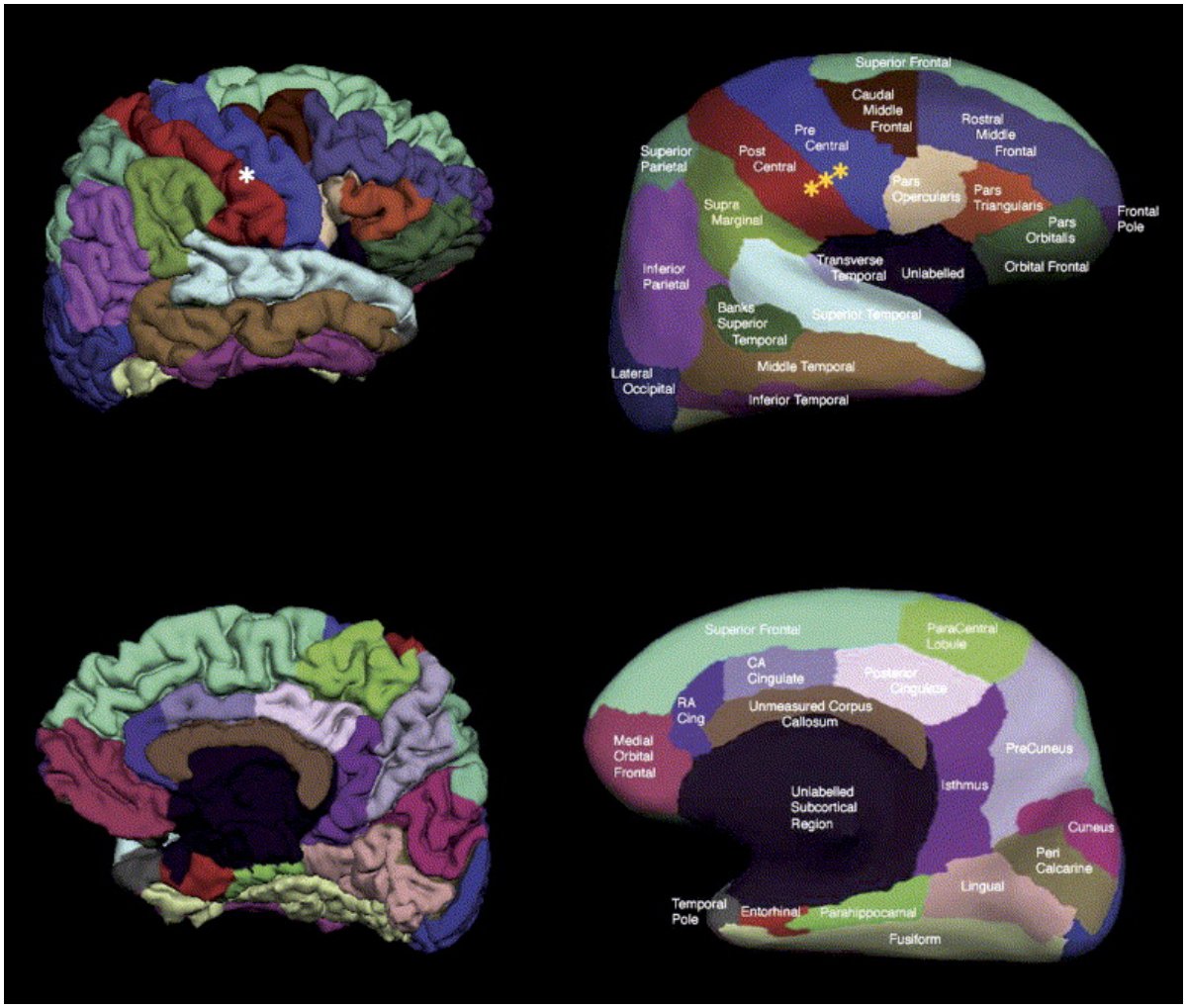

Illustration 7 Example of the Desikan-Killiany anatomical parcellation. 34 ROIs are delineated on each hemisphere based, mainly, on local curvature.

For example with the ***Desikan-Killiany atlas*** (Desikan et al. 2006) the procedure was to manually parcellate the cortical surface of 40 brains coming from various profiles (different sex, age, condition) based on heterogeneous information including: standard conventions, previous atlas definitions, and local curvature. They generated an atlas by mean of a registration - i.e. the cortical folding patterns alignment - and probabilistic assignment of a label to each vertex of the cortical surface. 34 parcels on each hemisphere. A similar process was also used for the ***Destrieux atlas*** (Christophe Destrieux et al. 2010) which is based on the work of (Duvernoy 1999) and ended up being composed with 148 ROIs. Both of these parcellation can be automatically generated using the largely distributed ***FreeSurfer*** software (https://surfer.nmr.mgh.harvard.edu/) making them ones of the most used anatomical parcellations.

The ***Automated Anatomical Labeling (AAL)*** (Tzourio-Mazoyer et al. 2002) is another widely used brain parcellation also based on cortical curvature and standard nomenclature but it has the following advantages: *(i)* it is freely available inside the ***SPM software*** (Litvak et al. 2011); *(ii)* it provides a volumetric parcellation (and not only a parcellation of the cortical surface) adapted for fMRI-based functional connectivity; *(iii)* it has been defined directly in the ***MNI space***[4] from the high resolution Colin27[5] brain; and *(iv)* the number of ROIs (or AVOI, as described in the paper) is particularly suited for a brain connectivity analysis at reasonable scale.

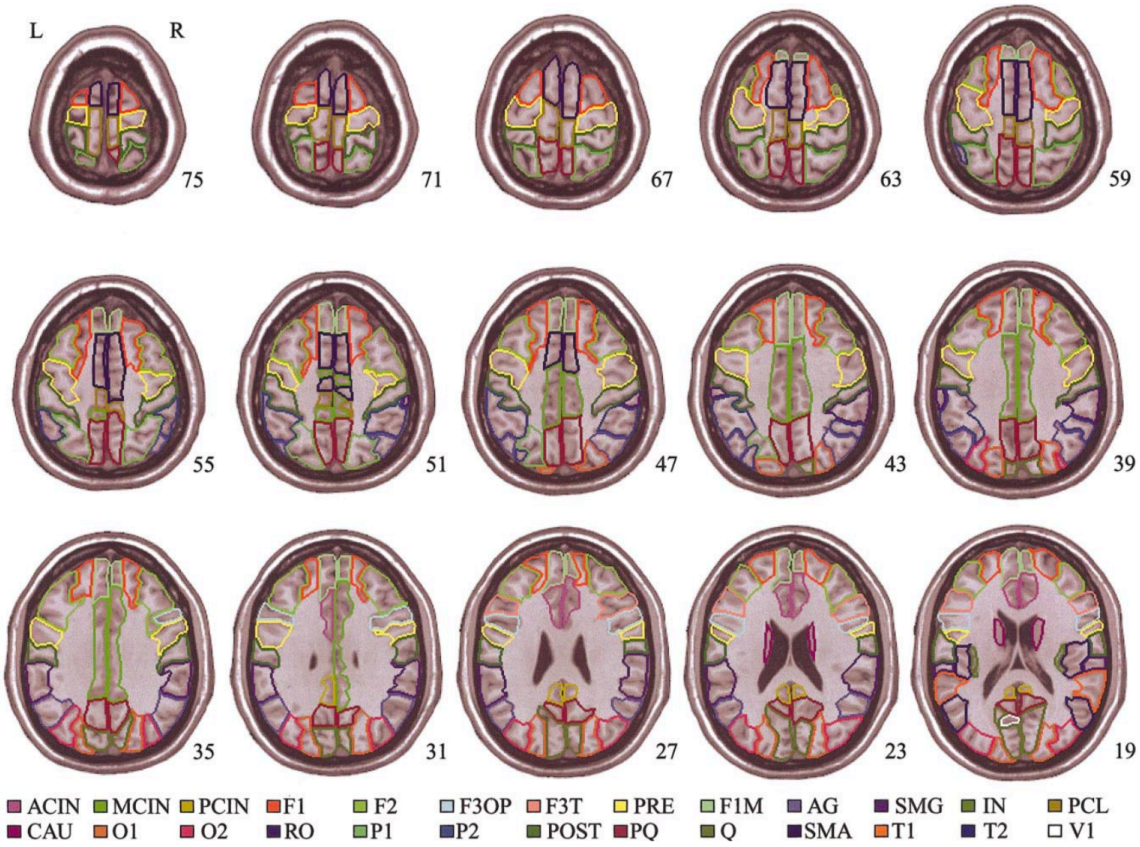

Illustration 8 Regions of interest of the AAL atlas (Tzourio-Mazoyer et al. 2002), drawn on axial 1-mm-thick T1 MNI single-subject slices (only one slice every 4 mm is reproduced). Values on the lower right of each slice indicate the stereotaxic z coordinate in millimeters (from $z = 75$ to $z = 19$ mm).

[4] The MNI space consists in the average of 305 (then 152) T1 brain scans linearly transformed to the Talairach stereotaxic template.

[5] T1 brain template computed as the average of the 27 scans of a single young man. After a non-linear registration to the MNI305 space, this template has been adopted by many standard software e.g., AFNI (Cox 1996); Brainstorm (Tadel et al. 2011); SPM (Litvak et al. 2011); Fieldtrip (Oostenveld et al. 2011).

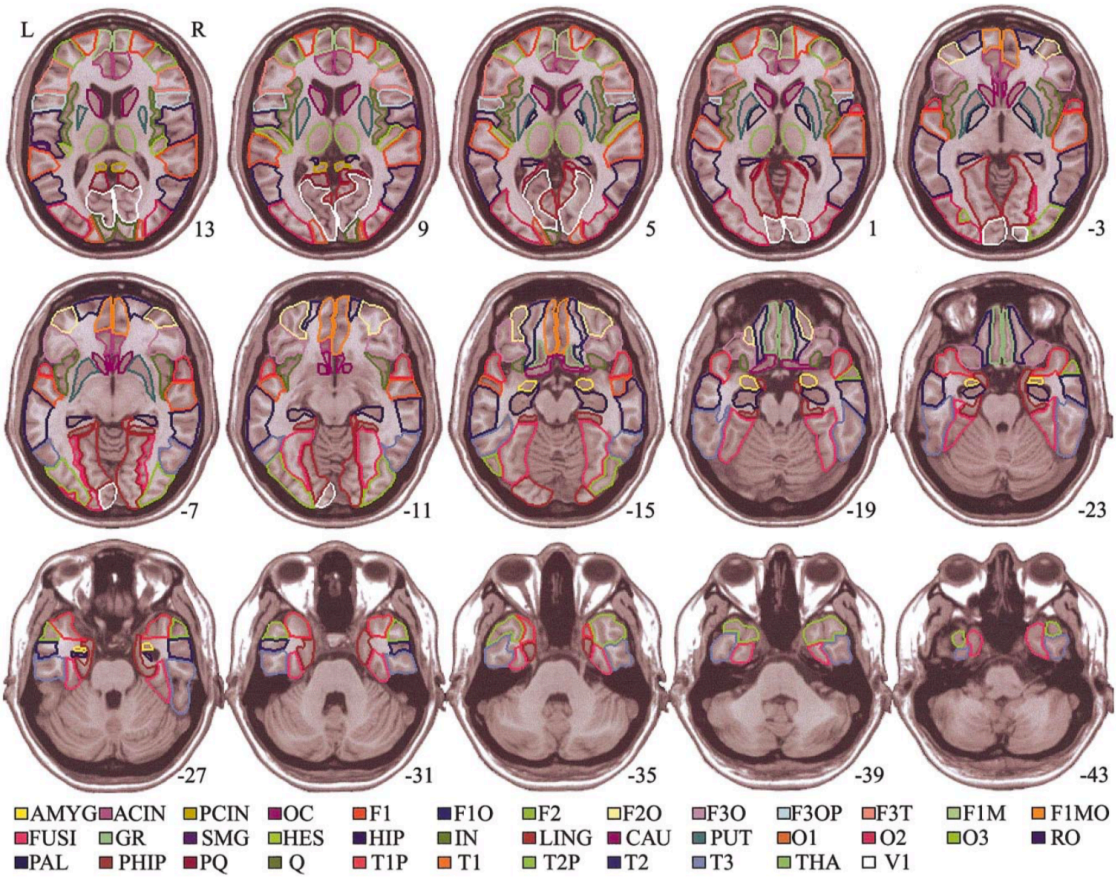

Illustration 9 Regions of interest of the AAL atlas (Tzourio-Mazoyer et al. 2002), drawn on axial 1-mm-thick T1 MNI single-subject slices (only one slice every 4 mm is reproduced). Values on the lower right of each slice indicate the stereotaxic z coordinate in millimeters (from $z = 13$ to $z = -43$mm).

This parcellation method have some limitations. First, inter-individual anatomical variability (Zilles et al. 1997; Destrieux et al. 1998) which remains from 9 to 18 mm, depending on the brain regions considered (Thompson et al. 1996). Second, the heterogeneity of structural and/or functional connectivity inside each macroscopic brain parcels. For example, the works of Margulies et al. (2007) and Beckmann, Johansen-Berg, and Rushworth (2009) showed respectively that structural and functional connectivity in the anterior cingulate (AAC) was highly heterogenous thought it was typically represented as a single ROI (in AAL for instance, Arslan et al. 2018).

ii Connectivity-based parcellation

The common concept between most of the connectivity-based parcellation (CBP) algorithms is to cluster vertices or voxels of the brain images/signals based on a local similarity measure such as Pearson's correlation, Euclidian distance, etc.; or on a global metrics such as Newman's modularity (see Chapter 2 for more details), using various unsupervised clustering algorithm such

as k-means, hierarchical clustering (Ward Jr. 1963) or spectral clustering. A spatial constraint is usually added such that only neighboring clusters or voxels/vertices can merge into one single cluster. Most CBP are single-subject's parcellations; their scan-to-scan reproducibility, thus, cannot be assured. But being directly obtained from the underlying data, they can provide much more coherent parcels for subsequent connectivity analysis.

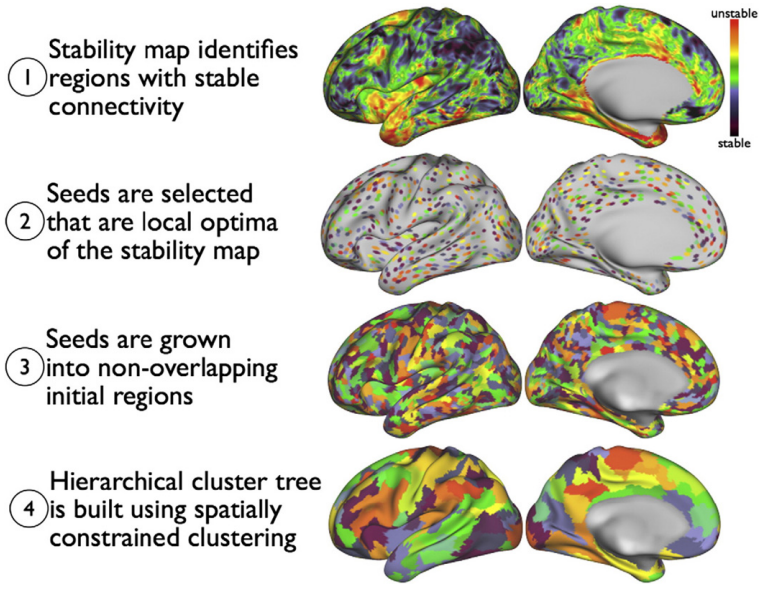

Illustration 10 Typical example of connectivity-based parcellation procedure from Blumensath et al. (2013). After preprocessing, clustering proceeds in four steps. In step (1) a slightly smoothed stability map is computed (black: more stable, red: less stable). Local optima are identified in step (2). The locations of these optima will be the seed regions used in the next step. In step (3) the seeds are grown into disjoint clusters, giving the finest clustering. Finally, in step (4), a spatially constrained hierarchical clustering method builds a cluster tree, giving not only a single parcellation, but an entire spectrum of parcellations at different resolutions (only one of these is shown here).

There is a growing list of exhaustive reviews specifically treating the subject of CBP: Eickhoff et al. (2015), Thirion et al. (2014), and de Reus and van den Heuvel (2013).

> *"Importantly, no single package permitting CBP is, to the best of our knowledge, openly distributed at the moment. Rather, it seems that different research groups perform CBP analyses based on their own script library, in-house databases, and laboratory setups. However, sharing of code implementations and international collaboration on its successive improvement will hopefully contribute towards a widely accepted software infrastructure (cf. Pradal, Varoquaux, and Langtangen 2012)."*
>
> *Eickhoff et al. (2015)*

CBP algorithms have been evaluated again this year by Arslan et al. (2018) which associated to their paper a website (https://biomedia.doc.ic.ac.uk/brain-parcellation-survey/) that lists some links to some of the source codes used to generate the parcellations and a GitHub repository containing all the scripts used to evaluate the 24 parcellations as depicted below.

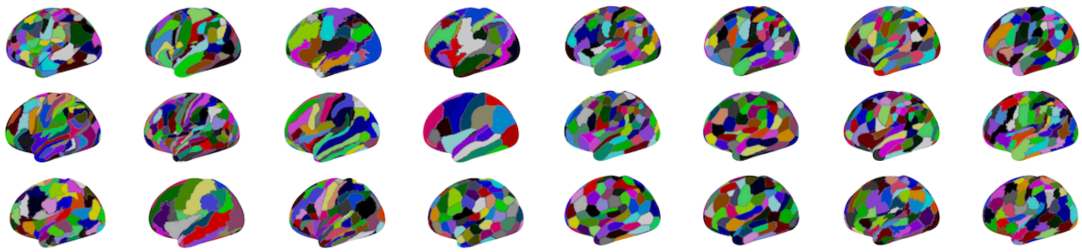

C Connectivity estimators

Once the nodes of the brain network are chosen, depending on the modalities available, you can define the links between them using a **connectivity estimator**.

i Structural connectivity estimators

Structural connectivity almost exclusively refers to a quantification of the white matter fiber tracts density or quality computed using ***tractography*** algorithms on DWI images. A tractography algorithm can be divided in two steps: *(i)* the *local modeling*, which defines at each voxel the distribution of directions of propagation; and *(ii)* the *fiber tracking* that uses this local information to build 3D trajectories called **streamlines** or **fiber tracts** (Yo et al. 2009; Khalsa et al. 2014).

Two types of local models exist: the one, most common, describing a single main fiber orientation of whiter matter inside each voxel, known as the diffusion tensor model (DT, P J Basser, Mattiello, and LeBihan 1994); and those capturing multiple fiber orientations such as the **multiple tensor model** (Tuch et al. 2002), **q-ball imaging** (QBI, Tuch et al. 2003), **diffusion spectrum imaging** (DSI, Cohen Veterans Bioscience n.d.), [constrained] **spherical deconvolution** (Tournier et al. 2004; Tournier, Calamante, and Connelly 2007), etc. (review by Alexander 2005; Lazar 2010). The former type of methods has been proven limited since it cannot capture crossing/kissing/fanning/branching fibers inside a single voxel (Seunarine and Alexander 2014; Jones 2010).

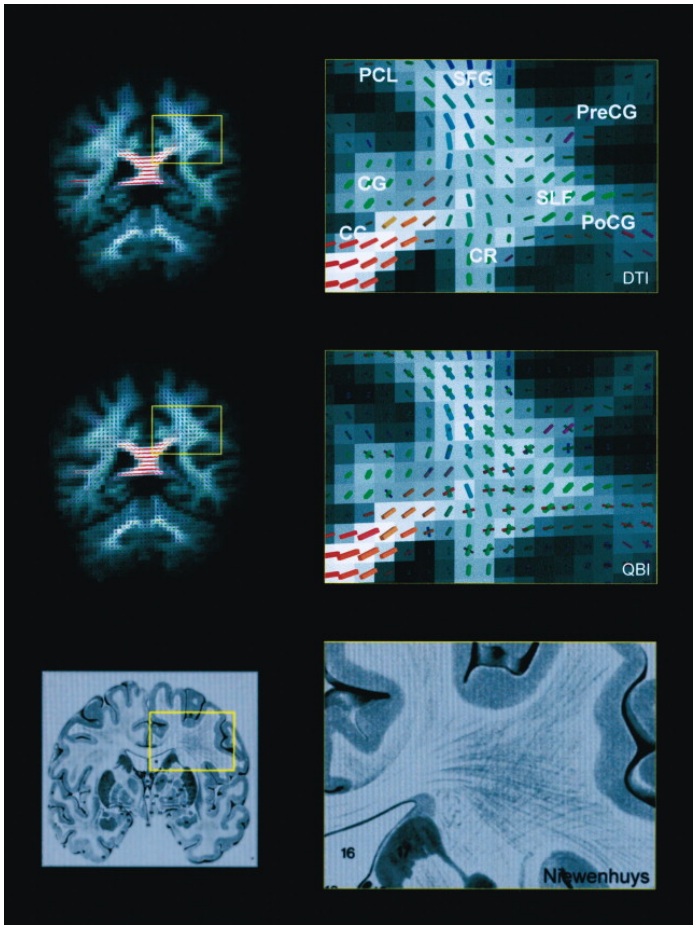

Illustration 11 Comparison of DTI, QBI, and Nieuwenhuys Atlas.(Tuch et al. 2003)

Some of those advanced methods may require specific DWI sequences with, for example, a set of different b-values[6], high b-values ($b > 3000\text{s/mm}^2$), or many gradient encoding directions ($N_{\text{enc}} > 60$) such as models based on high angular resolution diffusion-weighted imaging (HARDI, Tuch et al. 2002). These setups may lengthen the time necessary for a scan, thus, making them not suited in clinical environments where young, diseased or old patients cannot support long periods inside an MRI scanner.

After the local modeling, the fiber tracking algorithm allows to estimate fiber tracts. The algorithms usually work as follow: a seed voxel is randomly chosen within a subset of possible voxels to start from, then a streamline starts to grow by making steps towards either *(i)* the most probable direction as dictated by the local model of the voxel in question - this is called *deterministic* tractography - or towards *(ii)* a direction sampled from the local **fiber orientation**

[6] The b-value is a factor that reflects the strength and timing of the gradients used to generate diffusion-weighted images. ("B-Value Diffusion" n.d.)

distribution (FOD) - this is *probabilistic* tractography. The most common deterministic tractography algorithms are FACT for Fiber Assigned by Continuous Tracking (Mori et al. 1999) or the streamline tracking algorithm (Peter J. Basser et al. 2000).

In practice

In order to compare all the variety of different preprocessing pipelines and tractography algorithm, a first initiave called FiberCup (Fillard et al. 2011) tried to define a common framework under the form of a challenge. More recently, Maier-Hein et al. (2017) reviewed 96 methods of tractography and associated a standalone tool to evaluate new submission (http://tractometer.org/).

Another interesting initiative is the gathering of HARDI-based methods in a MATLAB® toolbox ("NeuroImageN - High Angular Resolution Diffusion Imaging (HARDI) Tools" n.d.).

Once the set of tracts (or tractogram) is generated, different connectivity measures allow to quantify the strength of the connection between two ROIs. The most common one is known as number of streamlines (NOS) and simply counts the number of generated fiber tracts connecting the two sets of voxels/vertices, i.e. starting in ROI i to finish in ROI j. Some other estimators use the length of the fiber tracts as a factor of the weight (Hagmann et al. 2008), and/or normalize it by the size (area, number of vertices/voxels) of the connecting ROIs. One can also weight the connection based on its probability (for probabilistic tractography-based methods), or on the fractional anisotropy (FA) of the voxels it's crossing.

ii Functional connectivity estimators

The standard approach in functional connectivity is to estimate a statistical dependency between time series averaged inside each previously define ROI. Functional connectivity estimators can be *linear/nonlinear*, *bivariate/multivariate*, in the *time/frequency* domain or even based on *information theory*.

The simplest, linear, is the ***cross-correlation***, especially and widely used in fMRI-based connectivity analyses (introduced by Cao and Worsley (1999) discussed by Zalesky, Fornito, and Bullmore (2012) and Hlinkaa et al. (2011)). Another similar measure is the (sometimes called magnitude-squared-, spectral-, or phase-) ***coherence*** equivalent to the cross-correlation, but in

the frequency domain. It captures linear time-invariant relationship between two time series by resulting a coefficient between 0 and 1; 0 meaning no linear relationship, and 1 meaning that one time series can perfectly predict the other in a linear way, independently of the phase difference as long as it doesn't change through time (i.e. time-invariant) (Sun, Miller, and D'Esposito 2004). Coherence is function of the frequency and is usually averaged by frequency bands that have a neurophysiological meaning; making it the preferred connectivity measure for wide frequency range brain recordings (typically EEG and MEG). The ***phase lag index*** (PLI, by Stam, Nolte, and Daffertshofer (2007)) that works as a phase synchronization quantifier or the ***wavelet correlation*** and its multiresolution nature (Bullmore et al. 2004; Achard et al. 2006) are also adapted to time series of neural activities.

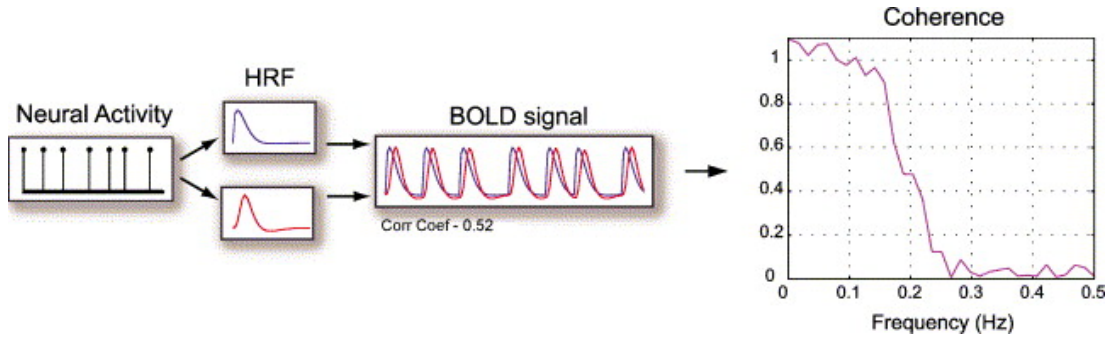

Illustration 12 Illustration of coherence as a measure of the linear time-invariant relationship between two time series. In this simulation, the same model of neural activity is linearly convolved with two different models of the hemodynamic response function. The correlation coefficient of the resulting time series is 0.52, which is low compared to the coherence in the bandwidth of the hemodynamic response function (HRF). Within the bandwidth of the model HRF, coherence is near 1, and above the HRF bandwidth, coherence is near 0. (Sun, Miller, and D'Esposito 2004)

Granger causality is very well appreciated for its directed aspect. Indeed, the granger causality evaluates differently the connection from node i to node j, from the one from j to i. It is said that i causes j if the past information contained in the signal of i helps in predicting the signal of j.

Many other dependency estimators exist such as the ***directed transfer function*** (DTF, by Kaminski and Blinowska (1991), the ***phase locking value*** (PLV, by Lachaux et al. (1999)), the ***partial directed coherence*** (PDC, by Baccalá and Sameshima (2001)), the ***synchronization likelihood*** (SL, by C. J. Stam and van Dijk (2002)), or the ***imaginary part of coherency*** (Nolte et al. 2004). And novel methods based on deep learning are also appearing (Y. Wang et al. 2018). Colclough et al. (2016), Sakkalis (2011) and Jalili (2016) reviewed some of the connectivity estimators and discussed the binarization methods.

CHAPTER 2

Complex brain networks

I Brain network as a graph

A set of connectivity coefficients for each pair of ROIs can be stored in a $N \times N$ matrix, with N the number of ROIs, called an ***adjacency matrix*** $A = \{w_{ij}\}, \forall i, j \in 1..N$, where w_{ij} is the connectivity coefficient (or weight of connection) between ROI i and ROI j. It can be represented as a fully connected graph of N nodes, and $N \times (N-1)$ directed (or $\frac{N \times (N-1)}{2}$ undirected) edges weighted by their corresponding coefficient in A. Basic operations on A are *(i)* the ***thresholding*** that allows to remove weak links that may be spurious and due to noise in brain signals and images; *(ii)* ***binarization*** that can be useful when the strength of a link does not really make sense (such as in structural connectivity analysis where you could simply be interested if there is a connection or not) nor directly reflect the real physiological phenomenon *(iii)* ***symmetrization***, less usual, permits the conversion of directed to undirected links, when the direction of the connection is not of interest after a wrongly chosen connectivity estimator.

Thresholding generates information loss, but is often adopted to remove spurious links, reduces the false positives rate, and simplify the resulting network topology. It may be *absolute*, or *proportional*; it is, in many cases, arbitrarily chosen. While some studies analyze networks across

broad range of thresholds, a recent study have attempted to estimate *a priori* an optimal threshold value based on topological hypotheses (De Vico Fallani, Latora, and Chavez 2017), or other more standard methods filter networks based on the statistical significance of each link (Gourévitch, Bouquin-Jeannès, and Faucon 2006; Toppi et al. 2012; Craddock et al. 2013) which again depends on an arbitrarily chosen "significance" threshold. There exists other network filtering techniques that try to somehow optimize the topology of the network, such as by extracting the ***minimum spanning tree*** (MST) or ***minimum connected component*** (MCC), defined respectively as the subgraph minimizing the summation of link weights without forming any loops and the subgraph removing the weakest edges as soon as all the nodes are not disconnected from the main component (Vijayalakshmi et al. 2015; Jalili 2016).

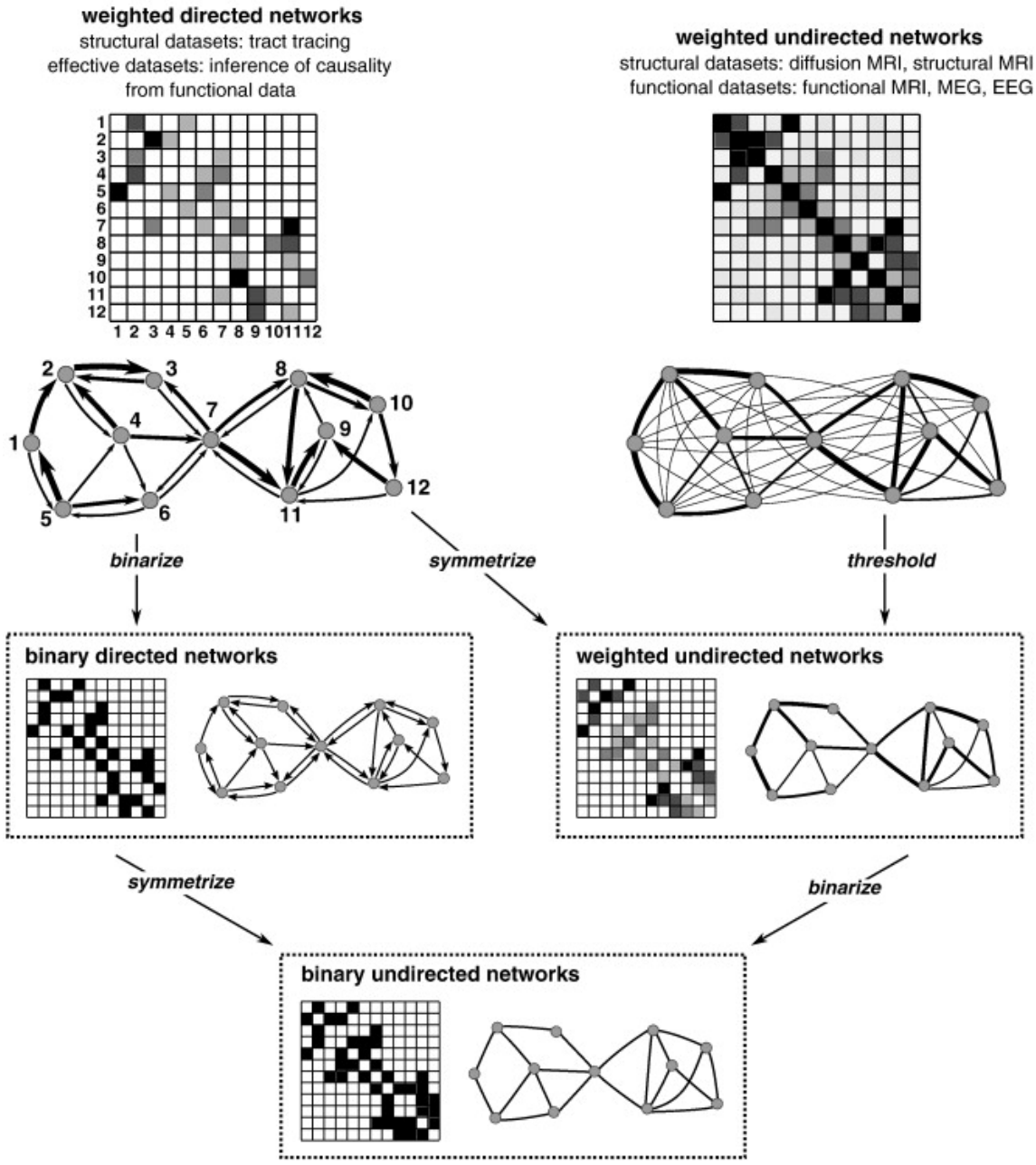

Illustration 13 Visual representations of brain networks' adjacency matrices and their associated graph after standard connectivity estimation and manipulation. Each rows and columns representing nodes and matrix entries representing links weighted by a connectivity estimator. Most of the connectivity estimators allow to start with a fully-connected and weighted network (top row) that are often reduced to sparse binary undirected form (bottom row) through thresholding, binarizing, and symmetrizing (Rubinov and Sporns 2010).

Binarizing and symmetrizing also generate great loss of information but also facilitate a lot the analysis, with in practice, a decreased computation time and power necessary for every operation (including visualization), simple graph metrics and more easily defined null-models for statistical comparisons (see below).

II Graph analysis tools

A Graph metrics

The brain networks topology can be quantified by metrics coming from graph theory. These are often segmented in function of the scale of the entity they are describing, that might be a single node, the *local scale*; a group of nodes (or modules), the *mesoscale*; or the whole network, the *global scale*.

Starting with local measures, the most standard is the ***node degree*** d_i which is the number of nodes to which a given node is connected and can mathematically written as follow:

$$k_i = \sum_{j \neq i} a_{ij} ,$$

where a_{ij} are the entries of the binarized adjacency matrix (zeros or ones). The degree reflects the *centrality*, i.e. the importance of a node in comparison with all the other nodes of the network. A lot of network metrics are derived from this first one, including the ***network density*** ρ or normalized average degree:

$$\rho = \frac{1}{N-1} \times \bar{k} = \frac{1}{N-1} \times \frac{1}{N} \sum_i k_i ,$$

With $\bar{k}$ the average node degree, ρ is comprised between 0 for disconnected networks and 1 for fully-connected networks (normalized by $N-1$, the maximum degree of a node). Note that global measures are usually averaged versions of local measures across the whole set of nodes.

i Functional integration metrics

such as for the ***global efficiency*** E, which is inversely proportional to the average shortest path length:

$$E = \frac{1}{N} \sum_i E_i = \frac{1}{N} \sum_i \frac{1}{N-1} \times \frac{1}{\sum_{j \neq i} d_{ij}},$$

With d_{ij} the shortest path length between node i and node j and E_i the efficiency of node i (local, but different from the "local efficiency" of node i, see below). This measures how globally efficient a network is in the sense of connecting distant nodes together. Global efficiency is related to another measure based on shortest paths called ***characteristic path length*** (Watts and Strogatz 1998):

$$L = \frac{1}{N}\sum_i L_i = \frac{1}{N}\sum_i \frac{\sum_{j\neq i} d_{ij}}{N-1},$$

Where L_i is the average distance between node i and all other nodes (local).

These two latter measures reflect the *functional integration* of the concerned network. Functional integration is the brain's ability to combine (integrate) information from distributed (long distance) brain regions. Here the *distance* definition depends on the type of brain network in question; it could be structural, functional or even metric if, for instance, your distance d_{ij} is defined as the physical distance separating two brain region's centroids based on a structural connectivity-based network topology. Though, the relationship between E, L and functional integration should be taken with care as highlighted by Achard and Bullmore (2007) and Estrada and Hatano (2008) since they do not take into account the redundancy of paths (and their length, longer than or equal to the shortest ones) connecting pairs of nodes.

Other local measures make use of the shortest paths in order to characterize the centrality of a nodes or edges, they are called ***node betweenness centrality*** $\mathrm{NBC_i}$ and ***edge betweenness centrality*** $\mathrm{EBC_{ij}}$ respectively and represent the number of all-to-all shortest paths making use of a given node or edge respectively. They can be defined as follow:

$$NBC_i = \sum_{p\neq i\neq u} \frac{\Gamma_{pu}(i)}{\Gamma_{pu}},$$

and,

$$EBC_{ij} = \sum_{p\neq u} \frac{\Gamma_{pu}(e_{ij})}{\Gamma_{pu}},$$

where Γ_{pu} is the number of shortest paths between node p and u, $\Gamma_{pu}(i)$ the number of these paths making use the *node* i, and $\Gamma_{\mathrm{pu}}(e_{ij})$ those making use of the *edge* between node i and j.

ii Functional segregation metrics

We say that the brain is functionally segregated if groups of brain regions are densely *intraconnected* but sparsely *interconnected.* Those groups of nodes are called *modules, clusters, rich-club, core or community structure* and can be quantified using the following metrics.

First, the ***clustering coefficient*** C, which is the fraction of the node's neighbors that are directly connected to each other (Watts and Strogatz 1998); or put differently, the number of triangles a given node belongs to over the total number of triangles it could belong to.

$$C = \frac{1}{N}\sum_i C_i = \frac{1}{N}\sum_i \frac{2t_i}{k_i(k_i-1)},$$

Where t_i is the number of triangles around node i and could be written as $t_i = \frac{1}{2}\sum_{j,h} a_{ij}a_{ih}a_{jh}$, and C_i is the (local) clustering coefficient of node i. A variation of the clustering coefficient that stays in a similar spirit is the ***local efficiency*** E_{loc} (*different from the local version of the efficiency* E_i, that measures how close a node is from *any other nodes* of the network). This one characterizes, like the clustering coefficient, and unlike the global efficiency, *only the neighborhood of a given node* i but instead of looking at direct connections between them, it puts emphasis on the length of the shortest path linking them.

$$E_{\text{loc}} = \frac{1}{N}\sum_i E_{\text{loc},i} = \frac{1}{N}\sum_i \frac{\sum_{j,k\in G_i} d_{jk}^{-1}}{k_i(k_i-1)},$$

Where G_i is the subgraph containing all the neighbors of i, but not i. For an extensive comparison between C, E, E_{loc}, and L, see the work of Latora and Marchiori (2003).

The segregation in a network can also be characterized globally through the concepts of community structure and modularity. The range of algorithms used to divide a network into partitions of densely connected nodes that are sparsely connected together is vast and complex but a majority of them are based on the ***modularity index Q*** (Newman 2004, 2006) defined as follow:

$$Q = \sum_{m=1}^{M}\left(q_{mm} - \left(\sum_{n=1}^{M} q_{mn}\right)^2\right),$$

With M the number of modules and q_{mn} the proportion of all links connecting nodes in module m with those in module n. Finally, the ***participation coefficient PC***, based on a previously computed partition of modules, evaluates how evenly distributed the connections of a given node are across module. It is defined as follow:

$$PC_i = 1 - \sum_{m=1}^{M} \left(\frac{k_i(m)}{k_i} \right)^2,$$

With $k_i(m)$ the number of connections the node i with nodes belonging to module m.

iii Other metrics

All the metrics presented above have been described in the context of a binary adjacency matrix, i.e. an undirected unweighted network, but *adaptations exist for both directed and weighted networks*. Also, a lot of other graph metrics exist, but I presented here the most useful ones for brain connectivity analysis, or at least, the most common.

In practice

Jalili (2016) reviewed a set of networks measures useful in brain connectivity analysis. And Rubinov and Sporns (2010) made an amazing work in summarizing a large number of metrics for which they provided source codes in their MATLAB® brain connectivity toolbox (https://sites.google.com/site/bctnet/) along with graph manipulation algorithms such as null models generation or thresholding. For Python users, the `networkx` library is now a standard and efficiently implemented a large number of metrics (https://networkx.github.io/documentation/networkx-1.10/reference/algorithms.html).

B Null-hypothesis networks

Since most of the *network measures indirectly depends on basic topological attributes* such as the number of nodes, the number of edges or the degree distribution which themselves depend on the parcellation and/or connectivity estimator; comparing two networks extracted from different subjects, or even different machines become difficult. Therefore, significance of network indices must be computed against ***null-hypothesis networks***, i.e. random networks that share the

topological attributes of the original one but are not supposed to expose any specific behavior that could be captured by the index in question.

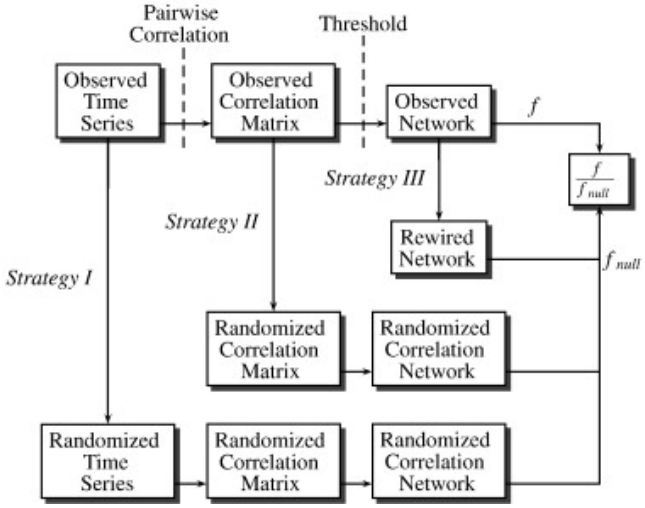

Figure 2.1 Strategies for generating null networks. Strategy I: time series randomization. Strategy II: correlation matrix randomization. Strategy III: topology randomization (e.g. random rewiring). f denotes the network measure calculated for the observed network, while f_{null} denotes the same network measure averaged over the ensemble of null networks. Adapted from Zalesky, Fornito, and Bullmore (2012).

Different strategies are presented in **Figure 2.1**, at different steps of the brain connectivity network creation pipeline. Each of them has their advantages and pitfalls, but a common approach is to randomly rewire (strategy III) the final networks while preserving the degree distribution. While this method's algorithm is quite simple for binary networks, it might become theoretically and computationally complex for weighted and/or directed networks. The only - probably obvious - rule is to choose a null model for which the original network topology does not have any influence from the point of view of the metric of interest; or, on the contrary, a null-model that greatly impact a metric. For example, time series randomization would generate networks with different densities if analyzed using a fixed threshold value; then studying a metric that depends on shortest path lengths would not make much sense since sparser (resp. denser) networks would have much more probability to have longer (resp. shorter) path lengths.

III Known characteristics of brain networks

A Small-world topology

The concept of small-world comes from a social experiment known as the **Milgram paradox** (Travers and Milgram 1969) stating that two people, from anywhere in the world, are separated by a small number of intermediates. Put differently, in the world's social network, where nodes are people and links are relationships, the characteristic path length is small (around six, according to experiments that followed Milgram's). This phenomenon was studied through the lens of complex networks by Watts and Strogatz (1998), by mean of randomization of a lattice network, and latter quantified thanks to a ***small-worldness index S*** (Humphries, Gurney, and Prescott 2006) defined as follow:

$$S = \frac{C/C_{\text{rand}}}{L/L_{\text{rand}}},$$

Where C and L are the clustering coefficient and the characteristic path length as defined in section "Graph metrics". C_{rand} and L_{rand} are the same measures for equivalent random networks with an identical number of nodes N and identical density ρ. A network is considered to have a high small-worldness when its characteristic path length is significantly shorter than for equivalent random networks and have, in the same time, a higher clustering coefficient than by random. Thus, it should be a *balance between integration and segregation* to be robust to single-node failures while keeping a cost-efficient propagation of information thanks to smartly distributed shortcuts (Bassett et al. 2006).

Human (and other mammalian) structural brain networks extracted from DWI have high-degree nodes, or hubs, and modular structure giving it small-world networks properties (Bullmore and Sporns 2009; Hagmann et al. 2007; Heuvel and Sporns 2011). This result has also been demonstrated in functional brain networks.

Bassett and Bullmore (2017) review the latest advances on this concept of small-world network and put emphasis on its generalization to weighted networks that carry much more information than the old simple but still popular unweighted/binary network model of the brain. In particular, it draws attention on weak connections that may play an important role in brain connectivity of both healthy and diseased.

B Default mode network

The ***default mode network*** (DMN) was observed by Shulman et al. (1997) who noticed a set of brain regions whose *activity was reduced* when performing non-self-referential, goal-directed tasks as compared to a control state of quiet rest or simple visual fixation. It was originally measured using **positron emission tomography** (PET) imaging[7] (Raichle et al. 2001), where the "activity" was defined as an increase of the **oxygen extraction fraction** (OEF), a ratio of *oxygen consumed to oxygen delivered*. But this effect can be detected in standard fMRI scans, even though the relationship between blood-flow and oxygen consumption may not be completely evident (Raichle and Mintun 2006).

In AD, relationships between amyloid-β (Aβ) deposition and the DMN have been observed (Buckner et al. 2005; Vlassenko et al. 2010; Mormino et al. 2011) as shown in **Figure 2.2**.

Buckner, Andrews-Hanna, and Schacter (2008) mention the possibility that activity in the default network augments a metabolic cascade that is conducive to the development of Alzheimer's disease.

The brain can also expose other more or less identified sub-networks such as visual, sensorimotor, auditory, ventral and dorsal attention, and executive control (Raichle 2010; Betzel et al. 2014). A recent paper from Raichle (2015) himself retraces the history of the DMN and its impact on the literature.

[7] PET is a functional imaging technique used to visualize metabolic processes in the body. It measures gamma-rays emitted by a position-emitting radioactive isotope usually embedded on an analogue of glucose molecule (called fludeoxyglucose) that serves as radiotracer. This allows to indirectly obtain 3D images of energy (i.e. glucose) consumption in the body by triangulating gamma-rays emission and evaluating the radiotracer concentration.

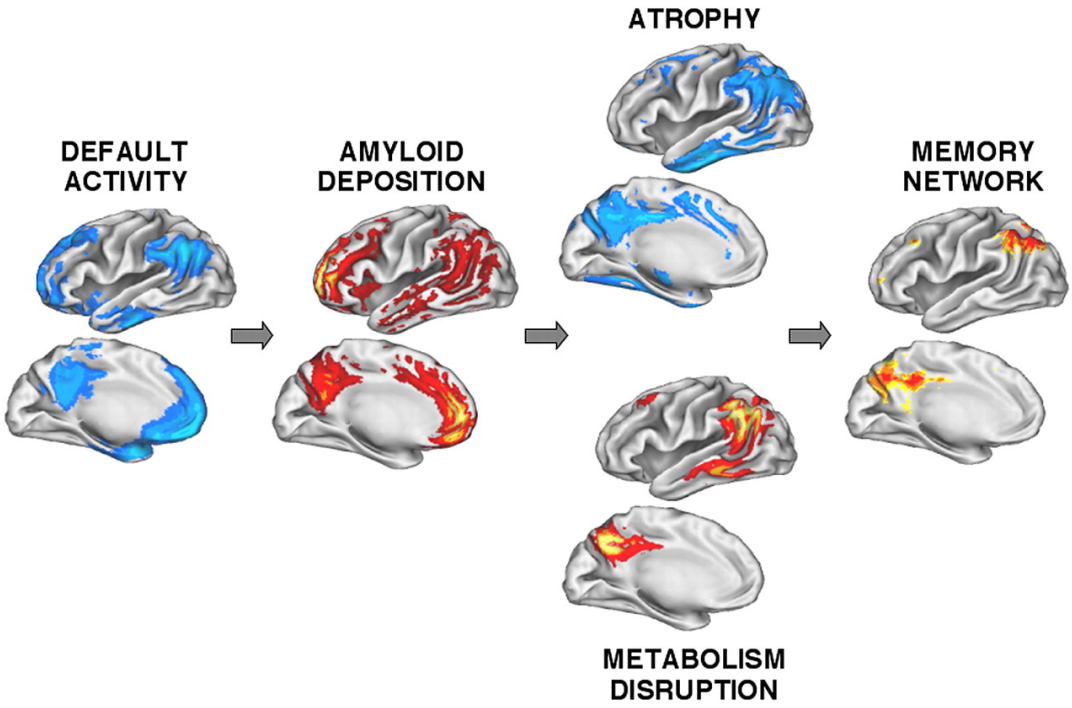

Figure 2.2 Convergence and hypothetical relationships across molecular, structural, and functional measures. This figure shows how default activity (DMN) pattern in young adults is highly similar to those of amyloid deposition in older adults with AD. Extracted from Buckner et al. (2005)

C Structural rich-club

A few studies have tried to identify hub regions in structural brain networks. Hubs are central nodes sharing high degree, strength and/or betweenness centrality. Hagmann et al. (2008) mapped whole brain structural pathways (between $N = 998$ ROIs) of five participants using diffusion spectrum imaging (DSI) followed by a tractography and found evidence for the existence of a structural core composed of posterior medial and parietal cortical regions that are densely interconnected and topologically central (see **Figure 2.3**). They emitted the hypothesis that those regions may play an important role in information integration and showed that the strengths of structural connections were highly predictive of the strengths of functional connections.

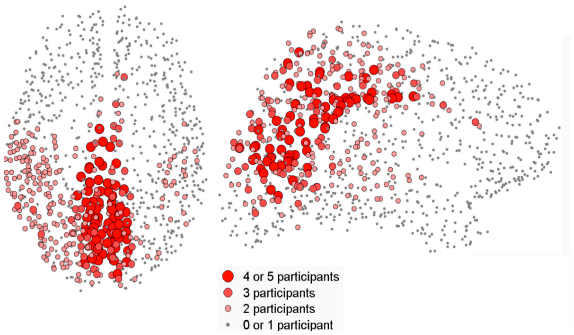

Figure 2.3 Average network core after the k-core decomposition of five subjects' binary connection matrix. Adapted from Hagmann et al. (2008).

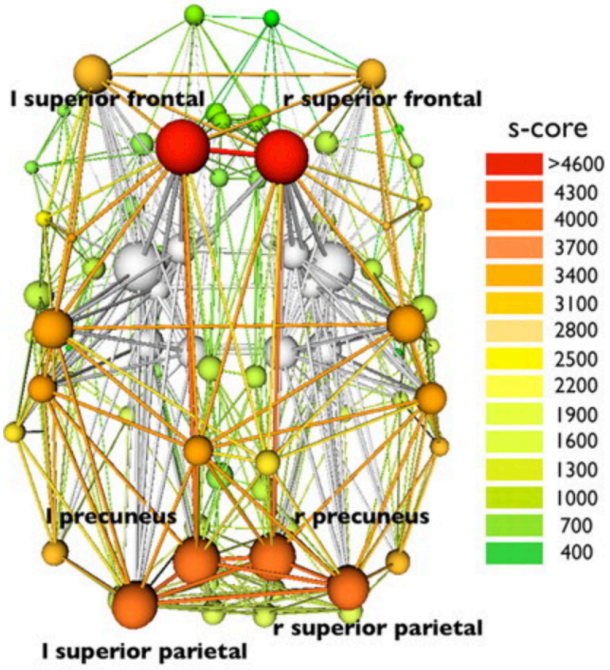

Figure 2.4 s-core decomposition of cortical regions. Adapted from Heuvel and Sporns (2011).

Few years later, Heuvel and Sporns (2011) confirmed those results by proving the existence of a rich-club organization[8] of the human connectome and overlapping its result with previous studies by identifying bilateral precuneus, superior frontal and superior parietal regions as part of the structural core of the brain (see **Figure 2.4**).

D Known characteristics of brain networks in health and AD

Alzheimer's disease is associated with a loss of small-world features, decreased nodal centrality in higher order association areas and abnormal community structure (Yu, Engels, Hillebrand, van Straaten, et al. 2017).

An extensive literature now exist about changes in brain connectivity due to Alzheimer's disease (for reviews see Tijms et al. 2013; Cornelis J. Stam 2014; Fornito, Zalesky, and Breakspear 2015; Jalili 2016).

[8] Rich-club is a set of nodes more densely connected among themselves than nodes of a lower degree.

Table 1 Previous studies reporting abnormalities of functional brain networks in AD. APL: Average Path Length, CC: Clustering Coefficient, GE: Global Efficiency, LE: Local Efficiency. Reproduced from (Jalili 2016)

Study	Brain signal	Connectivity measure	Binarization	Findings
Seo et al. (2013)	PET	Correlation	Density	Decreased CC and no change in APL
de Haan et al. (2012)	MEG	Synch Likelihood	NA	Decreased modularity in lower bands and increased modularity in higher bands
C. J. Stam et al. (2007)	EEG	Synch Likelihood	Threshold/Density	Increased APL and no change in CC
Willem de Haan et al. (2009)	EEG	Synch Likelihood	Density	Decreased CC in alpha and beta bands and decreased APL in alpha and gamma bands
Afshari and Jalili (2017)	EEG	Coherence	Density	Decreased GE and increased LE in alpha and beta bands
Supekar et al. (2008)	fMRI	Correlation	Threshold	Decreased CC
Zhao et al. (2012)	fMRI	Correlation	Density	Increased LE and decreased GE
Ciftçi (2011)	fMRI	Coherence	MST	No change in the degree distribution
Sanz-Arigita et al. (2010)	fMRI	Synch Likelihood	Threshold/Density	Decreased APL and no change in CC
C. J. Stam et al. (2009)	MEG	Phase Synch	NA	Decreased CC and APL in alpha band
Brier et al. (2014)	fMRI	Correlation	Density	No change in APL and reduced CC and modularity
Li et al. (2013)	fMRI	Correlation	Threshold	Decreased GE and CC
J. Wang et al. (2013)	fMRI	Correlation	Threshold	Increased APL

CHAPTER 3

Beyond the single-layer network

I Introduction

Networks and complex systems in general never are isolated, they evolve in contact with other networks, at different space and time scales. An evocative example would be transportation networks; embedded in space, an almost infinite number of network representation of human mobility could be superimposed; from subway stations network to airports without forgetting the good old road maps… Studying all of them in a single framework could be of interest. If we continue with our example, estimating the time necessary to go from the Eiffel Tower in Paris, France to a beach in Melbourne, Australia, would probably require to compute the shortest path on a metro, RER, planes, and a road network combined. In a network of networks, or a multilayer network.

Multilayer networks have really attracted attention only recently, most papers were published a couple of years before the beginning of my PhD thesis. De Domenico et al. (2013) started with

the mathematical formulation of it and first reviews on the subject appeared one year later, with Kivelä et al. (2014) and Boccaletti et al. (2014). As highlighted by Kivelä et al. (2014), there still is lack of a consensus on a set of terminology for studying multilayer networks. I will use in this report, the definition of **multilayer network** and **multiplex** given by De Domenico et al. (2013) where the set of networks (or layers) all have the same number of nodes, and where a node i from layer $\tilde{h}$ can be connected to any other node j in any other layer $\tilde{k}$. A multiplex network is a special type of multilayer network in which the only possible types of interlayer connections are ones in which a given node is connected to its counterpart nodes in the other layers.

In neuroscience, the application of multilayer networks is expected, due to the large panel of types of brain connectivity networks. An obvious example is the interdependence of structure and function in the brain. The fact that structure supports function could be abstracted using a multilayer network model (Simas et al. 2015; Chapter 5; Chapter 6, De Domenico (2017) called it ***structural and functional decomposition***. Functional brain networks are constantly evolving with time, especially during task; combining functional networks sampled in time could be a solution to study them all at once while keeping the whole set of information at disposal (Betzel and Bassett 2017; De Domenico 2017). This decomposition is called ***task-based decomposition***. Finally, it has been of common usage to study synchronizations of brain regions at different frequency bands, leading to another different set of functional networks that could be, again, somehow linked together in a multilayer network (Chapter 4; Brookes et al. 2016; Buldú and Porter 2017; De Domenico, Sasai, and Arenas 2016), it is the ***frequency-based decomposition***.

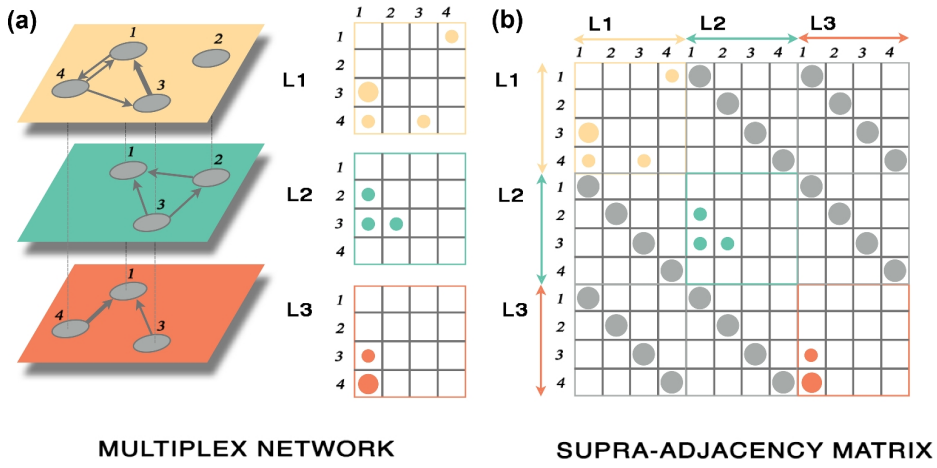

Figure 3.1 (a) A multilayer network consists of different networks encoded by layers, each one represented by a (possibly directed and weighted) adjacency matrix. (b) Common representation of multilayer networks generally known as supra-adjacency matrix. Adapted from De Domenico et al. (2013)

Buldú and Papo still call its application to brain connectivity a *terra incognita*.

> *"[…] a series of fundamental problems arise with this new approach, which make the interpretation of multilayer brain networks a* terra incognita *that will need to be explored in the near future."*
>
> *Buldú and Papo (2018)*

II Generalization of graph metrics

More and more single-layer graph metrics (as presented in 0) find their equivalent in multilayer settings. As mentioned above, community detection, an important feature for brain network, has been generalized by Mucha et al. (2010) that first need some clarification on the multilayer formalism.

In the following formulas, I will try to use script letters for indices and metrics relative to multilayer networks, whereas standard letters will be kept as defined in previous chapters, for monolayer networks.

Let's assume that our $\mathcal{L}$-layers network is fully described by its supra-adjacency matrix

$$\mathcal{A} = \begin{bmatrix} A^{[1]} & C^{[1,2]} & \dots & C^{[1,\mathcal{L}]} \\ C^{[2,1]} & A^{[2]} & \dots & C^{[2,\mathcal{L}]} \\ \vdots & \vdots & \ddots & \vdots \\ C^{[\mathcal{L},1]} & C^{[\mathcal{L},2]} & \dots & A^{[\mathcal{L}]} \end{bmatrix}$$

where $A^{[\ell]} = \left\{a_{ij}^{[\ell]}\right\}, \forall i,j \in 1..N, \forall \ell \in 1..\mathcal{L}$ is the adjacency matrix of layer ℓ containing the set of intra-layer edge weights and $C^{[k\ell]} = \left\{c_{ij}^{[k\ell]}\right\}, \forall i,j \in 1..N, \forall k,\ell \in 1..\mathcal{L}$ the coupling matrix between layers k and ℓ containing inter-layer edges weights. Then, the strength of node i in layer ℓ can be defined as $s_i^{[\ell]} = s_{\text{intra},i}^{[\ell]} + s_{\text{inter},i}^{[\ell]}$, with $s_{\text{intra},i}^{[\ell]} = \sum_j a_{ij}^{[\ell]}$ the standard strength of node i in the isolated layer ℓ network, and $s_{\text{inter},i}^{[\ell]} = \sum_{jk} c_{ij}^{[k\ell]}$ the inter-layer strength of node i (in multiplex networks, $\forall k,\ell \in 1..\mathcal{L}, j \neq i \Rightarrow c_{ij}^{[k\ell]} = 0$).

Then, on can define the multilayer modularity objective function as follow:

$$\mathcal{Q} = \frac{1}{2\mu} \sum_{k,\ell=1}^{\mathcal{L}} \sum_{i,j=1}^{N} \left[a_{ij}^{[k]} - \gamma_k a_{\text{null},ij}^{[k]} \delta(k,\ell) + c_{ij}^{[k\ell]} \delta(i,j)\right] \delta\left(g_i^{[k]}, g_j^{[\ell]}\right),$$

where:

- $\mu = \frac{1}{2}\sum_{ik} s_{ik}$ is the total weights sum of the network;
- γ_k is the structural resolution parameter of layer k;
- $a_{\text{null},ij}^{[k]}$ is the weight of the edge linking node i and node j in layer k of the null-model multilayer network[9];
- $\delta(a,b) = \begin{cases} 1 \text{ if } a = b \\ 0 \text{ if } a \neq b \end{cases}$ is the Kronecker symbol;
- $g_i^{[k]}$ is the community assigned to node i in layer k.

In order to study more basic segregation motifs, one can use the generalization of the clustering coefficient to the multiplex topology (Battiston, Nicosia, and Latora 2014):

$$C_{i,1} = \frac{\sum_\ell \sum_{k \neq \ell} \sum_{j \neq i, j' \neq i} a_{ij}^{[\ell]} a_{jj'}^{[k]} a_{j'i}^{[\ell]}}{(\mathcal{L}-1) \sum_\ell k_i^{[\ell]} \left(k_i^{[\ell]} - 1\right)}$$

[9] Here the null-model type is left to the appreciation of the user.

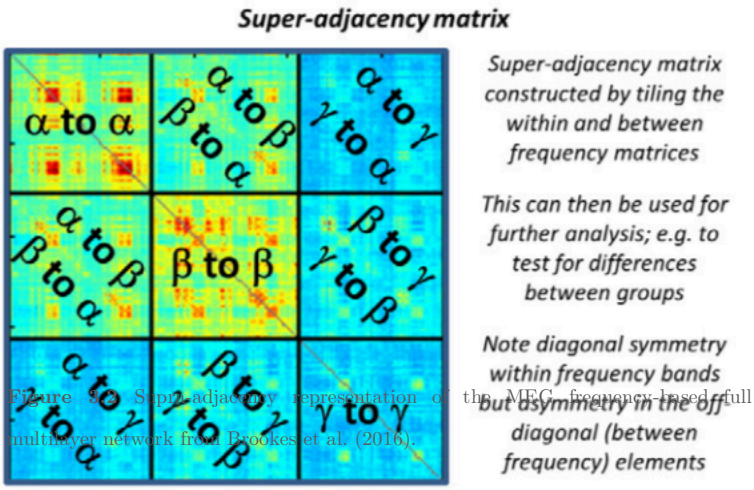

Figure 3.1 Supra-adjacency representation of the MEG frequency-based full multilayer network from Brookes et al. (2016).

Note that this version of the metric is based on the counting of two-triangles $\left(a_{ij}^{[\ell]}a_{jj'}^{[k]}a_{j'i}^{[\ell]}\right)$, i.e. triangles spanning over two layers. Another metric $\mathcal{C}_{i,2}$ is counting the three-triangles and may be suited, for instance, sparser networks. Note also that it was defined for *binary* multiplex networks but does not take advantage of the inter-layer links which may be convenient when there is no real motivation in using them or when their weight is arbitrary chosen.

Motifs (Battiston et al. 2017) and other metrics, such as the multi-participation coefficient (used in Chapter 4) or the multiplex coreness (introduced in Chapter 5 and used in Chapter 6) have be developed. For a brief review on the multilayer graph metrics, see recent work of Mandke et al. (2018).

III Multilayer brain networks topologies

A Multifrequency brain networks

As explained before, electrophysiological signals or BOLD signals are usually analyzed by frequency-bands, generating one functional brain connectivity network per frequency-band. With the arrival of the multilayer framework, we could combine those networks into one single mathematical object. To my knowledge, six studies explored this track so far, including ours.

First, Brookes et al. (2016), constructed frequency-based full multilayer networks from MEG data, in which each layer includes the interactions in a given frequency band, and weighted *interlayer links the cross-frequencies interactions*; all by using signals envelopes correlation. They showed that the corresponding supra-adjacency matrices (which encode a linear-algebraic representation of connections in a multilayer network, see **Figure 3.2**) convey statistically significant differences when comparing a control group with a group of schizophrenia sufferers.

Then, De Domenico, Sasai, and Arenas (2016) used fMRI data to build a frequency-based multiplex where each node is connected to its counterpart in all the other layers (see **Figure 3.3**). They showed that each frequency band (from 0.01Hz to 0.25Hz, by steps of 0.02Hz) carries unique topological information. They used a generalization of the page rank centrality measure to identify the multilayer definition of hubs and distinguish between healthy and schizophrenic populations.

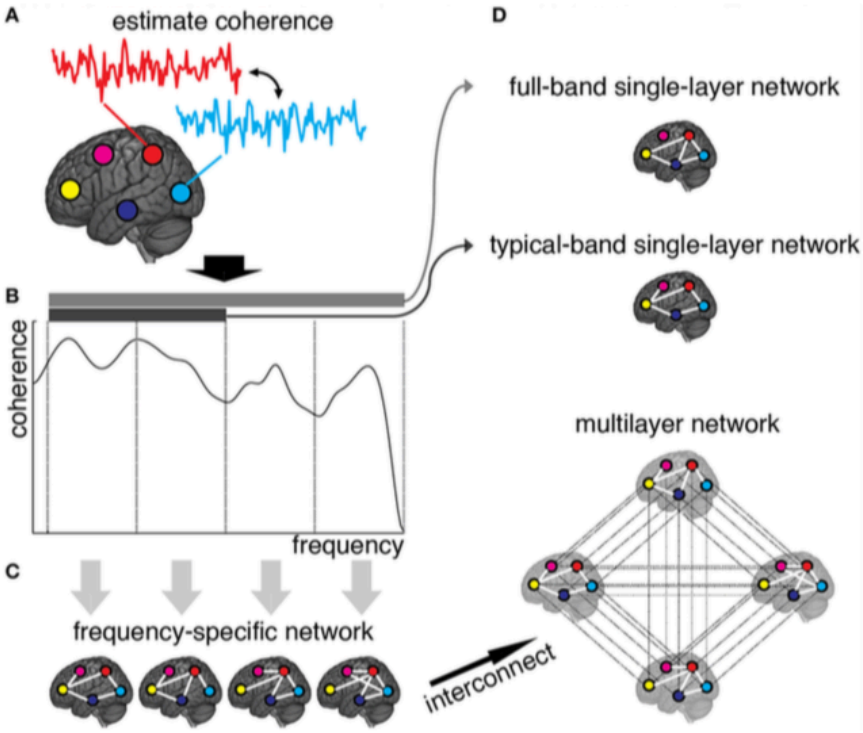

Figure 3.3 Schematic illustration of brain multiplex functional network construction. From any pairs of brain activity signals measured in 264 ROIs **(A)**, they estimated the coherence spectrum **(B)** that they averaged in 12 frequency bands, to quantify the strength of frequency-specific functional connectivity **(C).** These brain connectivity networks constituted the layers of the multiplex functional network once interconnected **(D).** Adapted from De Domenico, Sasai, and Arenas (2016).

They chose a *uniform weight for interlayer edges* linking similar ROIs in different layers using a data-driven approach.

It is in this context that we wrote the article that constitutes the next chapter (Guillon et al. 2017; Chapter 4).

Then, Tewarie et al. (2016a) used the same setup as in Brookes et al. (2016) to study inter- and intra-layer weights dependencies. They found that the strength of inter-layer coupling significantly correlated with the averaged magnitude of within layer interactions highlighting the fact that

within and between frequency interactions should not be treated separately, but rather integrated into a broader picture of brain function.

Yu et al. (2017) also used MEG frequency-based multiplex topology to study hub disruption in AD and showed an improvement of the discrimination between AD and healthy populations by using multilayer-based methodology.

More recently, Buldú and Porter (2017) interestingly compared 4 topologies, based on MEG: single-layer, with one network per frequency-band; aggregated network (also single-layer); multiplex and full multilayer (with inter-layer links) and showed that inter-layer weights strongly influence the value of λ_2, an indicator of synchronizability, emphasizing the fact that the way these edges are computed must be carefully chosen.

B Multimodal brain networks

As underlined by Buldú and Porter (2017), integrating *anatomical and functional networks* in a multiplex topology is an extremely natural approach. However, only two studies exploited this configuration; one in Human (Battiston et al. 2017), the other in Macaque (Crofts, Forrester, and O'Dea 2016).

In Battiston et al. (2017), fMRI- and DTI-based connectivity networks are combined in a two-layers multiplex to study recurrence of newly defined multilayer motifs. Significant variations of these *motifs were found to be overrepresented in the human brain* and differ from previous findings based simply on structural connectivity. This confirms again that non-trivial relationships exist between structural and functional brain networks and that the multilayer paradigm is an appropriate choice to study them.

In Crofts, Forrester, and O'Dea (2016), a new measure of structure-function clustering allowed them to investigate functional connections that are distinct from the underlying cortical structure.

Another recent study integrated *functional networks from two different modalities (MEG and fMRI*, see **Figure 3.4**) in a multilayer topology (Mandke et al. 2018) and evaluated what they called "correction schemes", i.e. filtering or thresholding methods (see section "Brain network as a graph" in Chapter 2), and their impact on different multilayer metrics.

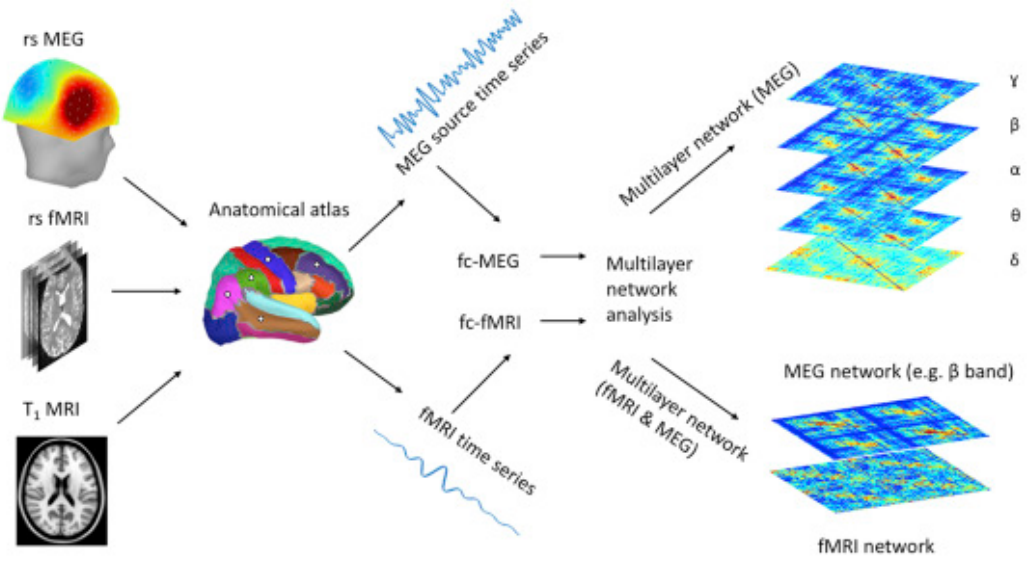

Figure 3.4 Multimodal brain network creation workflow from Mandke et al. (2018).

C Temporal brain networks

As noted in the introduction of this chapter, brain networks evolve. Obviously from a functional perspective but also structurally if the time-scale is large enough (days to years) (Betzel and Bassett 2017). Multilayer network is a flexible model that allows to add as many layers as needed, whose nodes are connected to any other node of any layers. Therefore, a natural way to represent temporal brain networks is to chain networks from different adjacent time points (Holme and Saramäki 2012). Thus, nodes would only be connected to their equivalent one time-step before and one time-step after, constraining the adapted topology to a specific type of multiplex, those with ordinal interlayer coupling (see Figure 3.5, red lines).

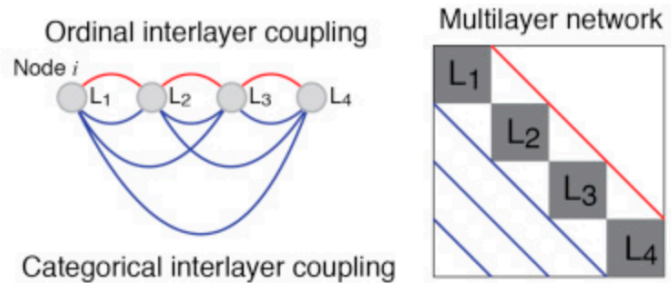

Figure 3.5 Illustration of two conventional ways of linking a node i to its counterparts in the layers of a multiplex (left) with their corresponding schematic representation on a supra-adjacency matrix (right). Adapted from Betzel and Bassett (2017)

This configuration was the most investigated of the three exposed here. Among the several studies that applied this methodology to study the brain, the most influential results were obtained a by

a series of papers from Danielle S. Basset et al. (Bassett et al. 2011; Mantzaris et al. 2013; Bassett et al. 2013, 2015) where they mainly analyzed modifications of the community (or core-periphery) structure during task and learning based on the famous generalization of the modularity metric by Mucha et al. (2010).

Recently, Griffa et al. (2017) built what they call spatio-temporal brain networks, that are structurally constrained functional temporal network; where a node corresponding to ROI i is connected to ROI j if they are (i) anatomically wired through a fiber tract AND (ii) functionally co-active at the same time-point layer (intra-layer edges) or at two following time points (inter-layer edges). It allowed them to describe wave-like activation propagation patterns.

CHAPTER 4

Inter-frequency hubs in AD

In this chapter, we exploit the multifrequency brain networks topology, explained in the last chapter, based on MEG recordings during resting state in AD patients and age-matched subjects. We apply the multi-participation coefficient (MPC) and detect abnormally distributed connections across frequency bands in the AD population; mainly localized in association areas and cingulate cortex. We measure correlation of this MPC with memory impairment, and finally we show that the multilayer network approach improves the diagnostic power as compared to single-layer approaches.

SCIENTIFIC REPORTS

OPEN

Loss of brain inter-frequency hubs in Alzheimer's disease

J. Guillon[1,2], Y. Attal[3], O. Colliot[1,2], V. La Corte[5,6], B. Dubois[4], D. Schwartz[2], M. Chavez[2] & F. De Vico Fallani[1,2]

eived: 28 March 2017
epted: 29 June 2017
ished online: 07 September 2017

Alzheimer's disease (AD) causes alterations of brain network structure and function. The latter consists of connectivity changes between oscillatory processes at different frequency channels. We proposed a multi-layer network approach to analyze multiple-frequency brain networks inferred from magnetoencephalographic recordings during resting-states in AD subjects and age-matched controls. Main results showed that brain networks tend to facilitate information propagation across different frequencies, as measured by the multi-participation coefficient (*MPC*). However, regional connectivity in AD subjects was abnormally distributed across frequency bands as compared to controls, causing significant decreases of *MPC*. This effect was mainly localized in association areas and in the cingulate cortex, which acted, in the healthy group, as a true inter-frequency hub. *MPC* values significantly correlated with memory impairment of AD subjects, as measured by the total recall score. Most predictive regions belonged to components of the default-mode network that are typically affected by atrophy, metabolism disruption and amyloid-β deposition. We evaluated the diagnostic power of the *MPC* and we showed that it led to increased classification accuracy (78.39%) and sensitivity (91.11%). These findings shed new light on the brain functional alterations underlying AD and provide analytical tools for identifying multi-frequency neural mechanisms of brain diseases.

Recent advances in network science has allowed new insights in the brain organization from a system perspective. Characterizing brain networks, or connectomes, estimated from neuroimaging data as graphs of connected nodes has not only pointed out important network features of brain functioning - such as small-worldness, modularity, and regional centrality - but it has also led to the development of biomarkers quantifying reorganizational mechanisms of disease[1]. Among others, Alzheimer's disease (AD), which causes progressive cognitive and functional impairment, has received great attention by the network neuroscience community[1–3]. AD is histopathologically defined by the presence of amyloid-β plaques and tau-related neurofibrillary tangles, which cause loss of neurons and synapses in the cerebral cortex and in certain subcortical regions[2]. This loss results in gross atrophy of the affected regions, including degeneration in the temporal and parietal lobe, and parts of the frontal cortex and cingulate gyrus[4].

Structural brain networks, whose connections correspond to inter-regional axonal pathways are therefore directly affected by AD because of connectivity disruption in several areas including cingulate cortices and hippocampus[5,6]. A decreased number of fiber connections eventually lead to a number of network changes on multiple topological scales. At larger scales, AD brain networks estimated from diffusion tensor imaging (DTI) showed increased characteristic path length as compared to healthy subjects leading to a global loss of network small-worldness[2,7]. Similar topological alterations have been also documented in resting-state brain networks estimated from functional magnetic resonance imaging (fMRI)[8], as well as from magneto/electroencephalographic (M/EEG) signals, the latter ones often reported within the *alpha* frequency range (8–13 Hz) which is typically affected in AD[9–11]. On smaller topological scales, structural brain network studies have demonstrated a loss of connector hubs in temporal and parietal areas that correlates with cognitive decline[2,12,13]. In addition, higher-order association regions appear to be affected in functional brain networks inferred from fMRI[2,14] and MEG signals, the latter showing a characteristic loss of parietal hubs in higher (>14 Hz) frequency ranges[15,16].

[1]Inria Paris, Aramis project-team, 75013, Paris, France. [2]CNRS UMR-7225, Sorbonne Universites, UPMC Univ Paris 06, Inserm U-1127, Institut du cerveau et la moelle (ICM), Hopital Pitie-Salpetriere, 75013, Paris, France. [3]MyBrain Technologies, Paris, France. [4]Department of Neurology, Institut de la Memoire et de la Maladie dAlzheimer - IM2A, Paris, France. [5]Institute of Psychology, University Paris Descartes, Sorbonne Paris Cite, France. [6]INSERM UMR 894, Center of Psychiatry and Neurosciences, Memory and Cognition Laboratory, Paris, France. Correspondence and requests for materials should be addressed to F.D. (email: fabrizio.devicofallani@gmail.com)

	Control (HC)	Alzheimer (AD)	*p*-value
Age	70.8 (9.1)	73.5 (9.4)	0.3142
MMSE	28.2 (1.4)	23.2 (3.6)	$<10^{-5}$
FR	31.5 (6.6)	14.9 (6.5)	$<10^{-5}$
TR	46.3 (1.5)	33.9 (10.0)	$<10^{-5}$

Table 1. Characteristics, cognitive and memory scores of experimental subjects. Mean values and standard deviations (between parentheses) are reported. The last column shows the *p*-values returned by a non-parametric permutation t-tests with 10000 realizations. MMSE = mini-mental state examination score; TR = total recall memory test score (/48); FR = free recall memory test (/48).

Graph analysis of brain networks has advanced our understanding of the organizational mechanisms underlying human cognition and disease, but a certain number of issues still remain to be addressed[17,18]. For example, conventional approaches analyze separately brain networks obtained at different frequency bands, or in some cases, they simply focus on specific frequencies, thus neglecting possible insights of other spectral contents on brain functioning[17]. However, several studies have hypothesized and reported signal interaction or modulations between different frequency bands that are supportive of cognitive functions such as memory formation[19–21]. Moreover, recent evidence shows that neurodegenerative processes in AD do alter functional connectivity in different frequency bands[16,22,23]. How to characterize this multiple information from a network perspective still remains poorly explored. Here, we proposed a multi-layer network approach to study multi-frequency connectomes, where each layer contains the brain network extracted at different bands. Multi-layer network theory has been previously used to synthesize MEG connectomes from a whole population[24], characterize temporal changes in dynamic fMRI brain networks[12], and integrating structural information from multimodal imaging (fMRI, DTI)[25,26]. Its applicability to multi-frequency brain networks has been recently illustrated in fMRI connectomes for which, however, the frequency ranges of interest remains quite limited[27].

We focused on source-reconstructed MEG connectomes, characterized by rich frequency dynamics, that were obtained from a group of AD and control subjects in eyes-closed resting-state condition. We hypothesized that the atrophy process in AD would lead to an altered distribution of regional connectivity across different frequency bands and we used the multi-participation coefficient to quantify this effect both at global and local scale[28]. We evaluated the obtained results, which provide a novel view of the brain reorganization in AD, with respect to standard approaches based on single-layer network analysis and flattening schemes[29]. Finally, we tested the diagnostic power of the measured brain network features to discriminate AD patients and healthy subjects.

Methods

Experimental design and data pre-processing. The study involved 25 Alzheimer's diseased (AD) patients (13 women) and 25 healthy age-matched control (HC) subjects (18 women). All participants underwent the Mini-Mental State Examination (MMSE) for global cognition[30] and the Free and Cued Selective Reminding Test (FCSRT) for verbal episodic memory[31–33]. Specifically, we considered the Total Recall (TR) score - given by the sum of the free and cued recall scores - which has been demonstrated to be highly predictive of AD[34] (Table 1).

Inclusion criteria for all participants were: *i)* age between 50 and 90; *ii)* absence of general evolutive pathology; *iii)* no previous history of psychiatric diseases; *iv)* no contraindication to MRI examination; *v)* French as a mother tongue. Specific criteria for AD patients were: *i)* clinical diagnosis of Alzheimer's disease; *ii)* Mini-Mental State Examination (MMSE) score greater or equal to 18. Magnetic resonance imaging (MRI) acquisitions were obtained using a 3T system (Siemens Trio, 32-channel system, with a 12-channel head coil). The MRI examination included a 3D T1-weighted volumetric magnetization-prepared rapid-gradient echo (MPRAGE) sequence with 1 mm isotropic resolution and the following parameters: repetition time (TR) = 2300 ms, echo time (TE) = 4.18 ms, inversion time (TI) = 900 ms, matrix = 256×256. This sequence provided a high contrast-to-noise ratio and enabled excellent segmentation of high grey/white matter.

The magnetoencephalography (MEG) experimental protocol consisted in a resting-state with eyes-closed (EC). Subjects seated comfortably in a dimly lit electromagnetically and acoustically shielded room and were asked to relax. MEG signals were collected using a whole-head MEG system with 102 magnetometers and 204 planar gradiometers (Elekta Neuromag TRIUX MEG system) at a sampling rate of 1000 Hz and on-line low-pass filtered at 330 Hz. The ground electrode was located on the right shoulder blade. An electrocardiogram (EKG) Ag/AgCl electrodes was placed on the left abdomen for artifacts correction and a vertical electrooculogram (EOG) was simultaneously recorded. Four small coils were attached to the participant in order to monitor head position and to provide co-registration with the anatomical MRI. The physical landmarks (the nasion, the left and right pre-auricular points) were digitized using a Polhemus Fastrak digitizer (Polhemus, Colchester, VT).

We recorded three consecutive epochs of approximately 2 minutes each. All subjects gave written informed consent for participation in the study, which was approved by the local ethics committee of the Pitie-Salpetriere Hospital. All experiments were performed in accordance with relevant guidelines and regulation. Signal space separation was performed using MaxFilter[35] to remove external noise. We used in-house software to remove cardiac and ocular blink artifacts from MEG signals by means of principal component analysis. We visually inspected the preprocessed MEG signals in order to remove epochs that still presented spurious contamination. At the end of the process, we obtained a coherent dataset consisting of three clean preprocessed epochs for each subject.

Source reconstruction, power spectra and brain connectivity. We reconstructed the MEG activity on the cortical surface by using a source imaging technique[36,37]. We used the FreeSurfer 5.3 software (surfer.nmr.mgh.harvard.edu) to perform skull stripping and segment grey/white matter from the 3D T1-weighted images of each single subject[38,39]. Cortical surfaces were then modeled with approximately 20000 equivalent current dipoles (i.e., the vertices of the cortical meshes). We used the Brainstorm software[40] to solve the linear inverse problem through the wMNE (weighted Minimum Norm Estimate) algorithm with overlapping spheres[41]. Both magnetometer and gradiometer, whose position has been registered on the T1 image using the digitized head points, were used to localize the activity over the cortical surface. The reconstructed time series were then averaged within 148 regions of interest (ROIs) defined by the Destrieux atlas[42].

We computed the power spectral density (PSD) of the ROI signals by means of the Welch's method; we chose a 2 seconds sliding Hanning window, with a 25% overlap. The number of FFT points was set to 2000 for a frequency resolution of 0.5 Hz. We estimated functional connectivity by calculating the spectral coherence (Supplementary Text) between each pair of ROI signals[43]. As a result, we obtained for each subject and epoch, a set of connectivity matrices of size 148×148 where the (i, j) entry contains the value of the spectral coherence between the signals of the ROI i and j at a frequency $f = 0{,}0.5, \ldots, 499$.

We then averaged the connectivity matrices within the following characteristic frequency bands[44,45]: *delta* (2–4 Hz), *theta* (4.5–7.5 Hz), *alpha1* (8–10.5 Hz), *alpha2* (11–13 Hz), *beta1* (13.5–20 Hz), *beta2* (20.5–29.5 Hz) and *gamma* (30–45 Hz). We finally averaged the connectivity matrices across the three available epochs to obtain a robust estimate of the individual brain networks whose nodes were the ROIs ($n = 148$) and links, or edges, were the spectral coherence values.

Single-layer network analysis. In order to cancel the weakest noisy connections, we thresholded and binarized the values in the connectivity matrices. Specifically, we retained the same number of links for each brain network. We considered six representative connection density thresholds corresponding to an average node degree $k = \{1, 3, 6, 12, 24, 48\}$. These values cover the density range [0.007, 0.327] which contains the typical density values used in complex brain network analysis[17,18,46]. The resulting sparse brain networks, or graphs, were represented by adjacency matrices A, where the a_{ij} entry indicates the presence or absence of a link between nodes i and j.

Participation coefficient. Given a network partition, the local participation coefficient (PC_i) of a node i measures how evenly it is connected to the different clusters, or modules of the network[47]. Nodes with high participation coefficients are considered as central hubs as they allow for information exchange among different modules. The global participation coefficient PC of a network at layer λ is then given by the average of the PC_i values:

$$PC^{[\lambda]} = \frac{1}{n}\sum_{i=1}^{N} PC_i^{[\lambda]} = \frac{1}{n}\sum_{i=1}^{N}\left[1 - \sum_{m=1}^{M^{[\lambda]}}\left(\frac{k_{i,m}^{[\lambda]}}{k_i^{[\lambda]}}\right)^2\right], \tag{1}$$

where $k_{i,m}^{[\lambda]}$ is the number of links from the node i to the nodes of the module m in layer λ and $k_i^{[\lambda]}$ is the degree of node i in layer λ. By construction, PC ranges from 0 to 1. Here, the partition of the networks into modules was obtained by maximizing the modularity function[48].

Flattened networks. We also computed the participation coefficients for brain networks obtained by flattening the frequency layers into a single *overlapping* or *aggregated* network[28]. In an overlapping network, the weight of an edge o_{ij} corresponds to the number of times that the nodes i and j are connected across layers:

$$o_{ij} = \sum_{\lambda} a_{ij}^{[\lambda]}, \tag{2}$$

In an aggregated network, the existence of an edge indicates that nodes i and j are connected in at least one layer:

$$a_{ij} = \begin{cases} 1 & \text{if } \exists\ \lambda\text{: } a_{ij}^{[\lambda]} \neq 0 \\ 0 & \text{otherwise} \end{cases}, \tag{3}$$

Notice that, by construction, flattened networks do not preserve the original connection density of the single layer networks.

Multi-layer network analysis. We adopted a multi-layer network approach to integrate the information from brain networks at different frequency bands, while preserving their original structure. Specifically, we built for each subject a multiplex network (Fig. 1a,b) where the different layers correspond to different frequency bands and each node in one layer is virtually connected to all its counterparts in the other layers[28,29].

Without loss of generality, the resulting supra-adjacency matrix A is given by the intra-layer adjacency matrices on the main diagonal:

$$\mathcal{A} = \{A^{[\delta]}, A^{[\theta]}, A^{[\alpha_1]}, A^{[\alpha_2]}, A^{[\beta_1]}, A^{[\beta_2]}, A^{[\gamma]}\}, \tag{4}$$

where $A^{[\lambda]}$ corresponds to the brain network at the frequency λ. Notice that inter-layer adjacency matrices of multiplexes are intrinsically defined as identity matrices[49,50].

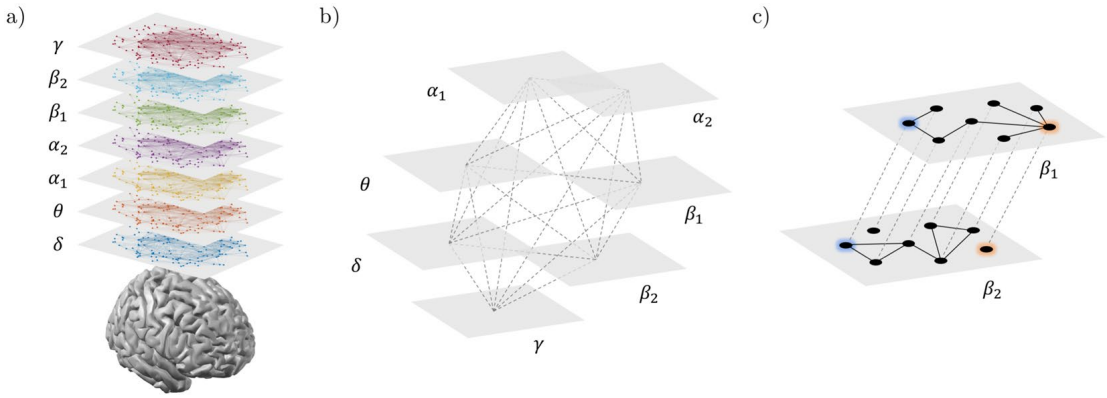

Figure 1. Multi-frequency brain networks. Panel (a) shows brain networks of a representative subject extracted from seven frequency bands. Links are inferred by means of spectral coherence and thresholded to have in each layer an average node degree $k = 12$. (**b**) Procedure to construct a multi-frequency network. Each layer corresponds to a different frequency band. Only nodes representing the same brain region in each layer are virtually connected. Hence, inter-layer links code for identity relationships. (**c**) Inter-frequency node centrality. A two-layer multiplex is considered for the sake of simplicity. The blue node acts as an inter-frequency hub (i.e., multi-participation coefficient $MPC = 1$) as it allows for a balanced information transfer between layer β_1 and β_2; the red node, who is disconnected in layer β_2, blocks the information flow and has $MPC = 0$.

Multi-participation coefficient. We considered the local multi-participation coefficient MPC_i, as an akin version of the local participation coefficient PC_i, to measure how evenly a node i is connected to the different layers of the multiplex[28]. This way, nodes with high MPC_i are considered central hubs as they would allow for a better information exchange among different layers. The global multi-participation coefficient is then given by the average of the MPC_i values:

$$MPC = \frac{1}{n}\sum_{i=1}^{N} MPC_i = \frac{1}{n}\sum_{i=1}^{N}\frac{M}{M-1}\left[1 - \sum_{\lambda}(NLP_i^{[\lambda]})^2\right], \tag{5}$$

where $NLP_i^{[\lambda]} = k_i^{[\lambda]}/o_i$ stands for *node-degree layer proportion*, which measures the tendency of the connectivity of a node i to concentrate in layer λ. By construction, if nodes tend to concentrate their connectivity in one layer, the global multi-participation coefficient tends to 0; on the contrary, if nodes tend to have the same number of connections in every layer, the MPC value tends to 1 (Fig. 1c). In the singular case where a node is disconnected in every layer, we assigned $MPC_i = 0$ to avoid indeterminate results.

From a statistical perspective, a random walker reaching a node with low MPC_i will jump with higher probability to layers where the node degree is higher, while it will tend to avoid layers with lower node degrees. On the contrary, if MPC_i is high, the random walker can jump with similar probability to any other layer, and this would facilitate the information passing (or communication) across all the layers.

We further used the standard coefficient of variation CV_i to measure the dispersion of the degree of a node i across layers. A global coefficient of variation CV is then obtained by averaging the CV_i values across all the nodes (Supplementary Text).

Statistical analysis. We first analyzed network features on global topological scales in order to detect statistical differences between AD and HC subjects at the whole system level. Only for the network features that resulted significantly different at the global scale, we also assessed possible group-differences at the local scale of single nodes. This hierarchical approach allowed us to associate brain network differences at multiple topological scales[51]. We used a non-parametric permutation t-test, to assess statistical differences between groups, with a significance level of 0.05[52,53]. The permutation test generated a set of 10000 surrogate data by randomly exchanging the group labels (i.e., AD or HC) of the brain network features. The t-statistic and p-value were then extracted from the simulated distributions. At the local scale, we performed a permutation test for each node separately. Due to the large number of tests (i.e., 148), we applied a correction for multiple comparisons by computing an adjusted version of the false discovery rate (FDR)[54].

To test the ability of the significant brain network features to predict the cognitive/memory impairment of AD patients, we used the non-parametric Spearman's correlation coefficient R. We set a significance level of 0.05 for the correlation of global network features, with a FDR correction in the case of multiple comparisons (local features).

Classification. We used a classification approach to evaluate the discriminating power of the local brain network features which resulted significantly different in the AD and HC group. Because we did not know in advance which were the most discriminating features, we tested different combinations. In particular, for each local network feature, we first ranked the respective ROIs according to the p-values returned by the between-group statistical analysis (see previous section). For each subject s, we then tested different feature vectors obtained by concatenating, one-by-one, the values of the network features extracted from the ranked ROIs. The generic feature vector c_s reads:

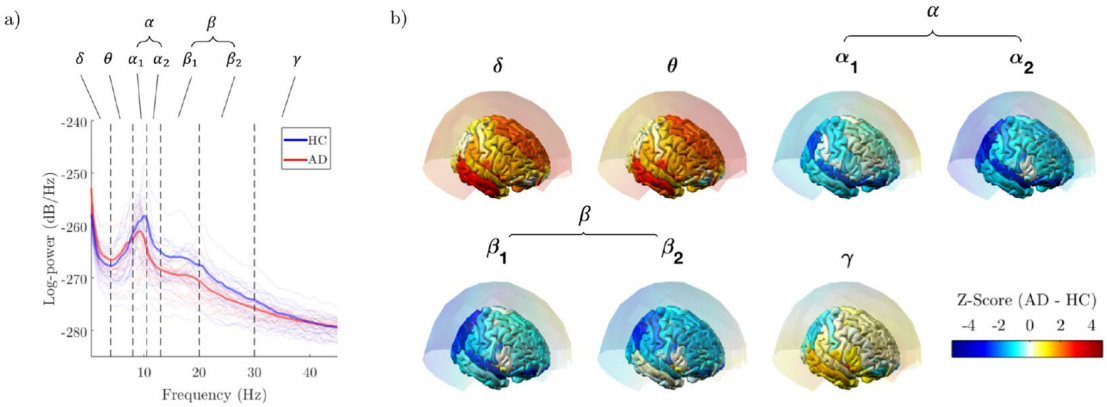

Figure 2. Spectral analysis of MEG signals. (**a**) Power spectrum density (PSD) for a representative occipital sensor before source reconstruction. Each line corresponds to a subject. Bold lines show the group-averaged values in the Alzheimer's disease group (AD) and in the healthy control group (HC). (**b**) Statistical PSD group differences. Z-scores are obtained using a non-parametric permutation t-test. Results are represented both as sensor and source space.

$$c_s = [g_1, \ldots, g_k] \tag{6}$$

where g_k is a generic local network feature and k is a rank that ranges from 1 (the most significant ROI) to the total number of significant ROIs. When different network features were considered (e.g., *PC* and *MPC*), we concatenated the respective c_s feature vectors allowing for all the possible combinations.

To quantify the separation between the feature vectors of AD and HC subjects, we used a Mahalanobis distance classifier. We applied a repeated 5-folds cross-validation procedure where we randomly split the entire dataset into a training set (80%) and a testing test (20%). This procedure was eventually iterated 10000 times in order to obtain more accurate classification rates. To assess the classification performance we computed the sensitivity (*Sens*), specificity (*Spec*) and accuracy (*Acc*), defined respectively as the percentage of AD subjects correctly classified as AD, the percentage of HC subjects classified as HC and the total percentage of subjects (AD and HC) properly classified. We also computed the receiver operating characteristic (ROC) curve and its area under the curve (AUC)[55].

Data availability. The Matlab code for the manipulation of multi-layer networks and the computation of the *MPC*, together with the connectivity matrices generated and analyzed in this study, are available at the Brain Network Toolbox repository (https://github.com/brain-network/bnt).

Results

Power analysis of source-reconstructed MEG signals confirmed the characteristic changes in the oscillatory activity of AD subjects compared to HC subjects (Fig. 2a)[56–59]. Significant *alpha* power decreases were more evident in the parietal and occipital regions ($Z < -2.58$), while significant *delta* power increases ($Z > 2.58$) were more localized in the frontal regions of the cortex (Fig. 2b).

Reduced gamma inter-modular connectivity. As expected, the value of the connection density threshold had an impact on the network differences between groups. We selected the first threshold for which we could observe a significant group difference for both single- and multi-layer analysis. The obtained results determined the choice of a representative threshold, common to all the brain networks, corresponding to an average node degree $k = 12$ (Fig. S1).

We first evaluated the results from the single-layer analysis. By inspecting the global participation coefficient *PC*, we reported in the *gamma* band a significant decrease of inter-modular connectivity in AD as compared to HC ($Z = -2.50$, $p = 0.017$; Fig. 3a inset). This behavior was locally identified in association ROIs including temporal and parietal areas ($p < 0.05$, FDR corrected; Fig. 3a; Table 2). No other significant differences were reported in other frequency bands or in flattened brain networks (Fig. S1).

Disrupted inter-frequency hub centrality. Then we assessed the results from the multi-layer analysis. Both AD and HC subjects exhibited high global multi-participation coefficients ($MPC > 0.9$), suggesting a general propensity of brain regions to promote interactions across frequency bands. However, such tendency was significantly lower in AD than HC subjects ($Z = -2.24$, $p = 0.028$; Fig. 3b inset). This loss of inter-frequency centrality was prevalent in association ROIs including temporal, parietal and cingulate areas, and with a minor extent in motor areas ($p < 0.05$, FDR corrected; Fig. 3b; Table 2).

Among those regions, the right cingulate cortex was classified as the main inter-frequency hub as revealed by the spatial distribution of the top 25% *MPC* values in the HC group (Fig. 4a). In HC subjects the connectivity of this region across bands, as measured by the node degree layer proportion *NLP*, was relatively stable (Kruskal-Wallis test, $\chi^2 = 10.79$, $p = 0.095$), while it was significantly altered in AD subjects (Kruskall-Wallis test, $\chi^2 = 14.98$, $p = 0.020$). In particular, the AD group exhibited a remarkably reduced $alpha_2$ connectivity

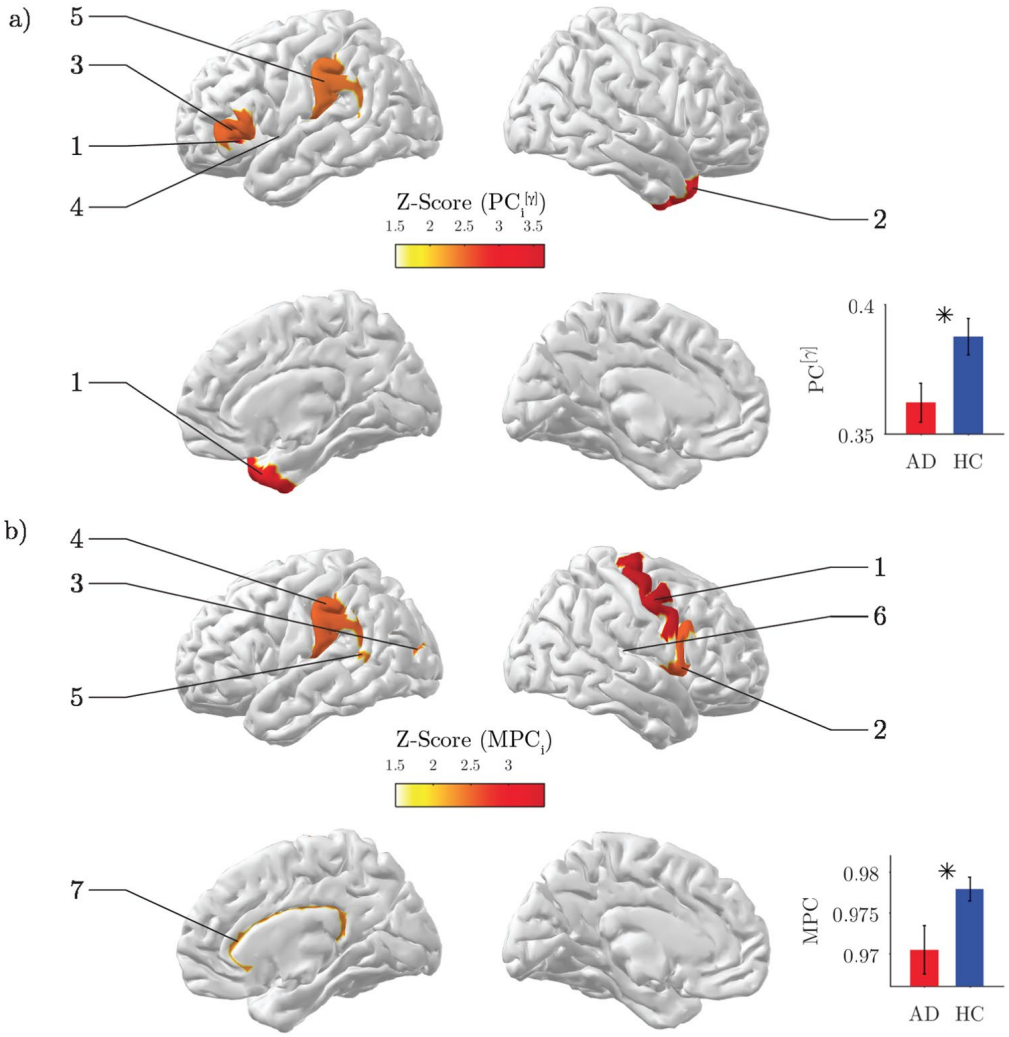

Figure 3. Network analysis of brain connectivity. (**a**) Inter-modular centrality. Statistical brain maps of group differences for local participation coefficients PC_i in the *gamma* band. Only significant differences are illustrated ($p < 0.05$, FDR corrected). The labels same ranks are used as labels. The inset shows the results for the global *PC*; vertical bars stand for group-averaged values while error bars denote standard error means. In both cases, Z-scores are computed using a non-parametric permutation t-test. b) Inter-frequency centrality. Statistical brain maps of group differences for local multi-participation coefficients MPC_i. The inset shows the results for the global *MPC*; same conventions as in (**a**).

Feature	Rank	ROI label	Cortex	Z score	*p*-value
$PC_i^{[\gamma]}$	1	Lat_Fis-ant-Horizont L	Frontal	−3.6507	0.0007
	2	Pole_temporal R	Temporal	−2.8642	0.0063
	3	G_front_inf-Triangul L	Frontal	−2.4562	0.0198
	4	**S_temporal_transverse L**	Temporal	−2.3887	0.0207
	5	**G_pariet_inf-Supramar L**	Parietal	−2.3820	0.0222
MPC_i	1	G_precentral R	Motor	−3.4735	0.0006
	2	G_front_inf-Opercular R	Motor	−2.5239	0.0127
	3	S_oc_middle_and_Lunatus L	Occipital	−2.4582	0.0138
	4	**G_pariet_inf-Supramar L**	Parietal	−2.4860	0.0142
	5	**S_interm_prim-Jensen L**	Parietal	−2.3708	0.0147
	6	**S_temporal_transverse R**	Temporal	−2.3996	0.0191
	7	**S_pericallosal R**	Limbic	−2.3041	0.0203

Table 2. Statistical group differences for local brain network features. ROI labels, abbreviated according to the Destrieux atlas, are ranked according to the resulting *p*-values. The same ranks are used as labels in Fig. 3. ROIs highlighted in bold belong to the default mode network (DMN).

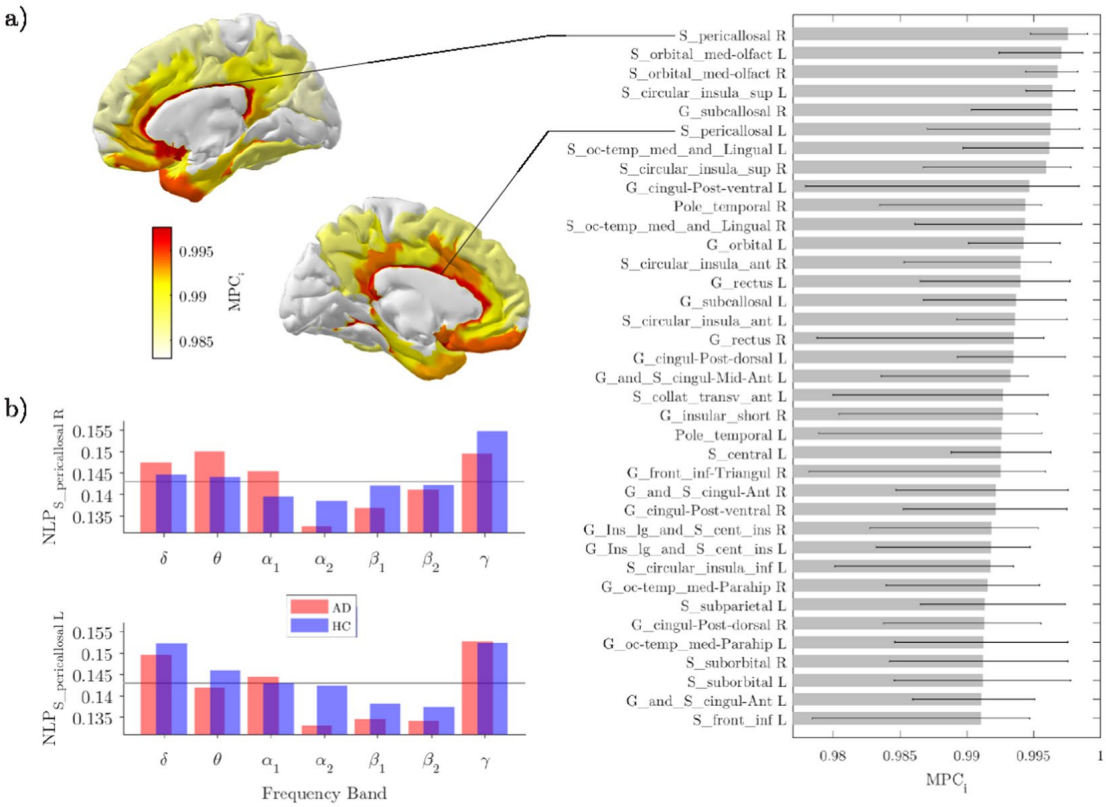

Figure 4. Inter-frequency hub centrality distribution. (**a**) The median values of local multi-participation coefficients (MPC_i) are shown over the cortical surface for the healthy group. Only the top 25% is illustrated for the sake of visualization. The corresponding list of ROIs is illustrated in the horizontal bar plot. (**b**) Group-median values of the node-degree layer proportion (NLP_i) for the right and left cingulate cortex. The grey line corresponds to the expected value if connectivity were equally distributed across frequency bands ($NLP_i = 1/7$).

and increased *theta* connectivity (Fig. 4b). Similar results were also reported for the left cingulate cortex (AD: $\chi^2 = 11.89$, $p = 0.064$; HC: $\chi^2 = 6.98$, $p = 0.323$), although it was not significant in terms of *MPC* differences (Fig. 3b; Table 2).

Diagnostic power of brain network features. We adopted a classification approach to evaluate the power of the most significant local network properties in determining the state (i.e., healthy or diseased) of each individual subject. The best results were achieved neither when we considered single-layer features (i.e., $PC_i^{[\gamma]}$) nor when we considered multi-layer features (MPC_i) (respectively, first column and row of panels in Fig. 5a). Instead, a combination of the two most significant features gave the best classification in terms of accuracy ($Acc = 78.39\%$) and area under the curve ($AUC = 0.8625$) (Fig. 5a,b). While the corresponding specificity was not particularly high ($Spec = 65.68\%$), the sensitivity was remarkably elevated ($Sens = 91.11\%$).

Relationship with cognitive and memory impairment. We finally evaluated the ability of the significant brain network changes to predict the cognitive and memory performance of AD subjects. We first considered the results from single-layer analysis. We found a significant positive correlation between the global participation coefficient *PC* in the *gamma* band and the MMSE score ($R = 0.4909$, $p = 0.0127$; Fig. 6a). Then we considered the results from multi-layer analysis. We reported a higher significant positive correlation between the global multi-participation coefficient *MPC* and the TR score ($R = 0.5547$, $p = 0.0074$; Fig. 6c). These relationships were locally identified in specific ROIs including parietal, temporal and cingulate areas of the default mode network (DMN)[60] ($p < 0.05$, FDR corrected; Fig. 6b,d; Table 3).

Discussion

Graph analysis of brain networks have been largely exploited in the study of AD with the aim to extract new predictive diagnostics of disease progression. Typical approaches in functional neuroimaging, characterized by oscillatory dynamics, analyze brain networks separately at different frequencies thus neglecting the available multivariate spectral information. Here, we adopted a method to formally take into account the topological information of multi-frequency connectomes obtained from source-reconstructed MEG signals in a group of AD and healthy subjects during EC resting states.

Main results showed that, while flattening networks of different frequency bands attenuates differences between AD and HC populations, keeping the multiplex nature of MEG connectomes allow to capture higher-order discriminant information. AD subjects exhibited an aberrant multiplex brain network structure

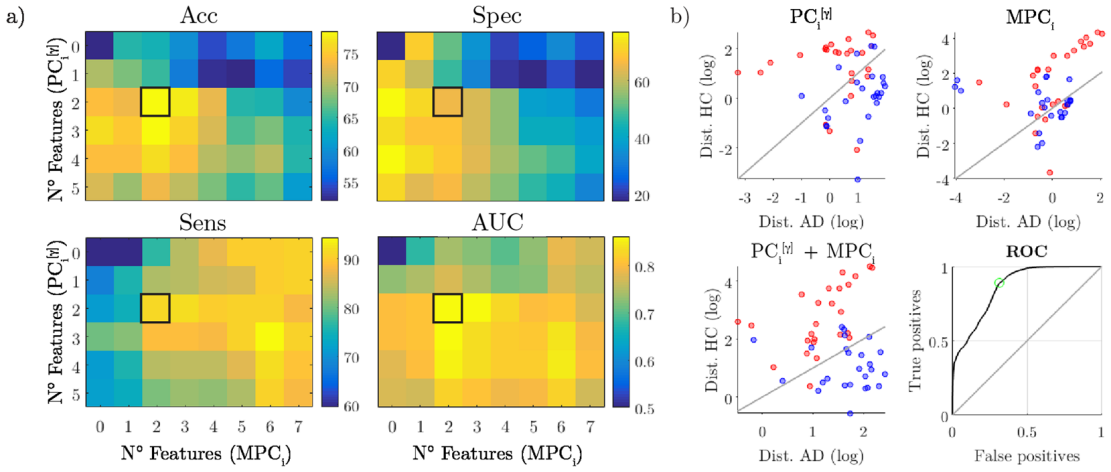

Figure 5. Classification performance of brain network features. (**a**) Matrices show the classification rates (accuracy = Acc, specificity = Spec, sensitivity = Sens, area under the curve = AUC) corresponding to the combination of the most significant $PC_i^{[\gamma]}$ and MPC_i network features, respectively on the rows and columns of each matrix. Black squares highlight the highest accuracy rate and the corresponding specificity, sensitivity and AUC. (**b**) Scatter plots show the Mahalanobis distance of each subject from the *AD* and *HC* classes. Separation lines ($y = x$: equal distances) are drawn in grey. Red circles stand for Alzheimer's disease (AD) subjects, blue ones for healthy controls (HC). The bottom right plot shows the ROC curve associated with the best network features configuration. The optimal point is marked by a green circle.

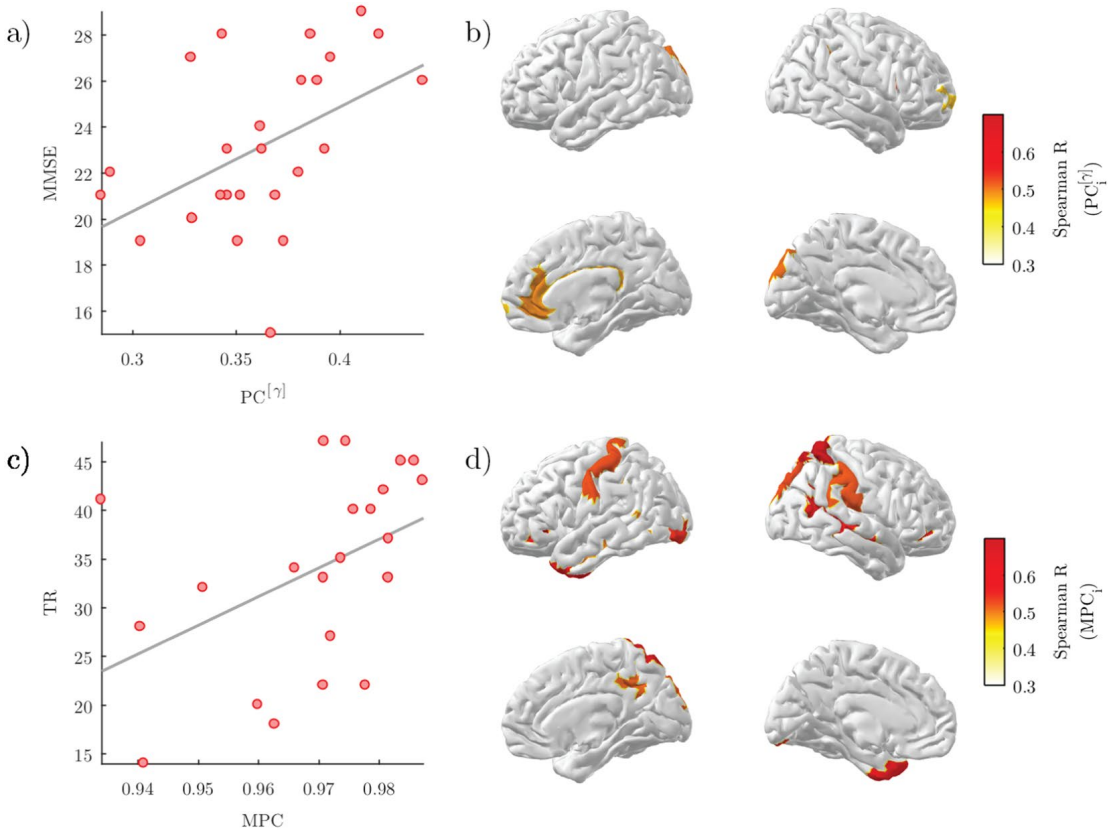

Figure 6. Correlation between brain network properties and cognitive/memory scores. (**a**) Scatter plot of the global participation coefficient in the *gamma* band ($PC^{[\gamma]}$) and the mini-mental state examination (MMSE) score of AD subjects (Spearman's correlation $R = 0.4909$, $p = 0.0127$). (**b**) Correlation brain maps of the local participation coefficient in the *gamma* band ($PC_i^{[\gamma]}$) and the mini-mental state examination (MMSE) score of AD subjects. Only significant R values are illustrated ($p < 0.05$, FDR corrected). (**c**) Scatter plot of the global multi-participation coefficient (PC) and the total recall (TR) score of AD subjects (Spearman's correlation $R = 0.5547$, $p = 0.0074$). (**d**) Correlation brain maps of the local multi-participation coefficient (MPC_i) and the total recall (TR) score of AD subjects. Only significant R values are illustrated ($p < 0.05$, FDR corrected).

Correlation	Rank	ROI label	Cortex	*R* coeff.	*p*-value
$PC_i^{[\gamma]}$ - MMSE	1	Lat_Fis-ant-Vertical R	Frontal	0.5480	0.0046
	2	G_occipital_sup L	Occipital	0.5005	0.0108
	3	**S_interm_prim-Jensen R**	Parietal	0.4948	0.0119
	4	**G_and_S_cingul-Ant R**	Limbic	0.4864	0.0137
	5	**S_pericallosal R**	Limbic	0.4735	0.0168
	6	G_and_S_transv_frontopol R	Frontal	0.4585	0.0212
MPC_i - TR	1	Lat_Fis-ant-Horizont L	Frontal	0.6915	0.0004
	2	S_collat_transv_post L	Occipital	0.6706	0.0006
	3	S_circular_insula_ant L	Frontal	0.6214	0.0020
	4	**G_parietal_sup R**	Parietal	0.6061	0.0028
	5	S_orbital_lateral R	Frontal	0.5920	0.0037
	6	Pole_temporal L	Temporal	0.5739	0.0052
	7	S_orbital_lateral L	Frontal	0.5462	0.0085
	8	**S_temporal_sup R**	Temporal	0.5457	0.0086
	9	G_and_S_occipital_inf L	Occipital	0.5368	0.0100
	10	G_occipital_sup R	Occipital	0.5208	0.0130
	11	G_postcentral L	Sensory	0.5191	0.0133
	12	**G_pariet_inf-Supramar R**	Parietal	0.5151	0.0142
	13	**S_subparietal R**	Parietal	0.5066	0.0161
	14	**S_interm_prim-Jensen L**	Parietal	0.4915	0.0202
	15	**S_temporal_inf L**	Temporal	0.4869	0.0216

Table 3. Correlations of local brain network features and cognitive/memory scores. ROI labels, abbreviated according to the Destrieux atlas, are ranked according to the resulting *p*-values. ROIs written in bold belong to the default mode network (DMN).

that significantly reduced the global propensity to facilitate information propagation across frequency bands as compared to HC subjects (Fig. 3b, inset). This could be in part explained by the higher variability of the individual node degrees across bands (Fig. S2).

Such loss of inter-frequency centrality was mostly localized in association areas as well as in the cingulate cortex (Fig. 3b; Table 2), which resulted the most important hub promoting interaction across bands in the HC group (Fig. 4a). Because all these areas are typically affected by AD atrophy[4] we hypothesize that the anatomical withering might have impacted the neural oscillatory mechanisms supporting large-scale brain functional integration. Notably, the significant alteration of the connectivity across bands observed in the cingulate cortex could be ascribed to typical M/EEG connectivity changes observed in AD, such as reduced *alpha* coherence[57–59, 61] (Fig. 4b). We also found a significant decrease in the primary motor cortex (right precentral gyrus). While previous studies have identified this specific region as a connector hub in human brain networks[2], its role in AD still needs to be clarified in terms of node centrality's changes with respect to healthy conditions.

While flattening network layers represents in general an oversimplification, analyzing single layers can still be a valid approach that is worth of investigation. Because the *MPC* is a pure multiplex quantity, we considered the conceptually akin version for single-layer networks, the standard participation coefficient *PC*, which evaluates the tendency of nodes to integrate information from different modules, rather than from different layers[28, 47]. AD patients exhibited lower inter-modular connectivity in the *gamma* band with respect to HC subjects (Fig. 3a; Table 2) that was localized in association areas including frontal, temporal, and parietal cortices (Fig. 3a; Table 2). Damages to these regions can lead to deficits in attention, recognition and planning[62]. Our results support the hypothesis that AD could include a disconnection syndrome[63–65]. Furthermore, they are in line with previous findings showing *PC* decrements in AD, although those declines were more evident in lower frequency bands and therefore ascribed to possible long-range low-frequency connectivity alteration[2, 15].

Put together, our findings indicated that AD alters the global brain network organization through connection disruption in several association regions (Figs 3a and 4a). In particular, we showed that the global loss of inter-modular interactions in the *gamma* band significantly affected the memory performance of AD patients as measured by the MMSE (Fig. 4a). These results suggest that the capacity of association areas to integrate information from other cortical regions through high-frequency channels, a crucial mechanism for sensory processing and memory retrieval[66–70], becomes critically compromised in AD patients. Interestingly, such loss was paralleled by a diffused decrease of inter-frequency centrality. Future studies, involving recordings of limbic structures and/or stimulation-based techniques, should elucidate whether these two distinct reorganizational processes are truly independent or linked through possible cross-frequency mechanisms which are known to be essential for normal memory formation[71–73].

As a confirmation of the complementary information carried out by the multi-layer approach, we reported an increased classification accuracy when combining the local *PC* and *MPC* features. The observed diagnostic power is in line with previous accuracy values obtained with standard graph theoretic approaches (around 80%) but exhibits slightly higher sensitivity (>90%), which is often desired to avoid false negatives[74–78]. Other approaches should determine if and to what extent the use of more sophisticated machine learning algorithms, or

the inclusion of basic connectivity features[79–81] and different imaging modalities[82], can lead to higher classification performance and better diagnosis[2].

Previous works have documented relationships between brain network properties and neuropsychological measurements in AD, suggesting a potential impact for monitoring disease progression and for the development of new therapies[7, 8, 10, 75, 83, 84]. This is especially true for the standard *PC* which has exhibited stronger correlations and larger between-group differences[2]. In line with this prediction, we also reported significant correlations between the MMSE cognitive scores and the *PC* values of the AD patients in the *gamma* band (Fig. 6a). An even stronger correlation was found, however, for the global *MPC* values and the TR scores (Fig. 6b, Table 3). Recent studies suggest that TR scores could be more specific for AD[85, 86] as compared to MMSE scores which could be biased by differences in years of education, lack of sensitivity to progressive changes occurring with AD, as well as fail in detecting impairment caused by focal lesions[87]. Locally, the regions whose *MPC* correlated with TR were part of the default-mode network (DMN) (Table 3), which is heavily involved in memory formation and retrieval[60, 88]. According to recent hypothesis, these areas are directly affected by atrophy and metabolism disruption, as well as amyloid-β deposition[89, 90].

Put together, our results suggest that AD symptoms related to episodic memory losses could be determined by the lower capacity of strategic DMN association areas to let information flow across different frequency channels. These results are in line with a recent study that adopted a similar multi-frequency network approach[91], but that, however, *i)* did not perform a direct comparison with standard single-frequency network measurements and, more importantly, *ii)* did not provide a possible interpretation of the MPC in terms of its ability to favor communication across frequencies.

Methodological considerations. As in many other biological systems, brain networks can be only inferred from experimentally obtained data[92, 93]. Hence, the resulting network only represents an estimate of the true underlying connectivity. In our study, MEG connectivity could be specifically influenced by linear mixing due to field spread effects (i.e., primary leakage) as well as by spurious interactions between areas spatially close to truly connected regions (i.e., secondary leakage)[91, 94].

Here, we estimated brain networks by means of spectral coherence, a functional connectivity measure widely used in the electrophysiological literature because of its simplicity and relatively intuitive interpretation[95]. While this measure, as any other existing ones, cannot solve the problem of primary and secondary leakage effects, recent evidence showed that source reconstruction techniques, like the one we adopted here, can *i)* mitigate this bias[96, 97], *ii)* generate connectivity patterns consistent within and between subjects[98], and *iii)* help the interpretation of results in terms of cortical regions[97].

To validate the obtained results we used, in a separate analysis, the imaginary coherence as a further approach to diminish field spread effects, at the cost, however, of removing possibly existing true interactions at zero-phase lag[94, 96, 99]. We demonstrated that while no significant between-group differences could be obtained in terms of *MPC* (data not shown here), the spatial distribution of the *MPC* values was very similar to that observed in brain networks obtained with the spectral coherence, especially for the internal regions along the longitudinal fissure (Fig. S3). Although, this is not a proof that we recovered true connectivity, it nevertheless validates the stability of our main results in terms of *MPC*.

Differently from other multiplex network quantities, such as those based on paths and walks[50], the *MPC* has the advantage to not depend on the weights of the inter-layer links which, in general, are difficult to estimate or to assign from empirically obtained biological data. This is especially true in network neuroscience where, so far, the strength of the inter-layer connections is parametric and subject to arbitrariness[27] or estimated through measures of cross-frequency coupling[21] whose biological interpretation remains still to be completely elucidated[20].

Conclusions

We proposed a multi-layer network approach to characterize multi-frequency brain networks in Alzheimer's disease. The obtained results gave new insights into the neural deterioration of Alzheimer's disease by revealing an abnormal loss of inter-frequency centrality in memory-related association areas as well as in the cingulate cortex. Longitudinal studies, including prodromal mild cognitive impairment subjects, will need to assess the predictive value of this new information as a potential non-invasive biomarker for neurodegenerative diseases.

References

1. Stam, C. J. Modern network science of neurological disorders. *Nat Rev Neurosci* **15**, 683–695 (2014).
2. Tijms, B. M. *et al.* Alzheimer's disease: connecting findings from graph theoretical studies of brain networks. *Neurobiol. Aging* **34**, 2023–2036 (2013).
3. Stam, C. J. Use of magnetoencephalography (MEG) to study functional brain networks in neurodegenerative disorders. *Journal of the Neurological Sciences* **289**, 128–134 (2010).
4. Wenk, G. L. Neuropathologic changes in Alzheimer's disease. *J Clin Psychiatry* **64**(Suppl 9), 7–10 (2003).
5. Rose, S. E. *et al.* Loss of connectivity in Alzheimer's disease: an evaluation of white matter tract integrity with colour coded MR diffusion tensor imaging. *J. Neurol. Neurosurg. Psychiatr.* **69**, 528–530 (2000).
6. Zhou, Y. *et al.* Abnormal connectivity in the posterior cingulate and hippocampus in early Alzheimer's disease and mild cognitive impairment. *Alzheimers Dement* **4**, 265–270 (2008).
7. Lo, C.-Y. *et al.* Diffusion tensor tractography reveals abnormal topological organization in structural cortical networks in Alzheimer's disease. *J. Neurosci.* **30**, 16876–16885 (2010).
8. Sanz-Arigita, E. J. *et al.* Loss of 'Small-World' Networks in Alzheimer's Disease: Graph Analysis of fMRI Resting-State Functional Connectivity. *PLOS ONE* **5**, e13788 (2010).
9. Stam, C. J. *et al.* Graph theoretical analysis of magnetoencephalographic functional connectivity in Alzheimer's disease. *Brain* **132**, 213–224 (2009).
10. de Haan, W. *et al.* Functional neural network analysis in frontotemporal dementia and Alzheimer's disease using EEG and graph theory. *BMC Neuroscience* **10**, 101 (2009).

11. Miraglia, F., Vecchio, F. & Rossini, P. M. Searching for signs of aging and dementia in EEG through network analysis. *Behavioural Brain Research* **317**, 292–300 (2017).
12. Bassett, D. S. *et al*. Dynamic reconfiguration of human brain networks during learning. *PNAS* **108**, 7641–7646 (2011).
13. Crossley, N. A. *et al*. The hubs of the human connectome are generally implicated in the anatomy of brain disorders. *Brain* **137**, 2382–2395 (2014).
14. Buckner, R. L. *et al*. Cortical hubs revealed by intrinsic functional connectivity: mapping, assessment of stability, and relation to Alzheimer's disease. *J. Neurosci.* **29**, 1860–1873 (2009).
15. de Haan, W. *et al*. Disrupted modular brain dynamics reflect cognitive dysfunction in Alzheimer's disease. *NeuroImage* **59**, 3085–3093 (2012).
16. Engels, M. M. *et al*. Declining functional connectivity and changing hub locations in Alzheimer's disease: an EEG study. *BMC Neurol* **15** (2015).
17. De Vico Fallani, F., Richiardi, J., Chavez, M. & Achard, S. Graph analysis of functional brain networks: practical issues in translational neuroscience. *Phil. Trans. R. Soc. B* **369**, 20130521 (2014).
18. Bullmore, E. & Sporns, O. Complex brain networks: graph theoretical analysis of structural and functional systems. *Nat. Rev. Neurosci.* **10**, 186–198 (2009).
19. Canolty, R. T. & Knight, R. T. The functional role of cross-frequency coupling. *Trends in Cognitive Sciences* **14**, 506–515 (2010).
20. Jirsa, V. & Müller, V. Cross-frequency coupling in real and virtual brain networks. *Front Comput Neurosci* **7** (2013).
21. Brookes, M. J. *et al*. A multi-layer network approach to MEG connectivity analysis. *NeuroImage* **132**, 425–438 (2016).
22. Fraga, F. J., Falk, T. H., Kanda, P. A. M. & Anghinah, R. Characterizing Alzheimer's Disease Severity via Resting-Awake EEG Amplitude Modulation Analysis. *PLoS One* **8** (2013).
23. Blinowska, K. J. *et al*. Functional and effective brain connectivity for discrimination between Alzheimer's patients and healthy individuals: A study on resting state EEG rhythms. *Clin Neurophysiol* (2016).
24. Ghanbari, Y. *et al*. Functionally driven brain networks using multi-layer graph clustering. *Med Image Comput Comput Assist Interv* **17**, 113–120 (2014).
25. Simas, T., Chavez, M., Rodriguez, P. R. & Diaz-Guilera, A. An algebraic topological method for multimodal brain networks comparisons. *Front Psychol* **6** (2015).
26. Battiston, F., Nicosia, V., Chavez, M. & Latora, V. Multilayer motif analysis of brain networks. Chaos. 27(4):047404 (2017).
27. De Domenico M, Sasai S, Arenas A. Mapping Multiplex Hubs in Human FunctionalBrain Networks. *Front Neurosci.* 15;10:326 (2016)
28. Battiston, F., Nicosia, V. & Latora, V. Structural measures for multiplex networks. *Phys. Rev. E* **89**, 032804 (2014).
29. De Domenico, M. *et al*. Mathematical Formulation of Multilayer Networks. *Phys. Rev. X* **3**, 041022 (2013).
30. Folstein, M. F., Folstein, S. E. & McHugh, P. R. "Mini-mental state". A practical method for grading the cognitive state of patients for the clinician. *J Psychiatr Res* **12**, 189–198 (1975).
31. Buschke, H. Cued recall in Amnesia. *Journal of Clinical Neuropsychology* **6**, 433–440 (1984).
32. Grober, E., Buschke, H., Crystal, H., Bang, S. & Dresner, R. Screening for dementia by memory testing. *Neurology* **38**, 900–903 (1988).
33. Pillon, B., Deweer, B., Agid, Y. & Dubois, B. Explicit memory in Alzheimer's, Huntington's, and Parkinson's diseases. *Arch. Neurol.* **50**, 374–379 (1993).
34. Sarazin, M. *et al*. Amnestic syndrome of the medial temporal type identifies prodromal AD: a longitudinal study. *Neurology* **69**, 1859–1867 (2007).
35. Taulu, S. & Simola, J. Spatiotemporal signal space separation method for rejecting nearby interference in MEG measurements. *Phys. Med. Biol.* **51**, 1759 (2006).
36. He, B. Brain electric source imaging: scalp Laplacian mapping and cortical imaging. *Crit Rev Biomed Eng* **27**, 149–188 (1999).
37. Baillet, S. *et al*. Evaluation of inverse methods and head models for EEG source localization using a human skull phantom. *Phys Med Biol* **46**, 77–96 (2001).
38. Fischl, B. *et al*. Whole brain segmentation: automated labeling of neuroanatomical structures in the human brain. *Neuron* **33**, 341–355 (2002).
39. Fischl, B. *et al*. Sequence-independent segmentation of magnetic resonance images. *Neuroimage* **23**(Suppl 1), S69–84 (2004).
40. Tadel, F. *et al*. Brainstorm: A User-Friendly Application for MEG/EEG Analysis, Brainstorm: A User-Friendly Application for MEG/EEG Analysis. *Computational Intelligence and Neuroscience*, *Computational Intelligence and Neuroscience* **2011**, e879716 (2011).
41. Lin, F.-H. *et al*. Assessing and improving the spatial accuracy in MEG source localization by depth-weighted minimum-norm estimates. *NeuroImage* **31**, 160–171 (2006).
42. Destrieux, C., Fischl, B., Dale, A. & Halgren, E. Automatic parcellation of human cortical gyri and sulci using standard anatomical nomenclature. *Neuroimage* **53**, 1–15 (2010).
43. Carter, G. C. Coherence and time delay estimation. *Proceedings of the IEEE* **75**, 236–255 (1987).
44. Stam, C. J. *et al*. Generalized synchronization of MEG recordings in Alzheimer's Disease: evidence for involvement of the gamma band. *J Clin Neurophysiol* **19**, 562–574 (2002).
45. Babiloni, C. *et al*. Abnormal fronto-parietal coupling of brain rhythms in mild Alzheimer's disease: a multicentric EEG study. *Eur. J. Neurosci.* **19**, 2583–2590 (2004).
46. Rubinov, M. & Sporns, O. Complex network measures of brain connectivity: Uses and interpretations. *NeuroImage* **52**, 1059–1069 (2010).
47. Guimerà, R. & Amaral, L. A. N. Cartography of complex networks: modules and universal roles. *J Stat Mech* **2005**, P02001–1–P02001–13 (2005).
48. Newman, M. E. J. Finding community structure in networks using the eigenvectors of matrices. *Phys. Rev. E* **74**, 036104 (2006).
49. Kivelä, M. *et al*. Multilayer networks. *jcomplexnetw* **2**, 203–271 (2014).
50. Boccaletti, S. *et al*. The structure and dynamics of multilayer networks. *Physics Reports* **544**, 1–122 (2014).
51. De Vico Fallani, F. *et al*. Interhemispheric Connectivity Characterizes Cortical Reorganization in Motor-Related Networks After Cerebellar Lesions. *Cerebellum* (2016).
52. Benjamini, Y. & Hochberg, Y. Controlling the False Discovery Rate: A Practical and Powerful Approach to Multiple Testing. *Journal of the Royal Statistical Society. Series B (Methodological)* **57**, 289–300 (1995).
53. Zar, J. H. *Biostatistical analysis* (Prentice Hall PTR, 1999).
54. Benjamini, Y. & Yekutieli, D. The Control of the False Discovery Rate in Multiple Testing under Dependency. *The Annals of Statistics* **29**, 1165–1188 (2001).
55. Hastie, T., Tibshirani, R. & Friedman, J. *The Elements of Statistical Learning*. Springer Series in Statistics (Springer New York, New York, NY, 2009).
56. Babiloni, C. *et al*. Mapping distributed sources of cortical rhythms in mild Alzheimer's disease. A multicentric EEG study. *Neuroimage* **22**, 57–67 (2004).
57. Jeong, J. EEG dynamics in patients with Alzheimer's disease. *Clin Neurophysiol* **115**, 1490–1505 (2004).
58. Dauwels, J., Vialatte, F. & Cichocki, A. Diagnosis of Alzheimer's Disease from EEG Signals: Where Are We Standing? *Current Alzheimer Research* **7**, 487–505 (2010).
59. Wang, R. *et al*. Power spectral density and coherence analysis of Alzheimer's EEG. *Cogn Neurodyn* **9**, 291–304 (2015).

60. Buckner, R. L., Andrews-Hanna, J. R. & Schacter, D. L. The Brain's Default Network. *Annals of the New York Academy of Sciences* **1124**, 1–38 (2008).
61. Stam, C. J. *et al*. Magnetoencephalographic evaluation of resting-state functional connectivity in Alzheimer's disease. *NeuroImage* **32**, 1335–1344 (2006).
62. Purves, D. *et al*. (eds) *Neuroscience*, 2nd edn. (Sinauer Associates, 2001).
63. Pearson, R. C., Esiri, M. M., Hiorns, R. W., Wilcock, G. K. & Powell, T. P. Anatomical correlates of the distribution of the pathological changes in the neocortex in Alzheimer disease. *Proc. Natl. Acad. Sci. USA* **82**, 4531–4534 (1985).
64. Arnold, S. E., Hyman, B. T., Flory, J., Damasio, A. R. & Van Hoesen, G. W. The topographical and neuroanatomical distribution of neurofibrillary tangles and neuritic plaques in the cerebral cortex of patients with Alzheimer's disease. *Cereb. Cortex* **1**, 103–116 (1991).
65. Catani, M. & Ffytche, D. H. The rises and falls of disconnection syndromes. *Brain* **128**, 2224–2239 (2005).
66. Miltner, W. H., Braun, C., Arnold, M., Witte, H. & Taub, E. Coherence of gamma-band EEG activity as a basis for associative learning. *Nature* **397**, 434–436 (1999).
67. Buschman, T. J. & Miller, E. K. Top-down versus bottom-up control of attention in the prefrontal and posterior parietal cortices. *Science* **315**, 1860–1862 (2007).
68. Siegel, M., Donner, T. H., Oostenveld, R., Fries, P. & Engel, A. K. Neuronal Synchronization along the Dorsal Visual Pathway Reflects the Focus of Spatial Attention. *Neuron* **60**, 709–719 (2008).
69. Gregoriou, G. G., Gotts, S. J., Zhou, H. & Desimone, R. High-frequency, long-range coupling between prefrontal and visual cortex during attention. *Science* **324**, 1207–1210 (2009).
70. Hipp, J. F., Engel, A. K. & Siegel, M. Oscillatory synchronization in large-scale cortical networks predicts perception. *Neuron* **69**, 387–396 (2011).
71. Canolty, R. T. *et al*. High Gamma Power Is Phase-Locked to Theta Oscillations in Human Neocortex. *Science* **313**, 1626–1628 (2006).
72. Axmacher, N. *et al*. Cross-frequency coupling supports multi-item working memory in the human hippocampus. *PNAS* **107**, 3228–3233 (2010).
73. Goutagny, R. *et al*. Alterations in hippocampal network oscillations and theta–gamma coupling arise before Aß overproduction in a mouse model of Alzheimer's disease. *Eur J Neurosci* **37**, 1896–1902 (2013).
74. Li, Y. *et al*. Discriminant analysis of longitudinal cortical thickness changes in Alzheimer's disease using dynamic and network features. *Neurobiol. Aging* **33** (2012).
75. Wang, J. *et al*. Disrupted functional brain connectome in individuals at risk for Alzheimer's disease. *Biol. Psychiatry* **73**, 472–481 (2013).
76. Wee, C.-Y. *et al*. Enriched white matter connectivity networks for accurate identification of MCI patients. *Neuroimage* **54**, 1812–1822 (2011).
77. Wee, C.-Y. *et al*. Identification of MCI individuals using structural and functional connectivity networks. *Neuroimage* **59**, 2045–2056 (2012).
78. Horwitz, B. & Rowe, J. B. Functional biomarkers for neurodegenerative disorders based on the network paradigm. *Progress in Neurobiology* **95**, 505–509 (2011).
79. Dai, D., He, H., Vogelstein, J. & Hou, Z. Network-Based Classification Using Cortical Thickness of AD Patients. In Hutchison, D. *et al*. (eds) *Machine Learning in Medical Imaging*, vol. 7009, 193–200 (Springer Berlin Heidelberg, Berlin, Heidelberg, 2011).
80. Shao, J. *et al*. Prediction of Alzheimer's disease using individual structural connectivity networks. *Neurobiol Aging* **33**, 2756–2765 (2012).
81. Zhou, L. *et al*. Hierarchical Anatomical Brain Networks for MCI Prediction: Revisiting Volumetric Measures. *PLOS ONE* **6**, e21935 (2011).
82. Dai, Z. *et al*. Discriminative analysis of early Alzheimer's disease using multi-modal imaging and multi-level characterization with multi-classifier (M3). *NeuroImage* **59**, 2187–2195 (2012).
83. Shu, N. *et al*. Disrupted topological organization in white matter structural networks in amnestic mild cognitive impairment: relationship to subtype. *Radiology* **265**, 518–527 (2012).
84. Stam, C. J., Jones, B. F., Nolte, G., Breakspear, M. & Scheltens, P. Small-world networks and functional connectivity in Alzheimer's disease. *Cereb. Cortex* **17**, 92–99 (2007).
85. Grober, E., Sanders, A. E., Hall, C. & Lipton, R. B. Free and cued selective reminding identifies very mild dementia in primary care. *Alzheimer Dis Assoc Disord* **24**, 284–290 (2010).
86. Velayudhan, L. *et al*. Review of brief cognitive tests for patients with suspected dementia. *Int Psychogeriatr* **26**, 1247–1262 (2014).
87. Tombaugh, T. N. & McIntyre, N. J. The mini-mental state examination: a comprehensive review. *J Am Geriatr Soc* **40**, 922–935 (1992).
88. Sperling, R. A. *et al*. Functional Alterations in Memory Networks in Early Alzheimer's Disease. *Neuromolecular Med* **12**, 27–43 (2010).
89. Buckner, R. L. *et al*. Molecular, structural, and functional characterization of Alzheimer's disease: evidence for a relationship between default activity, amyloid, and memory. *J. Neurosci.* **25**, 7709–7717 (2005).
90. Greicius, M. D., Srivastava, G., Reiss, A. L. & Menon, V. Default-mode network activity distinguishes Alzheimer's disease from healthy aging: Evidence from functional MRI. *Proc Natl Acad Sci USA* **101**, 4637–4642 (2004).
91. Yu, M. *et al*. Selective impairment of hippocampus and posterior hub areas in Alzheimer's disease: an MEG-based multiplex network study. *Brain* **140**, 1466–1485 (2017).
92. Vidal, M., Cusick, M. E. & Barabási, A.-L. Interactome networks and human disease. *Cell* **144**, 986–998 (2011).
93. Craddock, R. C. *et al*. Imaging human connectomes at the macroscale. *Nat. Methods* **10**, 524–539 (2013).
94. Palva, S. & Palva, J. M. Discovering oscillatory interaction networks with M/EEG: challenges and breakthroughs. *Trends in Cognitive Sciences* **16**, 219–230 (2012).
95. Srinivasan, R., Winter, W. R., Ding, J. & Nunez, P. L. EEG and MEG coherence: measures of functional connectivity at distinct spatial scales of neocortical dynamics. *J. Neurosci. Methods* **166**, 41–52 (2007).
96. Sekihara, K., Owen, J. P., Trisno, S. & Nagarajan, S. S. Removal of Spurious Coherence in MEG Source-Space Coherence Analysis. *IEEE Transactions on Biomedical Engineering* **58**, 3121–3129 (2011).
97. Schoffelen, J.-M. & Gross, J. Source connectivity analysis with MEG and EEG. *Hum Brain Mapp* **30**, 1857–1865 (2009).
98. Colclough, G. L. *et al*. How reliable are MEG resting-state connectivity metrics? *Neuroimage* **138**, 284–293 (2016).
99. Nolte, G. *et al*. Identifying true brain interaction from EEG data using the imaginary part of coherency. *Clinical Neurophysiology* **115**, 2292–2307 (2004).

Acknowledgements

We are grateful to F. Battiston for his useful comments and suggestions. This work has been partially supported by the program "Investissements d'avenir" ANR-10-IAIHU-06. FD acknowledges support from the "Agence Nationale de la Recherche" through contract number ANR-15-NEUC-0006–02. The content is solely the responsibility of the authors and does not necessarily represent the official views of any of the funding agencies.

Author Contributions

J.G. conceived and perfomed data analysis, wrote the manuscript and prepared all figures. Y.A. and D.S. performed data preprocessing. V.C. and B.D. conceived the experimental protocol, included patients and acquired neuroimaging and clinical data. O.C. conceived the experimental protocol and wrote the manuscript. F.D.V.F. conceived data analysis and wrote the manuscript. All authors reviewed the manuscript.

Additional Information

Supplementary information accompanies this paper at doi:10.1038/s41598-017-07846-w

Competing Interests: The authors declare that they have no competing interests.

Publisher's note: Springer Nature remains neutral with regard to jurisdictional claims in published maps and institutional affiliations.

Open Access This article is licensed under a Creative Commons Attribution 4.0 International License, which permits use, sharing, adaptation, distribution and reproduction in any medium or format, as long as you give appropriate credit to the original author(s) and the source, provide a link to the Creative Commons license, and indicate if changes were made. The images or other third party material in this article are included in the article's Creative Commons license, unless indicated otherwise in a credit line to the material. If material is not included in the article's Creative Commons license and your intended use is not permitted by statutory regulation or exceeds the permitted use, you will need to obtain permission directly from the copyright holder. To view a copy of this license, visit http://creativecommons.org/licenses/by/4.0/.

© The Author(s) 2017

CHAPTER 5

Core-periphery organization in multilayer networks

In this chapter, we define the core-periphery structure in multiplex networks and apply it to, first, synthetic network, and then, to a bimodal brain multiplex (DTI- and fMRI-based). Results confirm the role of the main known cortical and subcortical hubs, but also suggest the presence of new areas in the sensorimotor cortex that are crucial for intrinsic brain functioning.

Downloaded from http://rsif.royalsocietypublishing.org/ on September 12, 2018

INTERFACE

rsif.royalsocietypublishing.org

Research

Cite this article: Battiston F, Guillon J, Chavez M, Latora V, De Vico Fallani F. 2018 Multiplex core–periphery organization of the human connectome. *J. R. Soc. Interface* **15**: 20180514. http://dx.doi.org/10.1098/rsif.2018.0514

Received: 6 July 2018
Accepted: 16 August 2018

Subject Category:
Life Sciences–Physics interface

Subject Areas:
biocomplexity, computational biology, systems biology

Keywords:
complex networks, multilayer networks, rich-club, brain connectivity, multimodal integration

Author for correspondence:
Fabrizio De Vico Fallani
e-mail: fabrizio.devicofallani@gmail.com

Electronic supplementary material is available online at https://dx.doi.org/10.6084/m9.figshare.c.4209884.

THE ROYAL SOCIETY PUBLISHING

Multiplex core–periphery organization of the human connectome

Federico Battiston[1,2,3], Jeremy Guillon[1,2], Mario Chavez[2], Vito Latora[3,4] and Fabrizio De Vico Fallani[1,2]

[1]Inria Paris, Aramis project-team, 75013 Paris, France
[2]CNRS, Sorbonne Universites, UPMC Univ Paris 06, Inserm, Institut du cerveau et la moelle epiniere (ICM), Hopital Pitie-Salpetriere, 75013 Paris, France
[3]School of Mathematical Sciences, Queen Mary University of London, London E1 4NS, UK
[4]Dipartimento di Fisica ed Astronomia, Università di Catania and INFN, 95123 Catania, Italy

FDVF, 0000-0001-8035-7883

What is the core of the human brain is a fundamental question that has been mainly addressed by studying the anatomical connections between differently specialized areas, thus neglecting the possible contributions from their functional interactions. While many methods are available to identify the core of a network when connections between nodes are all of the same type, a principled approach to define the core when multiple types of connectivity are allowed is still lacking. Here, we introduce a general framework to define and extract the core–periphery structure of multi-layer networks by explicitly taking into account the connectivity patterns at each layer. We first validate our algorithm on synthetic networks of different size and density, and with tunable overlap between the cores at different layers. We then use our method to merge information from structural and functional brain networks, obtaining in this way an integrated description of the core of the human connectome. Results confirm the role of the main known cortical and subcortical hubs, but also suggest the presence of new areas in the sensori-motor cortex that are crucial for intrinsic brain functioning. Taken together these findings provide fresh evidence on a fundamental question in modern neuroscience and offer new opportunities to explore the mesoscale properties of multimodal brain networks.

1. Introduction

Complex networks are characterized by the existence of non-random structures at different topological scales [1–3]. A peculiar structure is the so-called core–periphery organization [4], where the network exhibits a group of tightly connected nodes (i.e. the *core*), and a group made by the remaining weakly connected nodes (i.e. the *periphery*).

Core–periphery organization has been recognized as a fundamental property of complex networks to support integration of information [5–12]. A related concept is that of rich-club behaviour, where the tightly connected nodes are the network hubs, i.e. the nodes with a large number of links [13,14]. A rich-club organization has been observed in various real-world systems, such as social, technological and biological networks [13–16], including the brain [17–20]. More recently, a refined version of the rich-club analysis, based not only on the number of connections of the hubs, but also on their capability to bridge different communities, has been shown to be relevant to support the integrative properties of the nervous system [21].

In the human brain, rich-club and rich-core organization, associated with the efficiency in communication and distribution of information, have been mainly reported in anatomical, or structural, connectivity networks obtained experimentally from diffusion tensor imaging (DTI) data. It has been conjectured that rich cores, rather than shortest paths, may actually be responsible for the efficient integration of information between remote brain areas [17],

© 2018 The Author(s) Published by the Royal Society. All rights reserved.

Downloaded from http://rsif.royalsocietypublishing.org/ on September 12, 2018

which is a crucial prerequisite for normal cognitive performance [22,23]. Current evidence suggests that posterior medial and parietal cortical regions mainly constitute the core of the human connectome [17,24], while the role of other areas, such as the medial prefrontal cortex (mPFC) and the sensori-motor system [25], is yet to be clarified. Because brain regions are also characterized by functional interactions inferred from neuroimaging data, such as functional magnetic resonance imaging (fMRI) [26,27], we hypothesize that integrating information from both structural and functional networks can give a more accurate estimate of the regions that eventually constitute the core of the human cortex.

Instead of aggregating the two different types of connectivity or analysing them separately, we adopt a multiplex network approach that preserves and exploits the original information on how brain regions are structurally and functionally interconnected. In a multiplex network, different connectivity types are mathematically represented as networks at different layers. Notably, in a multiplex—a particular case of multilayer network—there is a one-to-one correspondence between the nodes at different layers [28–32]. Multiplex network theory has been recently used to successfully extract higher-order properties of multimodal [33] and multifrequency brain networks that cannot be retrieved by standard approaches [34,35].

Interestingly, the detection of core–periphery organization in multiplex networks has been poorly explored, with the exception of approaches based on *k*-core decomposition [36,37]. To address this gap, we introduce a criterion to define and detect core–periphery organization in multiplex networks. Our method works for any number of layers and is scalable to large networks, being non-parametric and based on local node information [16]. In the following, we first introduce the general framework and then we validate it on synthetic multiplex networks with tunable core similarity.

We finally apply our method to integrate information from structural and functional brain networks and extract the multiplex core–periphery organization of the human brain. The obtained results confirm the main core areas in the posterior medial and parietal cortex, but also highlights the central role played by the regions of the sensori-motor system, which has been surprisingly neglected by previous studies on core–periphery organization, despite being considered a fundamental component of the default-mode network [25].

Our research sheds new light on the emergence of core regions in the human connectome, and we hope it will spur further work towards a better understanding of the complex relationships in the nervous system.

2. Results

2.1. Extracting the rich core of a multiplex network

Let us consider a multiplex network described by a vector of adjacency matrices $\mathcal{M} = \{A^{[1]}, \ldots, A^{[M]}\}$, where all interactions of type α, $\alpha = 1, \ldots, M$, are encoded in a different layer described by a binary adjacency matrix $A^{[\alpha]} = \{a_{ij}^{[\alpha]}\}$. To detect the core–periphery structure of a multiplex network, we first compute the multiplex degree vector $\boldsymbol{k}_i = \{k_i^{[1]}, \ldots, k_i^{[M]}\}$ of each node i [31], where $k_i^{[\alpha]} = \sum_{j \neq i} a_{ij}^{[\alpha]}$. From now on, we refer to $k_i^{[\alpha]}$, $\alpha = 1, \ldots, M$, as the *richness* of node i at layer α. Notice that this is the simplest way to define the richness of a node, and different measures of richness, such as other measures of node centrality, can be as well used.

For each layer α, we then divide the links of a node i in two groups, those towards nodes with lower richness and those towards nodes with higher richness. Hence, in our case, we can specifically decompose the degree of node i at layer α as $k_i^{[\alpha]} = k_i^{[\alpha]-} + k_i^{[\alpha]+}$. Finally, the multiplex richness μ_i of node i is obtained by aggregating single-layer information:

$$\mu_i = \sum_{\alpha=1}^{M} c^{[\alpha]} k_i^{[\alpha]}, \tag{2.1}$$

where the coefficients $c^{[\alpha]}$ modulate the relative relevance of each layer and can, for instance, be determined by exogenous information. In analogy to the single-layer case, we define the multiplex richness of a node towards richer nodes as:

$$\mu_i^+ = \sum_{\alpha=1}^{M} c^{[\alpha]} k_i^{[\alpha]+}. \tag{2.2}$$

In the most simple set-up, we can assume $c^{[\alpha]} = c = 1/M \ \forall \alpha$. More general functional forms to aggregate the contributions from different layers, giving rise to alternative measures of μ_i and μ_i^+, are presented in the Methods section.

The nodes of the multiplex are ranked according to their richness μ, so that the node i with the best rank, i.e. $\text{rank}_i = 1$, is the node with the largest value of μ, the node ranked 2 is the one with the second largest value of μ, and so on. We then compute for each node i the value of μ_i^+ as a function of rank_i. The value of the rank corresponding to the maximum of μ_i^+ finally determines the core–periphery structure. All nodes with rank lower than such a value are assigned to the multiplex core, whereas the remaining ones become part of the periphery. Nodes in the multiplex core are not necessarily part of the core of each layer, but are topologically the most valuable ones when all types of connectivity are considered. Moreover, we notice that also in the simplest case, when $c^{[\alpha]} = c \ \forall \alpha$, the multiplex core–periphery partition cannot be obtained by simply combining the cores of the different layers, or by applying the single-layer algorithm on the corresponding aggregated network.

As an illustrative example, we report in figure 1 the curve μ_i^+ as a function of rank_i obtained in the case of the Top Noordin Terrorist network, a multiplex network of $N = 78$ individuals with three layers (encoding information about mutual trust, common operations and exchanged communication between terrorists), which has been used as a benchmark to test measures and models of multiplex networks [31].

Coefficients $c^{[\alpha]}$ were chosen, in this case, to be inversely proportional to $K^{[\alpha]}$ to compensate for the different densities of the three layers. The resulting multiplex rich core integrates information from all the layers and looks different from the rich cores obtained at each of the three layers by a standard single-layer rich core analysis. More details about the results of this analysis are reported in electronic supplementary material, table S1.

2.2. Testing the method on multiplex networks with tunable core similarity

A network with a well-defined core–periphery structure has a high density of links among core nodes. With a suitable

Downloaded from http://rsif.royalsocietypublishing.org/ on September 12, 2018

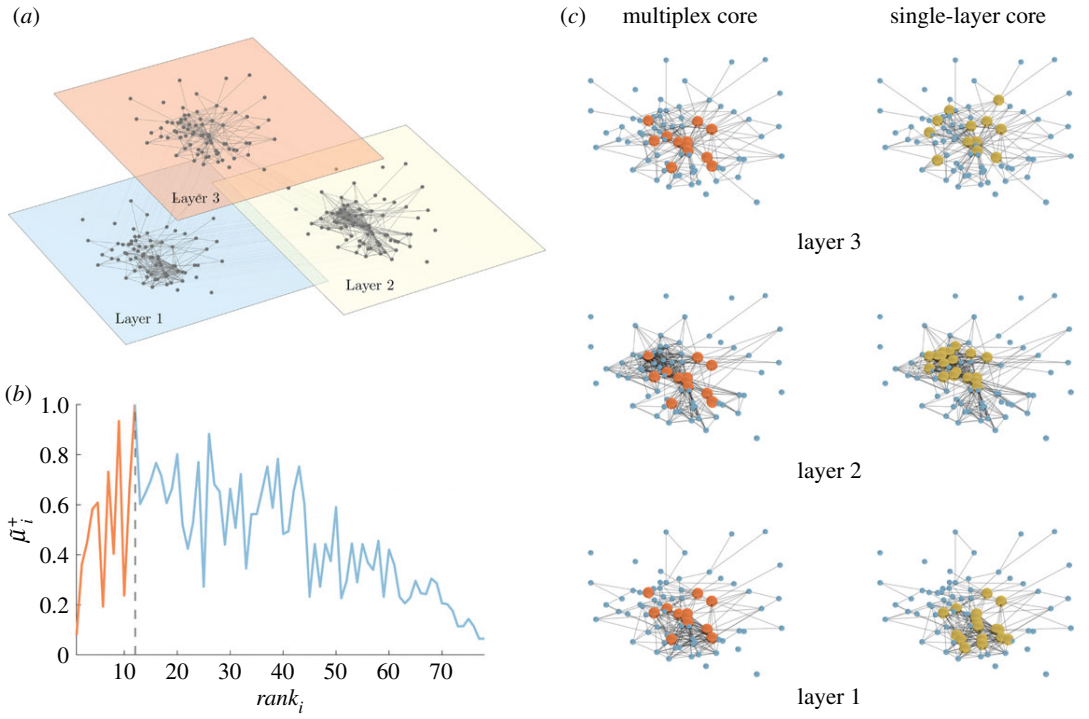

Figure 1. An illustrative example of the multiplex rich core analysis. In panel (*a*), we show a multiplex social network obtained from the Top Noordin Terrorists' contacts, with $N = 78$ nodes, $M = 3$ layers and $K^{[1]} = 259$, $K^{[2]} = 437$ and $K^{[3]} = 200$, for the three layers respectively. Panel (*b*) shows the curve $\tilde{\mu}_i^+ = \mu_i^+ / \max(\mu_i^+)$ as a function of rank_i. All nodes from rank equal to 1 up to the node with maximum $\tilde{\mu}^+$ are part of the core of the multiplex, which is shown in red colour in panel (*c*), first column. The cores obtained at each layer by the standard single-layer analysis are reported in yellow for the sake of comparison in the second column. The percentages of core nodes in the single layers that are in the multiplex core are 83.3% for layer 1, 66.7% for layer 2, and 58.3% for layer 3.

labelling of the nodes, the adjacency matrix of the network can be decomposed into four different blocks: a dense diagonal block encoding information on core–core links, a sparser diagonal block describing links among peripheral nodes and two off-diagonal blocks encoding core–periphery edges. The key feature of this block structure is that $\rho_1 \gg \rho_3$, i.e. the density ρ_1 of the core–core block is much higher than that of the periphery–periphery block, ρ_3. As first noted by Borgatti & Everett [4], the density ρ_2 of the off-diagonal blocks is typically not a crucial factor to characterize a core–periphery structure.

To test how our method works on multiplex networks with different structures, we have introduced a model to produce synthetic multiplex networks with tunable core similarity. In particular, we have constructed multiplexes where each of the $M = 2$ layers contains $N = 250$ nodes, only $N_c = 50$ of them belonging to the core. Each layer has the same average node degree $\langle k \rangle = 10$, and the same set of parameters $\rho_1 > \rho_2 > \rho_3$ to describe its core–periphery structure. Our model enables control of the number of nodes that are both in the core of layer 1 and 2. (see Methods for more details).

To quantify the similarity among cores at different layers, we introduce the core similarity $S_c^{[\alpha]}$ of layer α with respect to the other layers as:

$$S_c^{[\alpha]} = \frac{1}{(M-1)} \sum_{\beta \neq \alpha}^{M} \frac{I_c^{[\alpha\beta]}}{N_c^{[\alpha]}}, \tag{2.3}$$

where $I_c^{[\alpha\beta]}$ is the number of nodes in the core of both layer α and layer β, whereas $N_c^{[\alpha]}$ is the size of the core at layer α. The core similarity $S_c^{[\alpha]}$ ranges in [0,1]. When layer α does not share core nodes with any other layers we have $S_c^{[\alpha]} = 0$, when all its core nodes also belong to the cores of the other layers $S_c^{[\alpha]} = 1$, and when on average only half of them are part of the cores on each other level $S_c^{[\alpha]} = 1/2$. The average core similarity of the multiplex can then be computed as $S_c = (1/M) \sum_{\alpha=1}^{M} S_c^{[\alpha]}$.

In figure 2, we show the results for three multiplex networks with different core similarity. In the left column of figure 2, we consider a multiplex with $S_c = 0$. The cores of the two layers are not overlapping, as shown in panel (*a*). As a consequence, many nodes with high degree in one layer have low degree in the other one. When $c^{[1]} = c^{[2]} = 0.5$, the multiplex core of the system is formed by those nodes with sufficiently high multiplex richness, as shown in panel (*b*). In panel (*c*), we show the changes in the multiplex core when we partially ($c^{[1]} = 0.75$, $c^{[2]} = 0.25$, left subplot) or completely ($c^{[1]} = 1$, $c^{[2]} = 0$, right subplot) bias the algorithm towards the first layer.

In the central column of figure 2, we consider a multiplex with $S_c = \frac{1}{2}$. Half of the core nodes are common to both layers while half are typical of each layer. The block structure of the two layers is partially overlapping, and the nodes are spread uniformly over the $k_i^{[2]}$ versus $k_i^{[1]}$ plane. In the unbiased case, the multiplex core of the system is formed by nodes which are part of the core on both layers, but also by nodes scoring extremely high in one layer, despite being in the periphery in the other one (panel *b*). When $c^{[1]} > c^{[2]}$, this is particularly true for nodes which have high richness in the first layer and low richness in the second, while the opposite is much more unlikely (panel *c*).

In the right column of figure 2, we consider a multiplex with $S_c \approx 1$. The block structure of the two layers is now almost identical; the node degrees $k^{[1]}$ and $k^{[2]}$ are correlated

Downloaded from http://rsif.royalsocietypublishing.org/ on September 12, 2018

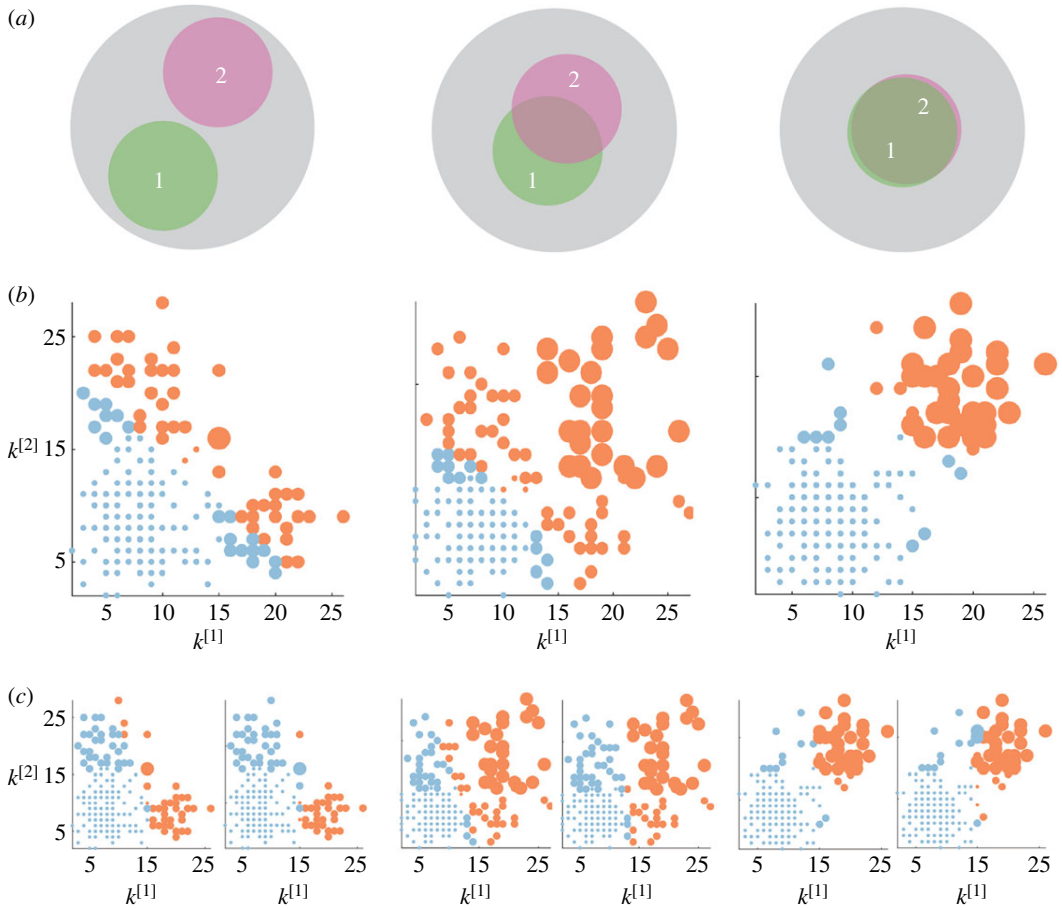

Figure 2. Core–periphery structure in synthetic multiplex networks with different core similarity. In panel (*a*), we sketch multiplex networks with $M = 2$ layers, $N = 250$ nodes and different levels of core similarity, namely $S_c = 0$ (left column), $S_c = \frac{1}{2}$ (central column) and $S_c = 1$ (right column). In panel (*b*), the nodes are placed in a two-dimensional plane according to their degree at each layer. The size of each dot is proportional to the multiplex richness μ_i of the node (unbiased case, $c^{[1]} = c^{[2]} = c = 0.5$). Nodes belonging to the multiplex cores are usually placed in the right-top corner of the plots and are coloured in orange, while the multiplex periphery is in blue. In panel (*c*), we report results obtained for two cases with $c^{[1]} \neq c^{[2]}$, namely: ($c^{[1]} = 0.75$,$c^{[2]} = 0.25$) where the core is biased towards the important nodes of the first layer (left), and ($c^{[1]} = 1$,$c^{[2]} = 0$), where the core corresponds to the core of the first layer (right).

and most of the nodes belonging to each core are in the multiplex core (panel *b*). As the core structure at the two layers are extremely similar, the biased cases do not differ significantly from the unbiased one (panel *c*).

2.3. Merging structure and function to extract the connectome's core

We have applied our method to investigate the human connectome by considering, at the same time, structural and functional information. We have therefore constructed a multiplex brain network formed by one structural layer and one functional layer. The two layers were obtained by first averaging brain connectivity matrices estimated, respectively, from DTI and fMRI data in 171 healthy individuals. Each of the two layers is then thresholded by fixing the average node degree $\langle k \rangle$. We have focused our analysis on 158 regions of interest (ROIs) of the cortex (see Methods for more details).

In figure 3, we report the cores found by analysing the two layers separately, as well as the multiplex core obtained with our method. The figure refers to the case of a representative threshold corresponding to an average node degree $\langle k \rangle = 7$. We notice that the cores of the structural and functional layers are only partially overlapping, with a value of core similarity of $S_c = 0.15$. For the sake of completeness, we also report the S_c values for the entire threshold range (electronic supplementary material, figure S1). A detailed analysis on the robustness of the multiplex core detection in the presence of random fluctuations is reported in the electronic supplementary material, text S1.

As shown in figure 3, ventral brain areas tend in general to form the structural core, while more dorsal regions appear in the functional core. Notably, brain ROIs (electronic supplementary material, table S2) that are in the core of both structural and functional layers also tend to be in the core of the multiplex. Instead, ROIs being in the periphery of both layers tend to be excluded from the multiplex core. However, exceptions may exist depending on the multiplex richness of the nodes. For example, the posterior part of the right precentral gyrus (RCGa3), which is in the periphery of both the structural and functional layer, is eventually assigned to the multiplex core, because of its relatively high rank score in the two layers. The situation appears even less predictable for ROIs that are in the core of one layer and in the periphery of the other layer. Only occasionally these will belong to the multiplex core. This is the case, for example, of the anterior part of right precentral gyrus (RCGa2) which exhibits a relatively low structural richness but high functional richness, i.e. ranked seventh in the functional core, or of the anterior part of the right parietal

Downloaded from http://rsif.royalsocietypublishing.org/ on September 12, 2018

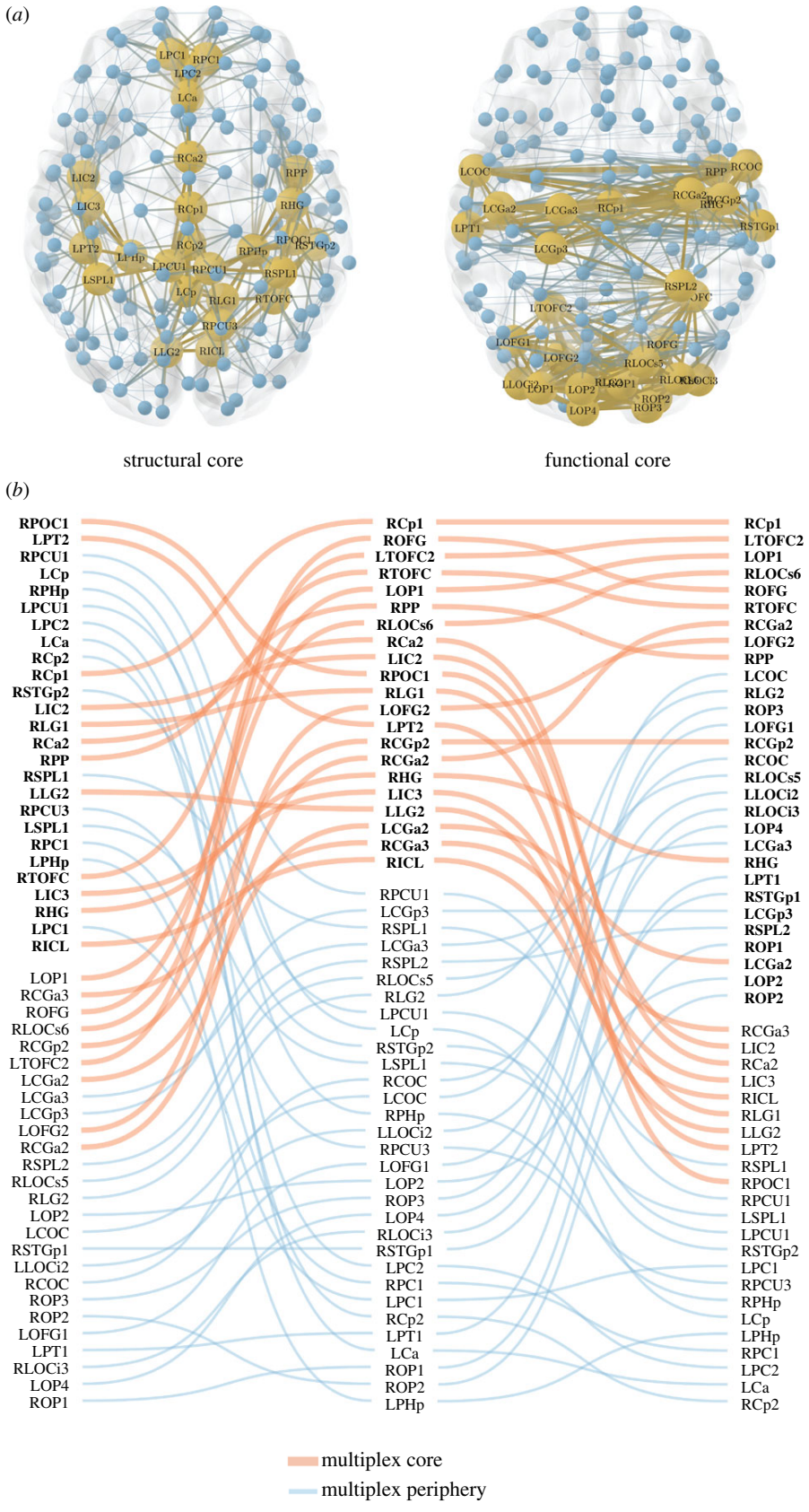

Figure 3. Extracting the multiplex core of the human brain from structural and functional information. (*a*) The structural and functional brain networks filtered with an average node degree $\langle k \rangle = 7$ are shown, respectively, on the left and right side. They are represented from above with the frontal lobe pointing upward. The position of the nodes corresponds to the actual location of the brain ROIs (electronic supplementary material, table S2). Yellow and large nodes represent the brain regions belonging to the core according to the standard single-layer method. Blue and small nodes code for the ROIs in the periphery. Links are yellow and thick if they connect two ROIs in the core, while they are blue and thin if they connect two peripheral nodes. (*b*) ROIs are ranked from top to bottom according to their richness in the structural (left column), functional (right column) and multiplex network (central column). In each column, the labels in bold/normal font stand for the ROIs that are in the core/periphery. For the sake of simplicity, only ROIs that are at least in one core (structural, functional or multiplex) are listed in the three columns. Red/blue and thick/thin lines identify ROIs that go into the core/periphery according to the multiplex approach.

Downloaded from http://rsif.royalsocietypublishing.org/ on September 12, 2018

operculum (RPOC1), which has the highest structural richness but a low functional richness.

2.4. Revealing new core regions of the human brain

We have extracted the multiplex core–periphery structure of the human brain for the full range of available thresholds $\langle k \rangle = 1,2,\ldots,120$ (see Methods for more details). In this way, we have been able to calculate the *coreness* C_i of each node i, defined as the normalized number of thresholds at which the corresponding ROI is present in the rich core. This allows us to rank ROIs according to their likelihood to be part of the multiplex core and to compare these to the rankings obtained separately for structural and functional layers. We note that the same approach of investigating the persistence across a set of different filtering thresholds can be applied to any node property. This can turn useful for statistical validation in the case no threshold is universally accepted, as often happens for brain networks [38–40].

Parietal (pre/cuneus PCU/LOC, superior parietal lobe SPL), cingulate (anterior Ca, posterior Cp), temporal (superior temporal gyrus), insular (insular cortex IC), as well as frontal ROIs (paracingulate PC) mainly constitute the structural core, as shown in electronic supplementary material, figure S2. While some overlap exists between the structural and the functional cores, the latter rather tends instead to include occipital (occipital fusiform gyrus OFG, temporo-occipital fusiform cortex TOFC) and central (pre/post central gyrus CGa/CGp) ROIs and, notably, to exclude regions in the frontal lobe (top 25% ROIs, electronic supplementary material, figure S3).

Figure 4 shows the coreness of the multiplex network. As expected, ROIs that are peripheral (i.e. low coreness) in both layers are also peripheral in the multiplex, while ROIs with both a high structural and high functional coreness are typically observed in the multiplex core (e.g. TOFC, OFG, Ca, Cp). Interesting behaviours emerge for those regions typically characterized by high coreness in one layer and low coreness in the other layer. In fact, some of these ROIs are part of the multiplex core, while others are usually found in the multiplex periphery, as shown in figure 5*a*. For areas with a different assignment in the two layers, we note that the main contribution to the multiplex richness μ_i comes from the richness in the layer where node i is identified as core. Interestingly, not only is the average richness of the node in the core layer higher than the one in the peripheral layer, but also its fluctuations around the mean.

As a consequence, among regions that are core in the structural layer but peripheral in the functional one, those with relatively higher structural richness (degree), such as precuneus PCU, insular cortex IC and posterior cingulate Cp, finally tend to join the multiplex core no matter the exact value of their functional richness (upper right corner of figure 5*a*). Conversely, ROIs with relatively lower structural degree are usually peripheral in the multiplex, and typically located in the pre-frontal cortex PC and frontal lobe FP (lower right corner of figure 5*a*), as illustrated in figure 5*b*,*c*. Similarly, among areas in the functional core, those with relatively higher functional degree, such as precentral gyrus CGa and central operculum COC, tend to join the multiplex core (upper left corner of figure 5*a*). By contrast, ROIs with relatively lower functional degree, are mostly peripheral in the multiplex, and are located in the parietal operculum POC and superior frontal gyrus SFG (lower left corner of figure 5*a*).

In a separate analysis, we have extracted the multiplex brain coreness from each individual and we show that, despite a normal inter-subject variability, the average multiplex brain coreness is very similar to the multiplex coreness of the group-averaged brain networks (electronic supplementary material, figure S4). Finally, we have evaluated the robustness of the results when also including subcortical ROIs in the brain networks. We report that thalamus, putamen and hippocampus are among the regions with highest coreness and therefore become part of the multiplex core (electronic supplementary material, figure S5). Interestingly, their presence does not significantly alter the coreness of the other ROIs (electronic supplementary material, figure S6), suggesting an assortative structure where highly connected subcortical regions preferentially get connected with core regions in the cortex.

3. Discussion

The existence of a network core in the brain is a prerequisite for neural functioning and cognition, and damage to the core have been associated with several neurological or psychiatric diseases [19,41,42]. Finding the router regions that ensure integration between the different brain modules and communication in the system is therefore a fundamental question in neuroscience. Previous studies have mainly considered the structural connectivity of the brain through disparate techniques, such as *k*-core decomposition, centrality measures and rich-club analysis [17,24]. While the results obtained agree on the implication of posterior medial and parietal cortical regions—as well as subcortical thalamus, putamen and hippocampus—in the network core [17,24], they neglect the possible role of other areas that are crucial from a functional perspective, such as those in the default-mode network (DMN) [25].

To integrate information from both structural and functional brain connectivity at the network level, we introduce a general criterion to define and extract the core when nodes are connected through links which can vary in meaning and nature, and the whole system can be described as a network with multiple layers [28–32]. Compared to standard approaches, this method has the theoretical advantage of providing a more robust solution, taking into account the relative importance of the nodes at each layer, rather than simply considering the union or intersection of the cores across layers, or extracting the core from the aggregated network.

The results obtained shed new light on the role of the regions characterizing the intrinsic brain function to eventually form the core of the human brain. First, we show that mPFC (e.g. PC and FP), exhibiting a high structural but low functional coreness, is eventually assigned to the periphery (figure 5*a*, lower-right corner). This outcome can be predicted by the lower multiplex richness and relatively low structural degree, and not solely by the attitude of frontal areas to be peripheral in the functional brain network (figure 5*b*,*c*). The exclusion of the mPFC from the rich core supports the hypothesis that default-mode network activity may be mainly driven from highly coupled areas of the posterior medial and parietal cortex, which in turn link to other highly connected regions, such as the medial orbitofrontal cortex [24].

Downloaded from http://rsif.royalsocietypublishing.org/ on September 12, 2018

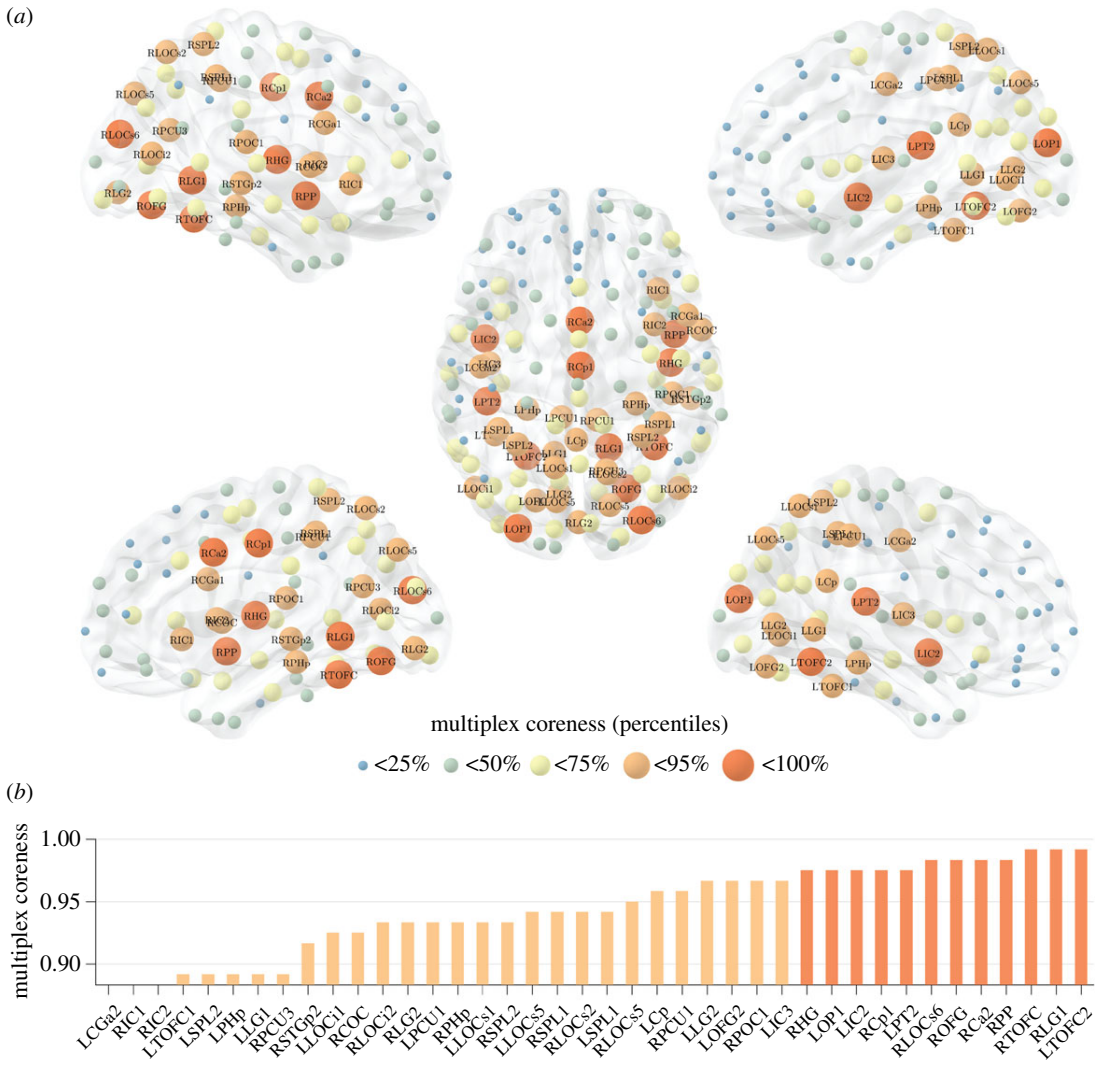

Figure 4. The multiplex core of the human connectome. Panel (*a*) shows the human brain, where ROIs are highlighted based on their multiplex coreness. The colour and size of the nodes are associated with the percentiles of multiplex coreness in each brain region, so that core nodes are larger in size and coloured in red. The left side shows the lateral view of the left hemisphere (top, dorsal; bottom, ventral). The right side shows the lateral view of the right hemisphere (top, dorsal; bottom, ventral). In the middle, the brain is shown from above, with the frontal lobe pointing upward. In panel (*b*), we report the ROIs corresponding to the 25% highest values of multiplex coreness. The colour follows the same legend as in panel (*a*).

Second, while frontal ROIs are excluded, new regions gain importance and become part of the core because of their higher multiplex richness (see figure 5*a*, upper left corner). Among them, we report areas of the central gyrus (CGa, CGp to a minor extent), which are characterized by a low structural but relatively high functional degree, as shown in figure 5*b*,*c*. These regions are part of the primary sensori-motor cortex, which has been shown to be the most extensive of the resting-state components, or networks (out of eight [43]), covering 27% of the total grey matter in the brain [44]. The primary sensori-motor component has a high degree of integration (overlap and activity coupling) with all other resting-state networks (e.g. DMN), which is consistent with the increased synchronization of neural activity in cortical regions during sensory processing [45]. Notably, ongoing functional connectivity in the primary sensori-motor network, originally revealed by seed-based analysis [46,47], has been extensively verified by ICA and clustering methods [48,49].

Our method provides an effective tool to integrate mesoscale topological information in brain networks derived from multimodal neuroimaging data. Multimodal integration of brain networks is gaining more and more interest [50–53] due, on the one hand, to the increasing availability of large heterogeneous datasets (e.g. HCP http://www.humanconnectomeproject.org, ADNI http://adni.loni.usc.edu) and, on the other hand, to the need of principled ways to characterize multiscale neural mechanisms (e.g. cross-frequency coupling) and to provide predictive diagnostics for multifactor brain diseases, such as Alzheimer's disease.

It is important to note, that our analysis of the human connectome relies on the assumption that each layer contributes with the same intensity to the definition of the multiplex core. In general, however, the contribution of a layer α can be weighted differently through a choice of the parameter $c^{[\alpha]}$, and this can be used to enhance or reduce the importance of the different types of connectivity. A larger value of $c^{[\alpha]}$ increases the relevance of the corresponding layer until when, in the limit in which $c^{[\alpha]} \to 1$ and the coefficients of all the other layers go to zero, the multiplex core is no longer defined by the topology of all the M layers, but coincides with the core at layer α. For instance,

Downloaded from http://rsif.royalsocietypublishing.org/ on September 12, 2018

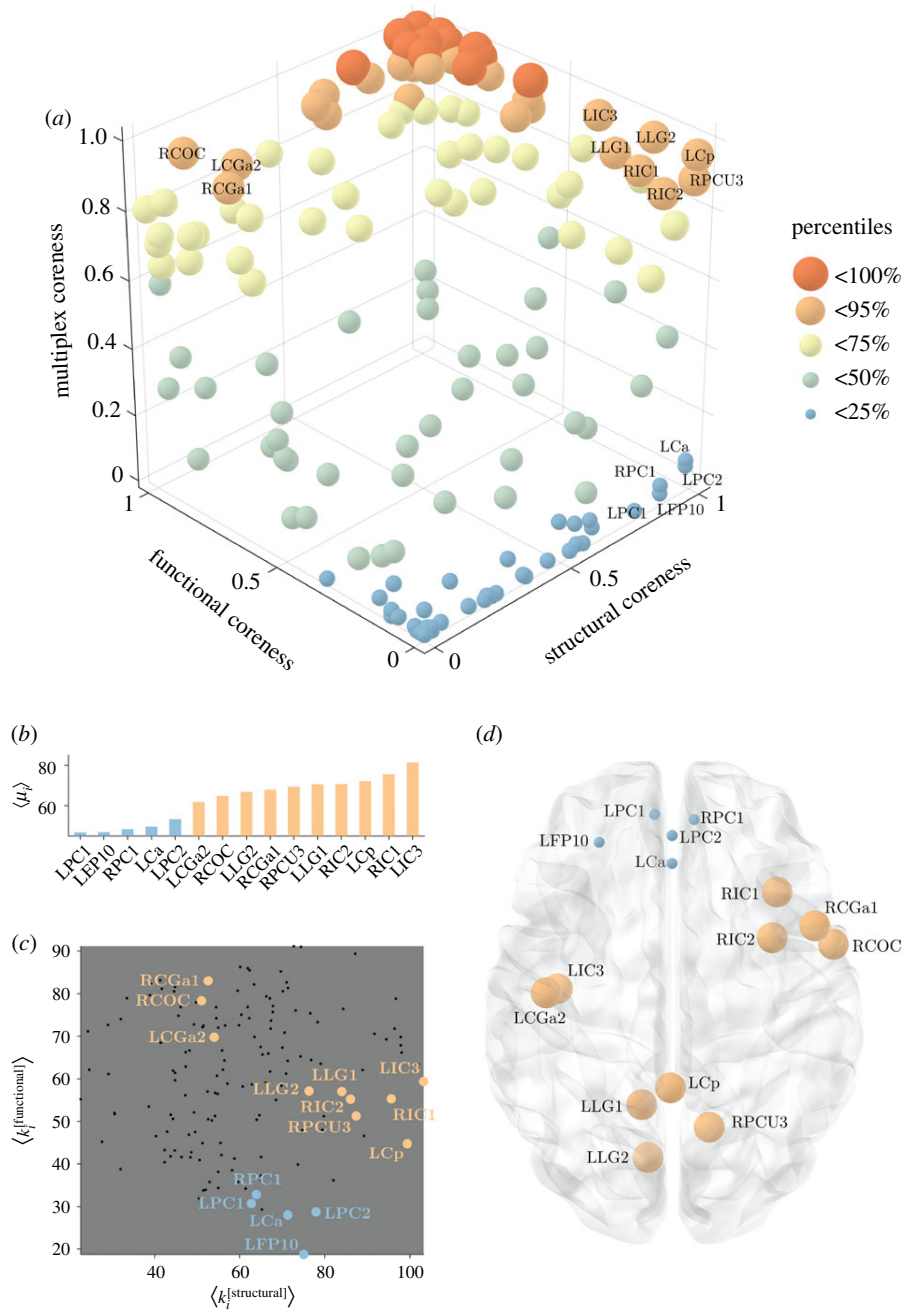

Figure 5. Emergent non-trivial core regions in the multiplex brain. Panel (*a*) shows the scatter plot of the structural, functional and multiplex coreness of the ROIs in the brain. The colour and size of the nodes are associated with the percentile of multiplex coreness across the set of brain regions, as in figure 4. Panel (*b*) reports the average value of multiplex richness $\langle \mu_i \rangle$ across the different thresholds for the ROIs with the strongest differences in structural and functional coreness. The colour follows the same legend as in panel (*a*). Panel (*c*) illustrates the distribution of the ROIs (black points) as a function of their averaged structural and functional degree across all the thresholds. Only the ROIs listed in panel (*b*) are highlighted according to the same colour legend as in panel (*a*).

setting $c^{[\text{structural}]} = 1$ and $c^{[\text{functional}]} = 0$ returns a core based on the anatomical information only, and in agreement with most of the previous literature on such topic (see electronic supplementary material, figure S2). As an unbiased way to characterize the multiplex core of the human brain, we have focused our analysis on the simplest and symmetric case, $c^{[\text{structural}]} = c^{[\text{functional}]} = 0.5$. We show in electronic supplementary material, figure S7 that the results are relatively stable for small perturbations around this unbiased condition. However, other combinations are in general possible and should be adopted if supported by a plausible rationale. For example, in the case of multifrequency brain networks one could assign different weights to the network layers taking into account the frequency scaling of the brain activity's power spectra [54,55].

In practice, the proposed method to detect the core–periphery organization of multiplex networks has two clear advantages: (i) it is fast and scalable, since it works using only local information; (ii) it is non-parametric, e.g. no need to input *a priori* information such as the core size. Moreover, it can be generalized in a straightforward way to the case of directed networks. A drawback of the method is that it focuses on highly connected rich nodes, and neglects the possible important role of the so-called *connectors*, i.e. central nodes with low degree [56]. We note that alternative core–periphery structures which include connectors can be

Downloaded from http://rsif.royalsocietypublishing.org/ on September 12, 2018

detected by more computationally demanding methods such as those based on stochastic block models, which have been recently proposed to extract the mesoscale structure of time-varying and multilayer networks [57]. We hope that our work can trigger further developments in the exploration of core–periphery structure of real-world large-scale multiplex networks.

To conclude, our method to investigate multiplex core–periphery organization in complex networks suggests that the core of the human cortex is made up of known cortical and subcortical hubs, as well as of areas in the sensorimotor system that were previously overlooked by standard approaches, but that are crucial for the brain functioning. Our findings offer an augmented definition of the rich core of the human brain, which takes into account not only the anatomical structure but also its function.

We hope that our work will contribute to advance our understanding of the mesoscale connectivity mechanisms in multiplex brain networks, in an effort to better integrate the one-to-many relationships that exist between structure and function in the human brain [26].

4. Methods

4.1. Multiplex stochastic block model with tunable core similarity

Stochastic block models for multiplex networks have been recently introduced by Peixoto [57]. Here, we introduce a stochastic block model that enables sampling of multiplex networks with an assigned value of core similarity S_C (see equation (3)). Suppose we have N nodes and we want to construct a multiplex network having a core–periphery structure at each layer $\alpha = 1, \ldots, M$, with $N_c^{[\alpha]}$ nodes in the core of layer α.

In particular, we set $M = 2$, $N = 250$, $N_c^{[1]} = N_c^{[2]} = N_c = 50$, and we create at each layer a core–periphery structure with the same set of densities: $\rho_1 = 0.2$, $\rho_2 = 0.04$ and $\rho_3 = 0.03$. Namely, for each of the two layers, we connect with a probability ρ_1 two nodes both in the core, with probability ρ_2 a node in the core and a node in the periphery, and finally with probability ρ_3 two peripheral nodes. The values of the three parameters were chosen in a way that $\langle k \rangle = 10$ on both layers, and the core–periphery structure of each layer is sufficiently strong to be detected with good accuracy, as discussed in the electronic supplementary material, text S2.

Different levels of core similarity are achieved by varying the overlap between core nodes at the two layers. When the two sets of core nodes are completely overlapping, $S_c = 1$, whereas when the two sets are disjoint $S_c = 0$. Despite other related formulations of S_c are possible, our definition reflects the intuition that when two layers with equal core size share half of the core nodes, then $S_c = \frac{1}{2}$.

4.2. Multiplex richness μ_i and μ_i^+

The multiplex richness μ_i and μ_i^+ introduced in equations (1) and (2) are obtained by means of a simple aggregation of information based on the single layers. In the simplest set-up $c^{[\alpha]} = c = 1/M$ for $\alpha = 1, \ldots, M$, and the multiplex richness μ_i of a node i is simply proportional to its overlapping degree o_i [31]. A layer with higher density weighs more in the computation of the multiplex core of a network.

In general, coefficients $c^{[\alpha]}$ can be used to modulate the relevance of the layers of the network in order to extract its core. If one wants to have equal contributions to μ_i and μ_i^+ from all the layers but their number of links $K^{[\alpha]}$ is different—for instance, because in some layers it might be easier to establish or measure a connection than in others—a natural choice is to set $c^{[\alpha]}$ to be proportional to $1/K^{[\alpha]}$. In other cases, independently from their density, it might be reasonable to assign different importance to different layers, because of exogenous information. Once again this can be achieved by assigning different values of the coefficients $c^{[\alpha]}$.

Our method inherits many advantageous properties of the original algorithm proposed for single-layer networks [16]. First, it can be easily extended to directed layers by replacing $k_i^{[\alpha]}$ with $(k_i^{[\alpha],\mathrm{in}} + k_i^{[\alpha],\mathrm{out}})/2$ in equation (1), where $k_i^{[\alpha],\mathrm{in}}$ and $k_i^{[\alpha],\mathrm{out}}$ correspond, respectively, to the in-degree and out-degree of node i at layer α, and by substituting $k_i^{[\alpha]+}$ with $(k_i^{[\alpha],\mathrm{in}+} + k_i^{[\alpha],\mathrm{out}+})/2$ in equation (2). Second, for weighted networks μ_i and μ_i^+ can be obtained by replacing the adjacency matrix binary entries $a_{ij}^{[\alpha]}$ with their weighted counterparts $w_{ij}^{[\alpha]}$, and by substituting the node degree with the strength $s_i^{[\alpha]} = \sum_{j \neq i} w_{ij}^{[\alpha]}$. Third, the core size is relatively stable with respect to randomly chosen different rankings of nodes with equal degree.

We finally notice that equation (1) is a particular choice of a more general scenario, where the multiplex richness μ_i is a generic function f of the degree of a node at the different layers:

$$\mu_i = f(k_i^{[1]}, \ldots, k_i^{[M]}) \tag{4.1}$$

and μ_i^+ is a generic function g:

$$\mu_i^+ = g(k_i^{+[1]}, \ldots, k_i^{+[M]}). \tag{4.2}$$

4.3. Multimodal brain networks

We have considered 171 healthy human subjects from the NKI Rockland dataset http://fcon_1000.projects.nitrc.org/indi/pro/nki.html. We have used diffusion weighted magnetic resonance imaging (dwMRI) and fMRI to derive, respectively, structural and functional brain networks in each subject.

We have gathered the corresponding connectivity matrices from the USC Multimodal Connectivity Database (http://umcd.humanconnectomeproject.org) [58].

In particular, structural connectivity has been obtained using anatomical fibre assignment through the continuous tracking (FACT) algorithm [59]. Functional connectivity has been computed by means of the Pearson's correlation coefficient between fMRI signals recorded during a 10 min resting state (RS). RS-based functional connectivity measures the amount of interaction—or temporal dependence—between different brain areas during spontaneous brain activity [27]. More details about the processing steps can be found here [60]. A total number of $N = 188$ ROIs are available for both structural and functional brain networks, thus resulting in connectivity matrices of size $N \times N$, spatially matched with the MNI152 template [61].

Because we are mainly interested in cortical networks, we focused our analysis on the network obtained by removing all subcortical ROIs and obtained connectivity matrices of size 158×158. The full names and acronyms for all the ROIs can be found in electronic supplementary material, table S1. We have then averaged the resulting connectivity matrices (after Fisher transformation) across subjects in order to have a population-level representation. At the end, we obtained a structural weighted connectivity matrix $\mathcal{S}$, whose entry $s_{ij} = s_{ji}$ contain the group-average number of axonal fibres between ROIs i and j, and a functional weighted connectivity matrix $\mathcal{F}$, whose entry $f_{ij} = f_{ji}$ correspond to the group-average correlation coefficient between the fMRI signals of ROIs i and j.

We have used density-based thresholding to derive structural and functional brain networks by removing the lowest values

Downloaded from http://rsif.royalsocietypublishing.org/ on September 12, 2018

from the connectivity matrices and binarizing the remaining ones [27]. We have considered a full range of density thresholds, corresponding to an increasing average node degree $\langle k \rangle = 1,2,\ldots,120$. The last value was given by the maximal $\langle k \rangle$ observed in the native structural connectivity matrices, which are originally not fully connected. After filtering, for each threshold we have combined the resulting structural and functional brain networks into a multiplex network $\mathcal{M} = \{\mathcal{S}, \mathcal{F}\}$.

Data accessibility. All the experimental data used in this work can be downloaded from the USC Multimodal Connectivity Database http://umcd.humanconnectomeproject.org. The Matlab code used to compute the core–periphery structure of multiplex networks is made available at https://github.com/brain-network/bnt.

Authors' contributions. F.B. carried out the theoretical work, participated in data analysis, participated in the design of the study and drafted the manuscript; J.G. participated in data analysis and drafted the manuscript; M.C. conceived and designed the study, and helped draft the manuscript. V.L. conceived the study and drafted the manuscript; F.D.V.F. coordinated the study, participated in the design of the study, participated in data analysis and drafted the manuscript. All authors gave final approval for publication.

Competing interests. We have no competing interests.

Funding. F.D.V.F. and M.C. acknowledge support by the ANR French programme through the contracts ANR-10-IAIHU-06 and ANR-15-NEUC-0006-02. The funders had no role in study design, data collection and analysis, decision to publish or preparation of the manuscript.

Reference

1. Milo R, Shen-Orr S, Itzkovitz S, Kashtan N, Chklovskii D, Alon U. 2002 Network motifs: simple building blocks of complex networks. *Science* **298**, 824–827. (doi:10.1126/science.298.5594.824)
2. Girvan M, Newman MEJ. 2002 Community structure in social and biological networks. *Proc. Natl Acad. Sci. USA* **99**, 7821–7826. (doi:10.1073/pnas.122653799)
3. Fortunato S. 2010 Community detection in graphs. *Phys. Rep.* **486**, 75–174. (doi:10.1016/j.physrep.2009.11.002)
4. Borgatti SP, Everett MG. 2000 Models of core/periphery structures. *Soc. Networks* **21**, 375–395. (doi:10.1016/S0378-8733(99)00019-2)
5. Csermely P, London A, Wu L-Y, Uzzi B. 2013 Structure and dynamics of core/periphery networks. *J. Complex Networks* **1**, 93–123. (doi:10.1093/comnet/cnt016)
6. Rombach M, Porter M, Fowler J, Mucha P. 2014 Core–periphery structure in networks. *SIAM J. Appl. Math.* **74**, 167–190. (doi:10.1137/120881683)
7. Boyd JP, Fitzgerald WJ, Mahutga MC, Smith DA. 2010 Computing continuous core/periphery structures for social relations data with MINRES/SVD. *Soc. Networks* **32**, 125–137. (doi:10.1016/j.socnet.2009.09.003)
8. Zhang X, Martin T, Newman MEJ. 2015 Identification of core–periphery structure in networks. *Phys. Rev. E* **91**, 032803. (doi:10.1103/PhysRevE.91.032803)
9. Luo F, Li B, Wan X-F, Scheuermann RH. 2009 Core and periphery structures in protein interaction networks. *BMC Bioinformatics* **10**, S8. (doi:10.1186/1471-2105-10-S4-S8)
10. Barucca P, Lillo F. 2016 Disentangling bipartite and core–periphery structure in financial networks. *Chaos Solitons Fractals* **88**, 244–253. (doi:10.1016/j.chaos.2016.02.004)
11. Verma T, Russmann F, Araújo NaM, Nagler J, Herrmann HJ. 2016 Emergence of core–peripheries in networks. *Nat. Commun.* **7**, 10441. (doi:10.1038/ncomms10441)
12. Fagiolo G, Reyes J, Schiavo S. 2010 The evolution of the world trade web: a weighted-network analysis. *J. Evol. Econ.* **20**, 479–514. (doi:10.1007/s00191-009-0160-x)
13. Colizza V, Flammini A, Serrano MA, Vespignani A. 2006 Detecting rich-club ordering in complex networks. *Nat. Phys.* **2**, 110–115. (doi:10.1038/nphys209)
14. Zhou S, Mondragon RJ. 2004 The rich-club phenomenon in the Internet topology. *IEEE Commun. Lett.* **8**, 180–182. (doi:10.1109/LCOMM.2004.823426)
15. Vaquero LM, Cebrian M. 2013 The rich club phenomenon in the classroom. *Sci. Rep.* **3**, 1174. (doi:10.1038/srep01174)
16. Ma A, Mondragón RJ. 2015 Rich-cores in networks. *PLoS ONE* **10**, e0119678. (doi:10.1371/journal.pone.0119678)
17. Heuvel MPvd, Sporns O. 2011 Rich-club organization of the human connectome. *J. Neurosci.* **31**, 15 775–15 786. (doi:10.1523/JNEUROSCI.3539-11.2011)
18. Harriger L, Heuvel MPvd, Sporns O. 2012 Rich club organization of macaque cerebral cortex and its role in network communication. *PLoS ONE* **7**, e46497. (doi:10.1371/journal.pone.0046497)
19. van den Heuvel MP, Sporns O, Collin G, Scheewe T, Mandl RCW, Cahn W, Goñi J, Hulshoff Pol HE, Kahn RS. 2013 Abnormal rich club organization and functional brain dynamics in schizophrenia. *JAMA Psychiatry* **70**, 783–792. (doi:10.1001/jamapsychiatry.2013.1328)
20. Ball G *et al.* 2014 Rich-club organization of the newborn human brain. *Proc. Natl Acad. Sci. USA* **111**, 7456–7461. (doi:10.1073/pnas.1324118111)
21. Bertolero MA, Yeo BTT, D'Esposito M. 2017 The diverse club. *Nat. Commun.* **8**, 1277. (doi:10.1038/s41467-017-01189-w)
22. Bullmore E, Sporns O. 2009 Complex brain networks: graph theoretical analysis of structural and functional systems. *Nat. Rev. Neurosci.* **10**, 186–198. (doi:10.1038/nrn2575)
23. Stam CJ. 2014 Modern network science of neurological disorders. *Nat. Rev. Neurosci.* **15**, 683–695. (doi:10.1038/nrn3801)
24. Hagmann P, Cammoun L, Gigandet X, Meuli R, Honey CJ, Wedeen VJ, Sporns O. 2008 Mapping the structural core of human cerebral cortex. *PLoS Biol.* **6**, e159. (doi:10.1371/journal.pbio.0060159)
25. Buckner RL, Andrews-Hanna JR, Schacter DL. 2008 The brain's default network. *Ann. NY Acad. Sci.* **1124**, 1–38. (doi:10.1196/annals.1440.011)
26. Friston KJ. 2011 Functional and effective connectivity: a review. *Brain Connect* **1**, 13–36. (doi:10.1089/brain.2011.0008)
27. De Vico Fallani F, Richiardi J, Chavez M, Achard S. 2014 Graph analysis of functional brain networks: practical issues in translational neuroscience. *Phil. Trans. R. Soc. B* **369**, 20130521. (doi:10.1098/rstb.2013.0521)
28. De Domenico M, Solé-Ribalta A, Cozzo E, Kivelä M, Moreno Y, Porter MA, Gómez S, Arenas A. 2013 Mathematical formulation of multilayer networks. *Phys. Rev. X* **3**, 041022. (doi:10.1103/PhysRevX.3.041022)
29. Kivelä M, Arenas A, Barthelemy M, Gleeson JP, Moreno Y, Porter MA. 2014 Multilayer networks. *J. Complex Networks* **2**, 203–271. (doi:10.1093/comnet/cnu016)
30. Boccaletti S, Bianconi G, Criado R, del Genio CI, Gómez-Gardeñes J, Romance M, Sendiña-Nadal I, Wang Z, Zanin M. 2014 The structure and dynamics of multilayer networks. *Phys. Rep.* **544**, 1–122. (doi:10.1016/j.physrep.2014.07.001)
31. Battiston F, Nicosia V, Latora V. 2014 Structural measures for multiplex networks. *Phys. Rev. E* **89**, 032804. (doi:10.1103/PhysRevE.89.032804)
32. Battiston F, Nicosia V, Latora V. 2017 The new challenges of multiplex networks: measures and models. *Eur. Phys. J. Spec. Top.* **226**, 401–416. (doi:10.1140/epjst/e2016-60274-8)
33. Battiston F, Nicosia V, Chavez M, Latora V. 2017 Multilayer motif analysis of brain networks. *Chaos* **27**, 047404. (doi:10.1063/1.4979282)
34. De Domenico M, Sasai S, Arenas A. 2016 Mapping multiplex hubs in human functional brain networks. *Front. Neurosci.* **10**, 326. (doi:10.3389/fnins.2016.00326)
35. Guillon J, Attal Y, Colliot O, Corte VL, Dubois B, Schwartz D, Chavez M, De Vico Fallani F. 2017 Loss of brain inter-frequency hubs in Alzheimer's disease. *Sci. Rep.* **7**, 10879. (doi:10.1038/s41598-017-07846-w)
36. Azimi-Tafreshi N, Gómez-Gardeñes J, Dorogovtsev SN. 2014 K-core percolation on multiplex networks.

Downloaded from http://rsif.royalsocietypublishing.org/ on September 12, 2018

Phys. Rev. E Stat. Nonlin. Soft Matter Phys. **90**, 032816. (doi:10.1103/PhysRevE.90.032816)

37. Corominas-Murtra B, Thurner S. 2016 The weak core and the structure of elites in social multiplex networks. In *Interconnected networks, understanding complex systems* (ed. A Garas), pp. 165–177. Cham, Switzerland: Springer.
38. van Wijk BCM, Stam CJ, Daffertshofer A. 2010 Comparing brain networks of different size and connectivity density using graph theory. *PLoS ONE* **5**, e13701. (doi:10.1371/journal.pone.0013701)
39. Fornito A, Zalesky A, Breakspear M. 2013 Graph analysis of the human connectome: promise, progress, and pitfalls. *NeuroImage* **80**, 426–444. (doi:10.1016/j.neuroimage.2013.04.087)
40. De Vico Fallani F, Latora V, Chavez M. 2017 A topological criterion for filtering information in complex brain networks. *PLoS Comput. Biol.* **13**, e1005305. (doi:10.1371/journal.pcbi.1005305)
41. Gollo LL, Zalesky A, Hutchison RM, van den Heuvel M, Breakspear M. 2015 Dwelling quietly in the rich club: brain network determinants of slow cortical fluctuations. *Phil. Trans. R. Soc. B* **370**, 20140165. (doi:10.1098/rstb.2014.0165)
42. Daianu M, Jahanshad N, Nir TM, Jack CR, Weiner MW, Bernstein MA, Thompson PM. 2015 Alzheimer's disease neuroimaging initiative. Rich club analysis in the Alzheimer's disease connectome reveals a relatively undisturbed structural core network. *Hum. Brain Mapp.* **36**, 3087–3103. (doi:10.1002/hbm.22830)
43. Heuvel MPvd, Pol HEH. 2010 Exploring the brain network: a review on resting-state fMRI functional connectivity. *Eur. Neuropsychopharmacol.* **20**, 519–534. (doi:10.1016/j.euroneuro.2010.03.008)
44. Tomasi D, Volkow ND. 2011 Association between functional connectivity hubs and brain networks. *Cereb. Cortex* **21**, 2003–2013. (doi:10.1093/cercor/bhq268)
45. Srinivasan R, Russell DP, Edelman GM, Tononi G. 1999 Increased synchronization of neuromagnetic responses during conscious perception. *J. Neurosci.* **19**, 5435–5448. (doi:10.1523/jneurosci.19-13-05435.1999)
46. Biswal B, Zerrin Yetkin F, Haughton VM, Hyde JS. 1995 Functional connectivity in the motor cortex of resting human brain using echo-planar MRI. *Magn. Reson. Med.* **34**, 537–541. (doi:10.1002/mrm.1910340409)
47. Xiong J, Parsons LM, Gao JH, Fox PT. 1999 Interregional connectivity to primary motor cortex revealed using MRI resting state images. *Hum. Brain Mapp.* **8**, 151–156. (doi:10.1002/(sici)1097-0193(1999)8:2/3<151::aid-hbm13>3.0.co;2-5)
48. Salvador R, Suckling J, Coleman M, Pickard J, Menon D, Bullmore E. 2005 Neurophysiological architecture of functional magnetic resonance images of human brain. *Cereb. Cortex* **15**, 1332–2342. (doi:10.1093/cercor/bhi016)
49. Damoiseaux J, Rombouts S, Barkhof F, Scheltens P, Stam C, Smith S, Beckmann C. 2006 Consistent resting-state networks across healthy subjects. *Proc. Natl Acad. Sci. USA* **103**, 13 848–13 853. (doi:10.1073/pnas.0601417103)
50. Rykhlevskaia E, Gratton G, Fabiani M. 2008 Combining structural and functional neuroimaging data for studying brain connectivity: a review. *Psychophysiology* **45**, 173–187. (doi:10.1111/j.1469-8986.2007.00621.x)
51. Lei X, Ostwald D, Hu J, Qiu C, Porcaro C, Bagshaw AP, Yao D. 2011 Multimodal functional network connectivity: an EEG-fMRI fusion in network space. *PLoS ONE* **6**, e24642. (doi:10.1371/journal.pone.0024642)
52. Simas T, Chavez M, Rodriguez PR, Diaz-Guilera A. 2015 An algebraic topological method for multimodal brain networks comparisons. *Front. Psychol.* **6**, 904. (doi:10.3389/fpsyg.2015.00904)
53. Amico E, Goñi J. 2017 Mapping hybrid functional-structural connectivity traits in the human connectome, [q-bio]. arXiv (http://arxiv.org/abs/1710.02199)
54. Bédard C, Kröger H, Destexhe A. 2006 Does the 1/f frequency scaling of brain signals reflect self-organized critical states? *Phys. Rev. Lett.* **97**, 118102. (doi:10.1103/PhysRevLett.97.118102)
55. Dehghani N, Bédard C, Cash SS, Halgren E, Destexhe A. 2010 Comparative power spectral analysis of simultaneous elecroencephalographic and magnetoencephalographic recordings in humans suggests non-resistive extracellular media. *J. Comput. Neurosci.* **29**, 405–421. (doi:10.1007/s10827-010-0263-2)
56. Corominas-Murtra B, Fuchs B, Thurner S. 2014 Detection of the elite structure in a virtual multiplex social system by means of a generalised K-core. *PLoS ONE* **9**, e112606. (doi:10.1371/journal.pone.0112606)
57. Peixoto TP. 2015 Inferring the mesoscale structure of layered, edge-valued, and time-varying networks. *Phys. Rev. E* **92**, 042807. (doi:10.1103/PhysRevE.92.042807)
58. Brown JA, Van Horn JD. 2016 Connected brains and minds—the UMCD repository for brain connectivity matrices. *NeuroImage* **124**, 1238–1241. (doi:10.1016/j.neuroimage.2015.08.043)
59. Mori S, van Zijl PCM. 2002 Fiber tracking: principles and strategies—a technical review. *NMR Biomed.* **15**, 468–480. (doi:10.1002/nbm.781)
60. Brown JA, Rudie JD, Bandrowski A, Van Horn JD, Bookheimer SY. 2012 The UCLA multimodal connectivity database: a web-based platform for brain connectivity matrix sharing and analysis. *Front. Neuroinform.* **6**, 28. (doi:10.3389/fninf.2012.00028)
61. Craddock RC, James G, Holtzheimer PE, Hu XP, Mayberg HS. 2012 A whole brain fMRI atlas generated via spatially constrained spectral clustering. *Hum. Brain Mapp.* **33**, 1914–1928. (doi:10.1002/hbm.21333)

View publication stats

CHAPTER 6

Impact of AD on the multimodal core-periphery organization

In this chapter, we apply again the previously defined core-periphery structure, and use its associated coreness index to study multimodal hub disruption in Alzheimer's disease. We show that core brain regions are the more susceptible to become peripheral as a consequence of the disease. We also show that the multimodal coreness is correlated with memory test scores (MMSE and FCSRT) in regions associated to working memory and language processing.

This chapter will soon be submitted as a journal article. I chose to incorporate it in this thesis as a whole in order to get a clear idea on what it should look like when it will be published.

Abstract

Many neurodegenerative diseases are recognized to include a disconnection syndrome initiated by the neuronal atrophy process. In Alzheimer's disease (AD), the progressive destruction of axonal pathways leads to aberrant network reconfigurations both at the structural and functional level. In such network reorganization, the core and peripheral nodes appear to be crucial for the prediction of clinical outcome due to their ability to influence large-scale functional integration. However, the role of the different types of brain connectivity in such prediction still remains unclear. Using a multiplex network approach, we integrated information from DWI, fMRI and MEG brain connectivity to extract an enriched description of the core-periphery structure in a group of AD patients and age-matched subjects. Results showed that the multiplex coreness - i.e., the probability of a region to be in the core - was mainly driven by DWI structural connectivity with significant contributions of fMRI and MEG functional connectivity, respectively at 0.1-0.3Hz and 8-10Hz. At the global scale, the multiplex coreness was significantly decreased in AD patients as a result of the randomization process initiated by the neurodegeneration. At the local scale, the most affected brain areas, such as medial temporal and occipital regions, tended to be in the core of the network and not in its periphery. In addition, the multiplex coreness significantly predicted the cognitive and memory impairment of patients as measured respectively by the MMSE and free-recall scores. Taken together these results indicate that a more accurate description of neurodegenerative diseases can be obtained from the multimodal integration of neuroimaging-derived network data.

I Introduction

The brain is a complex network where differently specialized areas are anatomically and functionally connected. Because of such interconnected structure, focal damages can affect the rest of the network through the interruption of communication pathways. Indeed, many neurological disorders affecting language, motor and sensory abilities are often due to a disconnection syndrome caused by the anatomical connectivity breakdown between the relevant

brain areas (SCHMAHMANN and PANDYA 2008). In the case of neurodegenerative diseases, the disconnection hypothesis is theoretically supported by a progressive death of neurons and synapses that induce gross atrophy. Empirical evidence has shown that Alzheimer's disease (AD) patients with severe motor and cognitive impairments exhibited anatomical disconnections among regions between cerebral hemispheres that resemble those observed in split-brain subjects (Delbeuck, Collette, and der Linden 2007; Lakmache et al. 1998). In Parkinson's disease (PD) intrahemispheric dissociations between subcortical and cortical structures have been linked to disturbances in cognition, perception, emotion, and sleep (Cronin-Golomb 2010). In addition, functional connectivity alterations within and between hemispheres have been reported in both AD (Blinowska et al. 2017; Sankari 2010; Adler, Brassen, and Jajcevic 2003; Babiloni et al. 2009) and PD (Luo et al. 2015; Dubbelink et al. 2013) suggesting their potential role in the early diagnosis.

Altogether, these findings suggest that neurodegenerative diseases must be considered as a network problem. Recent approaches based on network (or graph) theory have greatly advanced our understanding of the connection mechanisms characterizing brain diseases (Stam 2014). Among others, decreased efficiency, modularity and hub centrality have been largely reported in neurodegeneration and associated with the stage of disease. Increasing evidence suggests that the core-periphery structure of the human connectome - that supports global integration of information among distant areas - is highly affected by the AD process and that resulting changes might be effective predictors of cognitive declines. On the one hand, brain areas forming the core of the network - i.e. nodes with high connectivity and mutually interconnected - have been reported to be preferentially attacked by AD (Yan et al. 2018). On the other hand, brain regions forming the periphery of the network - i.e., nodes with low connectivity that are mutually interconnected - appear to be crucial for the degeneration, too (Daianu et al. 2013, 2015). While these results refer to structural brain connectivity, the relative contribution of functional brain connectivity into the network core-periphery changes remain poorly understood.

Based on the aforementioned empirical and theoretical grounds, we hypothesize that neurodegeneration would affect the core-periphery structure of the brain network at both anatomical and functional levels. More specifically, we expected that the extraction of the core-periphery organization by integrating information from multimodal brain networks would give more accurate predictor of AD and cognitive impairment. Finally, based on the evidence that

hubs are the most attacked nodes, we hypothesize that the core brain regions would be mostly impacted by the AD atrophy process.

To test these predictions, we considered multiple brain networks derived from DWI, fMRI and MEG data recorded in a group of AD patients and age-matched healthy controls. Cognitive impairments in AD patients were described using multidomain behavioral measurements. We extracted the multimodal core-periphery structure of the brain networks through a multiplex network approach, where all the available information is kept at different connectivity layers. We evaluated how AD impacted the multiplex core-periphery organization and we tested the correlation of the regional coreness with the cognitive and memory impairment of patients. See ??? for more details on the experimental design and methods of analysis.

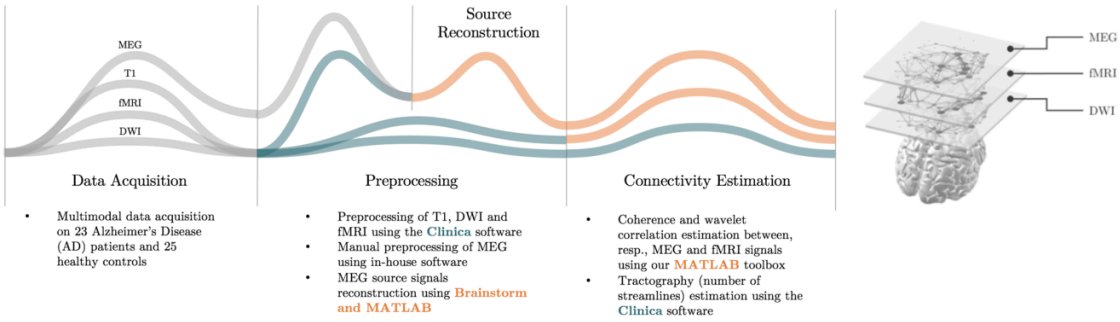

Figure 6.1 Multimodal brain network. This figure shows the multimodal brain networks of a randomly chosen subject. Layers correspond to structural or functional brain connectivity networks obtained from DWI, fMRI of MEG. All the layers have the same density (or average node degree $\overline{k}$) and weighted links whose weights are normalized between 0 and 1. The nodes are sized according to their strength, i.e. the sum of its connected edges weights.

II Results

Let us consider a 9-layers multiplex

$$\mathcal{M} = \left\{A^{[\mathrm{MEG}_\delta]}, A^{[\mathrm{MEG}_\theta]}, A^{[\mathrm{MEG}_{\alpha_1}]}, A^{[\mathrm{MEG}_{\alpha_2}]}, A^{[\mathrm{MEG}_{\beta_1}]}, A^{[\mathrm{MEG}_{\beta_2}]}, A^{[\mathrm{MEG}_\gamma]}, A^{[\mathrm{fMRI}]}, A^{[\mathrm{DTI}]}\right\},$$

where $A^{[m]} = \{w_{i,j}^{[m]}\}$ is the fully weighted adjacency matrix describing all connections associated to the couples of brain regions i and j in modality $m \in \{\mathrm{MEG}_\delta, \ldots, \mathrm{MEG}_\gamma, \mathrm{fMRI}, \mathrm{DTI}\}$. See section Methods for details.

In order to assess for changes in the core-periphery organization of this multimodal brain connectivity multiplex we use the *multiplex coreness* index $\mathcal{C}$ with the node strength as measure of richness, such as defined by (Battiston et al. 2017). The coreness index can be parametrized by a coefficients vector c of length M, the number of layers, that allows to modulate the importance of each layer in the computation of the multiplex richness of each node, and consequently in the final multiplex core-periphery organization.

A Complementarity of brain imaging modalities

In order to get the maximum out of the cohort's multimodal brain connectivities. We chose to tweak this coefficients vector c by using a data-driven approach in order to maximize the difference between AD and HC populations' coreness. We used the Particles Swarm Optimization algorithm (PSO, (Kennedy and Eberhart, n.d.)). The Fisher's criterion $F(c)$ maximizes the distance between the mean coreness of the two populations while minimizing the variance within each population (see Methods section for details). A minimum was obtained for the following coefficients vector c^*:

Layer m	$c^{*[m]}$
$\mathbf{MEG_\delta}$	**0.000**
$\mathbf{MEG_\theta}$	**0.001**
$\mathbf{MEG_{\alpha_1}}$	**0.258**
$\mathbf{MEG_{\alpha_2}}$	**0.000**
$\mathbf{MEG_{\beta_1}}$	**0.000**
$\mathbf{MEG_{\beta_2}}$	**0.002**
$\mathbf{MEG_\gamma}$	**0.000**
fMRI	**0.104**
DWI	**0.961**

Note that all coreness measures presented in the subsequent results have been computed using this optimal coefficient vector c^*, and should be written $\mathcal{C}(c^*)$ but will be refered to as $\mathcal{C}$ for readability purposes.

None of the three modalities has been discarded by the optimization, though, we notice the cancellation of the contribution of all MEG frequency-bands except for α_1. In Figure 6.2a, are shown the projection of the solution vectors (or particles) on the three main components axis. The other non-shown components are rapidly zeroing-out throughout 81 iterations of the 80

particles that have been necessary to converge to an optimum. The optimal configuration gives, in healthy subject, a high coreness on the central and superior frontal gyrii, and relatively high values in temporal cortices and superior parietal cortices as shown in the top row of Figure 6.2b. Coreness in AD respects the same pattern but with a general decrease in the values.

This global decrease of coreness in AD indicates a reduced size of the core structure at most of the network thresholds. The four highest coreness ROIs have values superior to 0.92 indicating that they almost always belong to the multimodal core in healthy subjects. As expected, most of the high-coreness-ROIs are regions already found in the literature to be key in structural or functional brain connectivity networks. The right and left superior frontal gyri (1st and 3rd highest coreness ROIs respectively) are the richest regions belonging to the structural rich club organization found in (van den Heuvel and Sporns 2011). And, the right and left precentral gyri (2nd and 4th highest coreness ROIs respectively) were already found at the top 12 among 1000 ROIs after a binary k-core decomposition in (Hagmann et al. 2008).

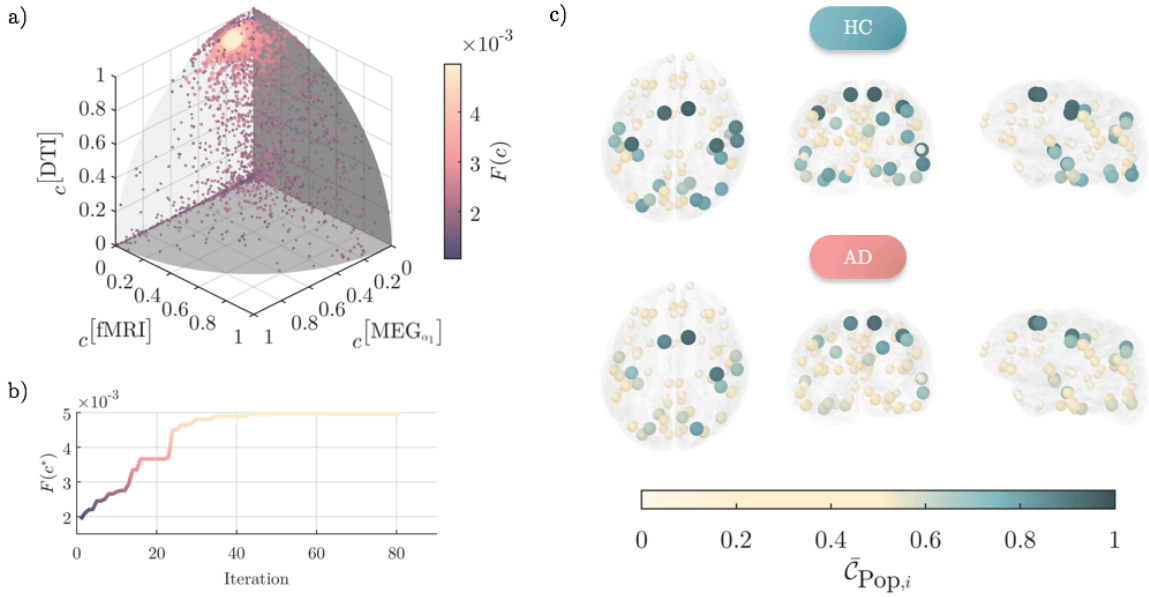

Figure 6.2 Particles Swarm Optimization of multimodal coreness difference. In panel **a)**, each dot represents the position of a particle at a given iteration in the 9-dimensions coreness coefficient vector space. Only three components of the vectors are depicted: MEG in the α_1 band, fMRI and DWI. In **b),** the evolution of the optimal value of the objective function $F(c^*)$, the fisher's criterion, in function of the iteration of the PSO (colorbar is identical to a)). In panel **c)** are represented the average multimodal coreness of the healthy controls (HC) population and the Alzheimer's disease (AD) population at the optimum shown in a).

B Core disruption in Alzheimer's disease

We have studied the coreness in AD by comparing it to those of the HC population. We observed that brain regions that are core in most of the healthy subjects tend to be the one losing the most coreness in AD. This trend can be quantified by measuring linear regression line's slope of the average coreness difference $\Delta\mathcal{C}_i = \bar{\mathcal{C}}_{\mathrm{AD},i} - \bar{\mathcal{C}}_{\mathrm{HC},i}$ in function of the average coreness of the healthy population $\bar{\mathcal{C}}_{\mathrm{HC}}$ (Figure 6.3a). We found a slope value $\overline{\kappa}_{\mathrm{AD}} = -0.26$ indicating AD will impact the coreness by 26% of reduction on average.

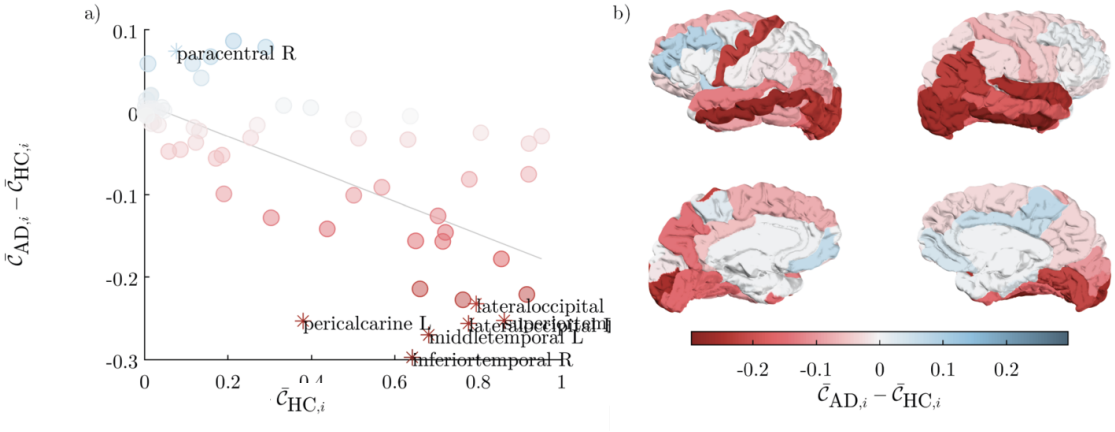

Figure 6.3 Local coreness disruption in AD. Panel **a)** plots the deviation of local coreness in AD as compared to HC on average. The gray line represents the hub disruption index line at $\overline{\kappa}_{\mathrm{AD}} = -0.26$. Stars show significantly different regions of interest (ROIs) according to a Wilcoxon test at $\alpha = 0.025$. Panel **b)** shows the same difference of local coreness on the cortical surface.

C Modelization of the Alzheimer's disease's impact on the individual core disruption

Based on the hypothesis that AD is a disconnection syndrome, we modelized our AD population by randomizing the HC one. The randomization process consists in shuffling a given proportion ρ of edges at each layer of our subjects' multimodal network. Thus, the weight distribution is kept unchanged; only the topology of the network is impacted, randomly. From each HC subject's multiplex, we generated $n_{\mathrm{rand}} = 3$ new randomized multiplexes that constituted three "fake" AD patients. This gave us a randomized population (RA) of size $N_{\mathrm{RA}} = n_{\mathrm{rand}} \times N_{\mathrm{HC}} = 63$ subjects. We then compared the core disruption of this randomized population and found that between 45 and 60 percent (Fig. 6.4) of the edges in the HC population must be randomly shuffled in order to get a core disruption similar to the one that is present in AD.

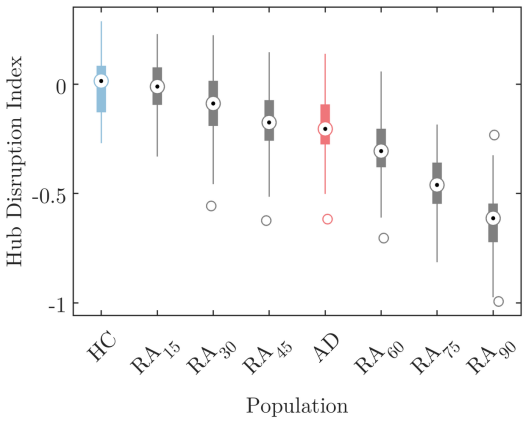

Figure 6.4 Hub disruption index in AD. This figure shows the hub disruption index distribution, represented as a gray box, in function of the proportion of edges that have been shuffled in healthy controls' (HCs) multiplexes. In blue and orange are inserted, respectively, the HCs' and the ADs' individual hub disruption indices distributions. Boxes are sorted in descending order based on their median.

D Individual core disruption and local coreness: associations to cognitive scores

We studied the coreness deviation of AD patients from normal population by the mean of the individual hub disruption index (HDI). HDI is computed as the linear regression line's slope obtained over all local coreness differences between a subject s's coreness and the coreness averaged over the HC population: $\mathcal{C}_{s,i} - \bar{\mathcal{C}}_{\mathrm{HC},i}$. The individual values HDI_s were then correlated to the cognitive tests scores such as the MMSE and the Free Recall score of the FCSRT, as presented in Figure 6.5.

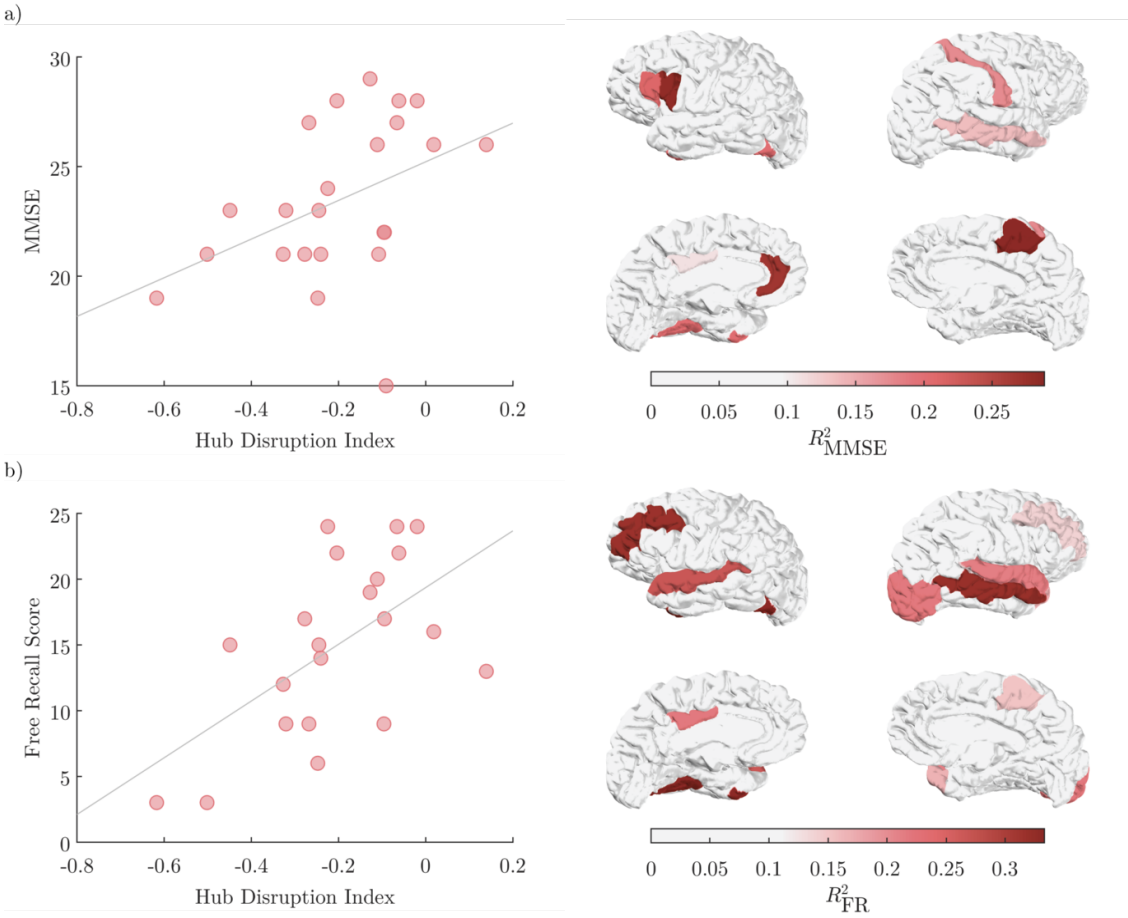

Figure 6.5 Local correlation with cognitive scores. In panels **a)** and **b)**, left column shows the linear regression curve between the global HDI and, respectively, the Mini-Mental State Examination (MMSE) score, and Free Recall (FR) score of the FCSRT in the Alzheimer's Disease (AD) population (one dot is one patient). And in right column, are shown the Spearman's correlation coefficients between the averaged local coreness of AD population and the same cognitive scores. Only significant ROIs are shown ($p < 0.025$).

III Conclusions and Discussions

Multiplex architecture has been recently applied to brain networks; as compositions of frequency-based functional networks (Brookes et al. 2016; Guillon et al. 2017), time-varying networks or structuro-fonctional networks such as reviewed by (Domenico 2017). This work is the first to combine three modalities covering a wide range of brain functional oscillations (0.1 to 45Hz with fMRI and MEG) and brain structure (with DWI). Results obtained by the PSO (Figure 6.2a and b) can be seen as a proof of the complementarity, in terms of information, of MEG, fMRI, and DWI in the study of brain connectivity and shows that combining those modalities together might lead to a better discrimination of AD patients versus healthy subjects. Our results on healthy

subjects (Figure 6.2c, top row) are in line with previously obtained results concerning structural or functional core-periphery structure (van den Heuvel and Sporns 2011, Hagmann et al. 2008). Especially the bilateral superior frontal and prefrontal gyri are known to be highly central regions from a structural point of view and the occipital gyri .

Results in Figure 6.3 indicate that AD disconnections are *targeted*, or follow an order based on structural *and* functional connectivity pathways. In general, brain regions belonging to the multimodal core will see their coreness decrease by 26% on average; the highest-coreness nodes have a higher probability of being discarded from the core after AD progression. This proves that the study of combined modalities is necessary to understand how AD progressively disrupt the different networks. The fact that the coreness disruption (measured using the HDI) can be reproduced by shuffling layers of the multiplex also supports the hypothesis that AD is a disconnection syndrome and encourages further research on finer models of AD progression, starting from healthy subject, by using for instance longitudinal datasets. One could also think to constrain the shuffling procedure on a subset of edges, on preferred nodes, or on preferred layers.

Multimodal coreness in AD showed a correlation with cognitive test scores implying intensive use of memory and language, especially in temporal and superior frontal areas. While episodic memory has long been known to depend on the medial temporal lobe (MTL) (Squire 1992; Gordon 1995) which is the most correlated region (Figure 6.5b); language and working memory are taking place in the superior frontal lobe (Pochon et al. 2002, and many other studies mainly based on fMRI).

The main advantage of using the coreness measure is that it avoids the fact of having to choose one specific threshold. It evaluates the core-periphery structure at every possible threshold (or more precisely only integer values of the average degree k) of a fully weighted multiplex. It could be interesting to study its optimal coefficient vector c^* in different protocols, conditions, diseases in order to evaluate on which physical medium (i.e. hematic, electromagnetic, or physiological) the differences are made. This coefficient c^* also address the problem mentioned by Buldú and Papo (2018) of translating the weights of the connections into the same units since it does not require any arbitrary choice concerning the contribution of each layer. However, the weights distribution between each layer can have a great impact on the core-periphery organization, and on the value of the components of c^* itself. This aspect might be a subject requiring more attention in future research. Mandke et al. (2018) already suggested to apply a singular value decomposition (SVD) to all layers obtained with a single connectivity estimator.

IV Methods

A Cohort inclusion

The study involved 23 Alzheimer's disease (AD) patients (13 women) and 26 healthy age-matched control (HC) subjects (19 women). All participants underwent the Mini-Mental State Examination (MMSE) for global cognition and the Free and Cued Selective Reminding Test (FCSRT) for verbal episodic memory. Inclusion criteria for all participants were: *i)* age between 50 and 90; *ii)* absence of general evolutive pathology; *iii)* no previous history of psychiatric diseases; *iv)* no contraindication to MRI examination; *v)* French as a mother tongue. Specific criteria for AD patients were: *i)* clinical diagnosis of Alzheimer's disease; *ii)* Mini-Mental State Examination (MMSE) score greater or equal to 18. All subjects gave written informed consent for participation in the study, which was approved by the local ethics committee of the Pitié-Salpêtrière Hospital. All experiments were performed in accordance with relevant guidelines and regulation.

B Data acquisition and pre-processing

i Structural and functional MRI

Magnetic resonance imaging (MRI) acquisitions were obtained using a 3T system (Siemens Trio, 32-channel system, with a 12-channel head coil). The MRI examination included:
i) 3D T1-weighted volumetric magnetization-prepared rapid gradient echo (MPRAGE) sequence with the following parameters: thickness = 1 mm isotropic, repetition time (TR) = 2300ms, echo time (TE) = 4.18ms, inversion time (TI) = 900ms, acquisition matrix = 256 × 256;
ii) echo planar imaging (EPI) sequence with the following parameters: one image with no diffusion sensitization (b0 image) and 50 diffusion-weighted images (DWI) at b = 1500 s/mm^2 , thickness = 2mm isotropic, TR = 13000ms, TE = 92ms, flip angle = 90°, acquisition matrix = 128 × 116;
iii) functional MRI (fMRI) resting-state sequence sensitive to blood oxygenation level-dependent (BOLD) contrast with the following parameters: 200 images, thickness = 3mm isotropic, TR = 2400ms, TE = 30ms, flip angle = 90°, acquisition matrix = 64 × 64.

All MR images were processed using the Clinica software (http://www.clinica.run). We first used the `t1-freesurfer-cross-sectional` pipeline to process T1-weighted images. This pipeline is a wrapper of different tools of the FreeSurfer software (http://surfer.nmr.mgh.harvard.edu/) (Fischl 2012). It includes segmentation of subcortical structures, extraction of cortical surfaces, cortical thickness estimation, spatial normalization onto the FreeSurfer surface template (FsAverage), and parcellation of cortical regions. Functional MRI images pre-processing have been conducted using the `fmri-preprocessing` pipeline. Slice timing correction, head motion correction and unwarping have been applied using SPM12 tools (www.fil.ion.ucl.ac.uk/spm). Separately the brain mask has been extracted from the T1 image of each subject using FreeSurfer. The resulting fMRI images have then been registered to the brain-masked T1 image of each subject using SPM's registration tool. Finally, diffusion-weighted images have been processed using the `dwi-preprocessing` pipeline of Clinica. For each subject, all raw DWI volumes were rigidly registered (6 degrees of freedom (dof)) to the reference b0 image (DWI volume with no diffusion sensitization) to correct for head motion. The diffusion weighting directions were appropriately updated [Leemans & Jones, 2009]. An affine registration (12 dof) was then performed between each DWI volume and the reference b0 to correct for eddy current distortions. These registrations were done using the FSL flirt tool (www.fmrib.ox.ac.uk/fsl). To correct for echo-planar imaging (EPI) induced susceptibility artifacts, the field map image was used as proposed by (Jezzard and Balaban 1995) with the FSL prelude/fugue tools. Finally, the DWI volumes were corrected for nonuniform intensity using the ANTs N4 bias correction algorithm (Tustison et al. 2010). A single multiplicative bias field from the reference b0 image was estimated, as suggested in (Jeurissen et al. 2014).

ii Magnetoencephalography

The magnetoencephalography (MEG) experimental protocol consisted in a resting-state with eyes-closed (EC). Subjects seated comfortably in a dimly lit electromagnetically and acoustically shielded room and were asked to relax. MEG signals were collected using a whole-head MEG system with 102 magnetometers and 204 planar gradiometers (Elekta Neuromag TRIUX MEG system) at a sampling rate of 1000 Hz and on-line low-pass filtered at 330 Hz. The ground electrode was located on the right shoulder blade. An electrocardiogram (EKG, Ag/AgCl electrodes) was placed on the left abdomen for artifacts correction and a vertical electrooculogram (EOG) was simultaneously recorded. Four small coils were attached to the participant in order to monitor

head position and to provide co-registration with the anatomical MRI. The physical landmarks (the nasion, the left and right pre-auricular points) were digitized using a Polhemus Fastrak digitizer (Polhemus, Colchester, VT). We extracted three consecutive clean epochs of approximately 2 minutes each.

Signal space separation was performed using MaxFilter (http://imaging.mrc-cbu.cam.ac.uk/meg/Maxfilter) to remove external noise. We used in-house software to remove cardiac and ocular blink artifacts from MEG signals by means of principal component analysis. We visually inspected the preprocessed MEG signals in order to remove epochs that still presented spurious contamination. At the end of the process, we obtained a coherent dataset consisting of three clean preprocessed epochs per subject.

We reconstructed the MEG activity on the cortical surface by using a source imaging technique (He 1999; Baillet et al. 2001): *i)* We used the previously segmented T1-weighted images of each single subject (Fischl et al. 2002; Fischl et al. 2004) to import cortical surfaces in the Brainstorm software (Tadel et al. 2011) where they were modeled with approximately 20000 equivalent current dipoles (i.e., the vertices of the cortical meshes). *ii)* We applied the wMNE (weighted Minimum Norm Estimate) algorithm with overlapping spheres (Lin et al. 2006) to solve the linear inverse problem. Both magnetometer and gradiometer, whose position has been registered on the T1 image using the digitized head points, were used to localize the activity over the cortical surface.

C Brain connectivity estimation

We built, for each modality, one or multiple brain connectivity networks whose nodes are regions of interests (ROIs) defined by the standard Desikan atlas (68 regions); and links are weighted by a given connectivity measure estimated between each pair of nodes resulting in 68×68 fully symmetric adjacency matrices.

i MEG-based functional connectivity

In the case of MEG, we used the spectral coherence as a connectivity estimator with the following parameters: window length = 2s, window type = sliding Hanning, overlap = 25% number of

FFT points (NFFT) = 2000 for a frequency resolution of 0.5Hz between 2Hz and 45Hz included.

We then averaged the connectivity matrices within the following characteristic frequency bands (Stam et al. 2002; Babiloni et al. 2004): *delta* (2–4Hz), *theta* (4.5–7.5Hz), *alpha1* (8–10.5Hz), *alpha2* (11–13Hz), *beta1* (13.5–20Hz), *beta2* (20.5–29.5Hz) and *gamma* (30–45Hz). We finally averaged the connectivity matrices across the three available epochs to obtain a robust estimate of the individual brain networks.

ii fMRI-based functional connectivity

We focused our analysis on the scale 2 wavelet correlation matrices that represented - with a TR = 2400ms - the functional connectivity in the frequency interval 0.05–0.10Hz (Biswal et al. 1995; Cordes et al. 2001). We wanted to study the highest possible frequencies in order to increase the robustness of the correlation (more periods) while staying in the most correlated frequency band.

iii DWI-based structural connectivity

We used again Clinica and its `tractography` pipeline that includes the following steps: estimation of the fiber orientation distributions (FODs) using *constrained spherical deconvolution* (CSD) algorithm from MRtrix3 `dwi2fod` tool and tractography based on *iFOD2* algorithm from MRtrix3 `tckgen` tool. The connectome is finally estimated by counting the *number of tracts* connecting each pair of nodes according to the given parcellation file using MRtrix3 `tck2connectome` tool.

D Particles swarm optimization

We used the PSO algorithm under the MATLAB® software with the default parameters to minimize the inverse of the Fisher's criterion $J(c) = 1/F(c)$. The Fisher's criterion $F(c)$ is defined as follow:

$$F(c) = \frac{\left(\bar{I}_{\mathrm{AD}}(c) - \bar{I}_{\mathrm{HC}}(c)\right)^2}{s_{\mathrm{AD}}^2 + s_{\mathrm{HC}}^2},$$

with $\bar{I}_{\mathrm{Pop}}(c)$, the average local (i.e. node level) index, here the coreness $\mathcal{C}$, over a population Pop, which in our case belongs to $\{\mathrm{AD}, \mathrm{HC}\}$, and,

$$s^2_{\mathrm{Pop}} = \sum_{s \in \mathrm{Pop}} (I_s(c) - \bar{I}_{\mathrm{Pop}}(c))^2,$$

with s a subject belonging the population Pop.

Since $F(c) = F(ac), \forall a \in \mathbb{R}^+$, and in order to save one dimension in the searching space, we expressed the coefficient c as a point on the positive section of the unitary hypersphere of dimension $M = 9$ such that:

$$c = \begin{pmatrix} \sin\phi_1 \dots \sin\phi_8 \\ \sin\phi_1 \dots \sin\phi_7 \cos\phi_8 \\ \sin\phi_1 \dots \sin\phi_6 \cos\phi_7 \\ \sin\phi_1 \dots \sin\phi_5 \cos\phi_6 \\ \sin\phi_1 \dots \sin\phi_4 \cos\phi_5 \\ \sin\phi_1 \dots \sin\phi_3 \cos\phi_4 \\ \sin\phi_1 \sin\phi_2 \cos\phi_3 \\ \sin\phi_1 \cos\phi_2 \\ \cos\phi_1 \end{pmatrix}, \phi_k \in [0, \frac{\pi}{2}], \forall k \in [1, M-1]$$

And used the angles vector ϕ as our particle position vector of dimension $M - 1$.

E Methodological considerations

Two-levels dimensionality limitations in the optimization of the core-periphery algorithm's contribution coefficients c:

- The dimension of the searching space; i.e. the number of layers can hardly be greater than what we used here (i.e. $M = 9$)
- The cost function, here the inverse of the Fisher's criterion, reduces to one the dimension of the features space (i.e. the space of nodal measures) in order to compare the two populations; therefore, it should be carefully chosen when the number of nodes increases, since the size of the feature's vectors will increase with it. One could think of the absolute difference between an average global measure on our populations' multiplexes, or a more advanced classification accuracy measure.

V References

Schmahmann, J., and D. Pandya. 2008. “Disconnection Syndromes of Basal Ganglia Thalamus, and Cerebrocerebellar Systems”. *Cortex* 44 (8). Elsevier BV: 1037–66. doi:10.1016/j.cortex.2008.04.004.

Delbeuck, X., F. Collette, and M. Van der Linden. 2007. “Is Alzheimers Disease a Disconnection Syndrome?”. *Neuropsychologia* 45 (14). Elsevier BV: 3315–23. doi:10.1016/j.neuropsychologia.2007.05.001.

Lakmache, Y., M. Lassonde, S. Gauthier, J.-Y. Frigon, and F. Lepore. 1998. “Interhemispheric Disconnection Syndrome in Alzheimers Disease”. *Proceedings of the National Academy of Sciences* 95 (15). Proceedings of the National Academy of Sciences: 9042–46. doi:10.1073/pnas.95.15.9042.

Cronin-Golomb, Alice. 2010. “Parkinson’s Disease as a Disconnection Syndrome”. *Neuropsychology Review* 20 (2). Springer Nature: 191–208. doi:10.1007/s11065-010-9128-8.

Blinowska, Katarzyna J., Franciszek Rakowski, Maciej Kaminski, Fabrizio De Vico Fallani, Claudio Del Percio, Roberta Lizio, and Claudio Babiloni. 2017. “Functional and Effective Brain Connectivity for Discrimination between Alzheimer’s Patients and Healthy Individuals: A Study on Resting State EEG Rhythms”. *Clinical Neurophysiology* 128 (4). Elsevier BV: 667–80. doi:10.1016/j.clinph.2016.10.002.

Sankari, Ziad T. 2010. “Local and Distal Coherence as a Measure of Cortical Connectivity in Alzheimers Disease”. *Alzheimers & Dementia* 6 (4). Elsevier BV: S373. doi:10.1016/j.jalz.2010.05.1250.

Adler, G., S. Brassen, and A. Jajcevic. 2003. “EEG Coherence in Alzheimer?s Dementia”. *Journal of Neural Transmission* 110 (9). Springer Nature: 1051–58. doi:10.1007/s00702-003-0024-8.

Babiloni, Claudio, Raffaele Ferri, Giuliano Binetti, Fabrizio Vecchio, Giovanni B. Frisoni, Bartolo Lanuzza, Carlo Miniussi, et al. 2009. “Directionality of EEG Synchronization in Alzheimers Disease Subjects”. *Neurobiology of Aging* 30 (1). Elsevier BV: 93–102. doi:10.1016/j.neurobiolaging.2007.05.007.

Luo, ChunYan, XiaoYan Guo, Wei Song, Bi Zhao, Bei Cao, Jing Yang, QiYong Gong, and Hui-Fang Shang. 2015. “Decreased Resting-State Interhemispheric Functional Connectivity in Parkinson’s Disease”. *BioMed Research International* 2015. Hindawi Limited: 1–8. doi:10.1155/2015/692684.

Dubbelink, Kim T. E. Olde, Arjan Hillebrand, Diederick Stoffers, Jan Berend Deijen, Jos W. R. Twisk, Cornelis J. Stam, and Henk W. Berendse. 2013. “Disrupted Brain Network Topology in Parkinson’s Disease: a Longitudinal Magnetoencephalography Study”. *Brain* 137 (1). Oxford University Press (OUP): 197–207. doi:10.1093/brain/awt316.

Stam, Cornelis J. 2014. “Modern Network Science of Neurological Disorders”. *Nature Reviews Neuroscience* 15 (10). Springer Nature: 683–95. doi:10.1038/nrn3801.

Battiston, Federico, Jeremy Guillon, Mario Chavez, Vito Latora, and Fabrizio De Vico Fallani. 2017. “Multiplex Core-Periphery Organization of the Human Connectome”. *ArXiv:1801.01913 [Physics, q-Bio]*, December. http://arxiv.org/abs/1801.01913.

Kennedy, J., and R. Eberhart. n.d. “Particle Swarm Optimization”. In *Proceedings of ICNN95 - International Conference on Neural Networks*. IEEE. doi:10.1109/icnn.1995.488968.

van den Heuvel, M. P., and O. Sporns. 2011. “Rich-Club Organization of the Human Connectome”. *Journal of Neuroscience* 31 (44). Society for Neuroscience: 15775–86. doi:10.1523/jneurosci.3539-11.2011.

Hagmann, Patric, Leila Cammoun, Xavier Gigandet, Reto Meuli, Christopher J Honey, Van J Wedeen, and Olaf Sporns. 2008. “Mapping the Structural Core of Human Cerebral Cortex”. Edited by Karl J Friston. *PLoS Biology* 6 (7). Public Library of Science (PLoS): e159. doi:10.1371/journal.pbio.0060159.

Brookes, Matthew J., Prejaas K. Tewarie, Benjamin A.E. Hunt, Sian E. Robson, Lauren E. Gascoyne, Elizabeth B. Liddle, Peter F. Liddle, and Peter G. Morris. 2016. “A Multi-Layer Network Approach to MEG Connectivity Analysis”. *NeuroImage* 132 (May). Elsevier BV: 425–38. doi:10.1016/j.neuroimage.2016.02.045.

Guillon, J., Y. Attal, O. Colliot, V. La Corte, B. Dubois, D. Schwartz, M. Chavez, and F. De Vico Fallani. 2017. “Loss of Brain Inter-Frequency Hubs in Alzheimers Disease”. *Scientific Reports* 7 (1). Springer Nature. doi:10.1038/s41598-017-07846-w.

Domenico, Manlio De. 2017. “Multilayer Modeling and Analysis of Human Brain Networks”. *GigaScience* 6 (5). Oxford University Press (OUP). doi:10.1093/gigascience/gix004.

Daianu, Madelaine, Neda Jahanshad, Talia M. Nir, Clifford R. Jack, Michael W. Weiner, Matt A. Bernstein, and Paul M. Thompson and. 2015. “Rich Club Analysis in the Alzheimers Disease Connectome Reveals a Relatively Undisturbed Structural Core Network”. *Human Brain Mapping* 36 (8). Wiley: 3087–3103. doi:10.1002/hbm.22830.

Vincent, Justin L., Abraham Z. Snyder, Michael D. Fox, Benjamin J. Shannon, Jessica R. Andrews, Marcus E. Raichle, and Randy L. Buckner. 2006. “Coherent Spontaneous Activity Identifies a Hippocampal-Parietal Memory Network”. *Journal of Neurophysiology* 96 (6). American Physiological Society: 3517–31. doi:10.1152/jn.00048.2006.

Wagner, Anthony D., Benjamin J. Shannon, Itamar Kahn, and Randy L. Buckner. 2005. “Parietal Lobe Contributions to Episodic Memory Retrieval”. *Trends in Cognitive Sciences* 9 (9). Elsevier BV: 445–53. doi:10.1016/j.tics.2005.07.001.

Squire, Larry R. 1992. “Memory and the Hippocampus: A Synthesis from Findings with Rats Monkeys, and Humans: Correction.”. *Psychological Review* 99 (3). American Psychological Association (APA): 582–82. doi:10.1037/0033-295x.99.3.582.

Gordon, Barry. 1995. “Memory Amnesia, and the Hippocampal System”. *Electroencephalography and Clinical Neurophysiology* 95 (6). Elsevier BV: 479. doi:10.1016/0013-4694(95)90026-8.

Buldú, Javier M., and David Papo. 2018. “Can Multilayer Brain Networks Be a Real Step Forward?”. *Physics of Life Reviews* 24 (March). Elsevier BV: 153–55. doi:10.1016/j.plrev.2017.12.007.

Fischl, Bruce. 2012. “FreeSurfer”. *NeuroImage* 62 (2). Elsevier BV: 774–81. doi:10.1016/j.neuroimage.2012.01.021.

Jezzard, Peter, and Robert S. Balaban. 1995. “Correction for Geometric Distortion in Echo Planar Images from B0 Field Variations”. *Magnetic Resonance in Medicine* 34 (1). Wiley: 65–73. doi:10.1002/mrm.1910340111.

Tustison, Nicholas J, Brian B Avants, Philip A Cook, Yuanjie Zheng, Alexander Egan, Paul A Yushkevich, and James C Gee. 2010. “N4ITK: Improved N3 Bias Correction”. *IEEE Transactions on Medical Imaging* 29 (6). Institute of Electrical and Electronics Engineers (IEEE): 1310–20. doi:10.1109/tmi.2010.2046908.

Jeurissen, Ben, Jacques-Donald Tournier, Thijs Dhollander, Alan Connelly, and Jan Sijbers. 2014. “Multi-Tissue Constrained Spherical Deconvolution for Improved Analysis of Multi-Shell Diffusion MRI Data”. *NeuroImage* 103 (December). Elsevier BV: 411–26. doi:10.1016/j.neuroimage.2014.07.061.

He, B. 1999. “Brain Electric Source Imaging: Scalp Laplacian Mapping and Cortical Imaging”. *Crit Rev Biomed Eng* 27 (3-5): 149–88.

Baillet, S., J. J. Riera, G. Marin, J. F. Mangin, J. Aubert, and L. Garnero. 2001. “Evaluation of Inverse Methods and Head Models for EEG Source Localization Using a Human Skull Phantom”. *Phys Med Biol* 46 (1): 77–96.

Fischl, Bruce, David H. Salat, Evelina Busa, Marilyn Albert, Megan Dieterich, Christian Haselgrove, Andre van der Kouwe, et al. 2002. “Whole Brain Segmentation: Automated Labeling of Neuroanatomical Structures in the Human Brain”. *Neuron* 33 (3): 341–55.

Fischl, Bruce, David H. Salat, AndrÃ© J. W. van der Kouwe, Nikos Makris, Florent SÃ©gonne, Brian T. Quinn, and Anders M. Dale. 2004. “Sequence-Independent Segmentation of Magnetic Resonance Images”. *Neuroimage* 23 Suppl 1: S69–84. doi:10.1016/j.neuroimage.2004.07.016.

Tadel, FranÃ§ois, Sylvain Baillet, John C. Mosher, Dimitrios Pantazis, Richard M. Leahy, FranÃ§ois Tadel, Sylvain Baillet, John C. Mosher, Dimitrios Pantazis, and Richard M. Leahy. 2011. “Brainstorm: A User-Friendly Application for MEG/EEG Analysis, Brainstorm: A User-Friendly Application for MEG/EEG Analysis”. *Computational Intelligence and Neuroscience, Computational Intelligence and Neuroscience* 2011, 2011 (April): e879716. doi:10.1155/2011/879716, 10.1155/2011/879716.

Lin, Fa-Hsuan, Thomas Witzel, Seppo P. Ahlfors, Steven M. Stufflebeam, John W. Belliveau, and Matti S. HÃ€mÃ€lÃ€inen. 2006. “Assessing and Improving the Spatial Accuracy in MEG Source Localization by Depth-Weighted Minimum-Norm Estimates”. *NeuroImage* 31 (1): 160–71. doi:10.1016/j.neuroimage.2005.11.054.

Stam, Cornelis J., Anne Marie van Cappellen van Walsum, Yolande A. L. Pijnenburg, Henk W. Berendse, Jan C. de Munck, Philip Scheltens, and Bob W. van Dijk. 2002. “Generalized Synchronization of MEG Recordings in Alzheimer’s Disease: Evidence for Involvement of the Gamma Band”. *J Clin Neurophysiol* 19 (6): 562–74.

Babiloni, Claudio, Raffaele Ferri, Davide V. Moretti, Andrea Strambi, Giuliano Binetti, Gloria Dal Forno, Florinda Ferreri, et al. 2004. “Abnormal Fronto-Parietal Coupling of Brain Rhythms in Mild Alzheimer’s Disease: a Multicentric EEG Study”. *Eur. J. Neurosci.* 19 (9): 2583–90. doi:10.1111/j.0953-816X.2004.03333.x.

van den Heuvel, Martijn P., René C.W. Mandl, René S. Kahn, and Hilleke E. Hulshoff Pol. 2009. “Functionally Linked Resting-State Networks Reflect the Underlying Structural Connectivity Architecture of the Human Brain”. *Human Brain Mapping* 30 (10). Wiley: 3127–41. doi:10.1002/hbm.20737.

Biswal, Bharat, F. Zerrin Yetkin, Victor M. Haughton, and James S. Hyde. 1995. "Functional Connectivity in the Motor Cortex of Resting Human Brain Using Echo-Planar Mri". *Magnetic Resonance in Medicine* 34 (4). Wiley: 537–41. doi:10.1002/mrm.1910340409.

Cordes, D, VM Haughton, K Arfanakis, JD Carew, PA Turski, CH Moritz, MA Quigley, and ME Meyerand. 2001. "Frequencies Contributing to Functional Connectivity in the Cerebral Cortex in Resting-State Data.". *AJNR Am J Neuroradiol* 22: 1326–33.

Conclusion

We proposed first a multilayer approach to study MEG-based multi-frequency brain connectivity. We identified a new type of hubs characterized by their ability to integrate information from different frequency bands. We showed that AD have an impact on those hubs, especially in cingulate and memory-related association areas. In the same study we also proved that multilayer metrics, such as the multi-participation coefficient, were complementary to the standard single-layer ones in the discrimination of AD versus healthy populations. In a second work, we generalized the concept of core-periphery structure to the case of multiplex networks where layers have different natures of links. We applied it to structuro-functional brain networks and showed that our method succeeds in identifying known core nodes coming from both modalities but also brain regions in the sensorimotor system that were previously overlooked by standard approaches. We applied again the coreness metric on a multimodal dataset that allowed us to build, for the first time, a multiplex network based on fMRI, DWI and multiple frequency bands of MEG. We showed that applying a multilayer index, such as the coreness, on a multiplex built as this one allows to consider multiple modalities in the same time and without any loss of information. Our results are perfectly in line with the literature, from a functional and structural point-of-view, in healthy and diseased subjects.

In general, this work shows the path to future study that might try various topologies of multilayer brain networks, and to combine different modalities. In the study of AD, one could think for instance to add a temporal component to incorporate the disease progression in the model.

I also really missed, from the dataset of the AD cohort we used in Chapter 4 and 6, information about Aβ and Tau proteins concentration, such as with PET scans. Especially with results that we obtained in Figure 6d of Chapter 4 where we show the local correlation between the Total Recall score of the FCSRT and the MPC_i values; regions that were the most correlated really overlap with the ones that are typically affected by amyloid deposition as shown with the **Figure 2.2** extracted from Buckner et al. (2005). I would have liked to explore connectivity-based

parcellation at the individual level. As shown multiple times in the literature, parcellation has a great effect on resulting networks, and since every brain is different, I don't see why parcellations should not be. The difficulty would be then to compare connectome between subjects. I would use ROI's centroid positions in a discretize MNI space to run group-wise analyses at a "meta-voxel" level.

Finally, this work also came with questions. In particular, one of the most urging methodological questions is about the inter-layer links. How are they computed and what do they express? Also, how to consider them in the generalization of network metrics? A few works, presented in Chapter 3 and 5, already proposed some solutions.

As many other elements of the brain multilayer networks construction pipeline, there is no consensus yet on which method to prefer. And I argue that this will slow down research focused on their possible application; since no framework has been precisely and commonly accepted, there is no possibility for neurologists (in this case) to compare results and finally use multilayer metrics as comprehensive indicators of neural structure or function. I deeply feel that open datasets and reproducible analyses will be the only way to get descent discussions in the field.

To conclude, we confirmed throughout this work that the multilayer networks framework is suited for an application to brain networks. Future research may now explore many different configurations of multilayer brain networks through time and modalities. Especially, multi-frequency and multimodal brain networks appeared to be a good choice for the investigation of the behavior of neurodegenerative disease such as Alzheimer's disease for which we gave new viewpoints about a few of its already known aspects.

Bibliography

Achard, Sophie, and Ed Bullmore. 2007. "Efficiency and Cost of Economical Brain Functional Networks." *PLOS Computational Biology* 3 (2): e17. https://doi.org/10.1371/journal.pcbi.0030017.

Achard, Sophie, Raymond Salvador, Brandon Whitcher, John Suckling, and Ed Bullmore. 2006. "A Resilient, Low-Frequency, Small-World Human Brain Functional Network with Highly Connected Association Cortical Hubs." *Journal of Neuroscience* 26 (1): 63–72. https://doi.org/10.1523/JNEUROSCI.3874-05.2006.

Afshari, Saeedeh, and Mahdi Jalili. 2017. "Directed Functional Networks in Alzheimer's Disease: Disruption of Global and Local Connectivity Measures." *IEEE Journal of Biomedical and Health Informatics* 21 (4): 949–55. https://doi.org/10.1109/JBHI.2016.2578954.

Alexander, Daniel C. 2005. "Multiple-Fiber Reconstruction Algorithms for Diffusion MRI." *Annals of the New York Academy of Sciences* 1064 (1): 113–33. https://doi.org/10.1196/annals.1340.018.

Arslan, Salim, Sofia Ira Ktena, Antonios Makropoulos, Emma C. Robinson, Daniel Rueckert, and Sarah Parisot. 2018. "Human Brain Mapping: A Systematic Comparison of Parcellation Methods for the Human Cerebral Cortex." *NeuroImage*, Segmenting the Brain, 170 (April): 5–30. https://doi.org/10.1016/j.neuroimage.2017.04.014.

Baccalá, Luiz A., and Koichi Sameshima. 2001. "Partial Directed Coherence: A New Concept in Neural Structure Determination." *Biological Cybernetics* 84 (6): 463–74. https://doi.org/10.1007/PL00007990.

Basser, P J, J Mattiello, and D LeBihan. 1994. "MR Diffusion Tensor Spectroscopy and Imaging." *Biophysical Journal* 66 (1): 259–67.

Basser, Peter J., Sinisa Pajevic, Carlo Pierpaoli, Jeffrey Duda, and Akram Aldroubi. 2000. "In Vivo Fiber Tractography Using DT-MRI Data." *Magnetic Resonance in Medicine* 44 (4): 625–32. https://doi.org/10.1002/1522-2594(200010)44:4<625::AID-MRM17>3.0.CO;2-O.

Bassett, Danielle S., and Edward T. Bullmore. 2017. "Small-World Brain Networks Revisited." *The Neuroscientist* 23 (5): 499–516. https://doi.org/10.1177/1073858416667720.

Bassett, Danielle S., Andreas Meyer-Lindenberg, Sophie Achard, Thomas Duke, and Edward Bullmore. 2006. "Adaptive Reconfiguration of Fractal Small-World Human Brain Functional Networks." *Proceedings of the National Academy of Sciences of the United States of America* 103 (51): 19518–23. https://doi.org/10.1073/pnas.0606005103.

Bassett, Danielle S., Nicholas F. Wymbs, Mason A. Porter, Peter J. Mucha, Jean M. Carlson, and Scott T. Grafton. 2011. "Dynamic Reconfiguration of Human Brain Networks during Learning." *Proceedings of the National Academy of Sciences* 108 (18): 7641–46. https://doi.org/10.1073/pnas.1018985108.

Bassett, Danielle S., Nicholas F. Wymbs, M. Puck Rombach, Mason A. Porter, Peter J. Mucha, and Scott T. Grafton. 2013. "Task-Based Core-Periphery Organization of Human Brain Dynamics." *PLOS Computational Biology* 9 (9): e1003171. https://doi.org/10.1371/journal.pcbi.1003171.

Bassett, Danielle S., Muzhi Yang, Nicholas F. Wymbs, and Scott T. Grafton. 2015. "Learning-Induced Autonomy of Sensorimotor Systems." *Nature Neuroscience* 18 (5): 744–51. https://doi.org/10.1038/nn.3993.

Battiston, Federico, Vincenzo Nicosia, Mario Chavez, and Vito Latora. 2017. "Multilayer Motif Analysis of Brain Networks." *Chaos: An Interdisciplinary Journal of Nonlinear Science* 27 (4): 047404. https://doi.org/10.1063/1.4979282.

Battiston, Federico, Vincenzo Nicosia, and Vito Latora. 2014. "Structural Measures for Multiplex Networks." *Physical Review E* 89 (3): 032804. https://doi.org/10.1103/PhysRevE.89.032804.

Becker, H., L. Albera, P. Comon, R. Gribonval, F. Wendling, and I. Merlet. 2015. "Brain-Source Imaging: From Sparse to Tensor Models." *IEEE Signal Processing Magazine* 32 (6): 100–112. https://doi.org/10.1109/MSP.2015.2413711.

Beckmann, Matthias, Heidi Johansen-Berg, and Matthew F. S. Rushworth. 2009. "Connectivity-Based Parcellation of Human Cingulate Cortex and Its Relation to Functional Specialization." *The Journal of Neuroscience: The Official Journal of the Society for Neuroscience* 29 (4): 1175–90. https://doi.org/10.1523/JNEUROSCI.3328-08.2009.

Bennett, Craig M., George L. Wolford, and Michael B. Miller. 2009. "The Principled Control of False Positives in Neuroimaging." *Social Cognitive and Affective Neuroscience* 4 (4): 417–22. https://doi.org/10.1093/scan/nsp053.

Betzel, Richard F., and Danielle S. Bassett. 2017. "Multi-Scale Brain Networks." *NeuroImage*, Functional Architecture of the Brain, 160 (October): 73–83. https://doi.org/10.1016/j.neuroimage.2016.11.006.

Betzel, Richard F., Lisa Byrge, Ye He, Joaquín Goñi, Xi-Nian Zuo, and Olaf Sporns. 2014. "Changes in Structural and Functional Connectivity among Resting-State Networks across the Human Lifespan." *NeuroImage* 102 (November): 345–57. https://doi.org/10.1016/j.neuroimage.2014.07.067.

Blumensath, Thomas, Saad Jbabdi, Matthew F. Glasser, David C. Van Essen, Kamil Ugurbil, Timothy E.J. Behrens, and Stephen M. Smith. 2013. "Spatially Constrained Hierarchical Parcellation of the Brain with Resting-State FMRI." *NeuroImage* 76 (August): 313–24. https://doi.org/10.1016/j.neuroimage.2013.03.024.

Boccaletti, S., G. Bianconi, R. Criado, C. I. del Genio, J. Gómez-Gardeñes, M. Romance, I. Sendiña-Nadal, Z. Wang, and M. Zanin. 2014. "The Structure and Dynamics of Multilayer Networks." *Physics Reports*, The structure and dynamics of multilayer networks, 544 (1): 1–122. https://doi.org/10.1016/j.physrep.2014.07.001.

Boccaletti, S., V. Latora, Y. Moreno, M. Chavez, and D. -U. Hwang. 2006. "Complex Networks: Structure and Dynamics." *Physics Reports* 424 (4): 175–308. https://doi.org/10.1016/j.physrep.2005.10.009.

Boer, Renske de, Henri A. Vrooman, M. Arfan Ikram, Meike W. Vernooij, Monique M. B. Breteler, Aad van der Lugt, and Wiro J. Niessen. 2010. "Accuracy and Reproducibility Study of Automatic MRI Brain Tissue Segmentation Methods." *NeuroImage* 51 (3): 1047–56. https://doi.org/10.1016/j.neuroimage.2010.03.012.

Bohan, David A., Corinne Vacher, Alireza Tamaddoni-Nezhad, Alan Raybould, Alex J. Dumbrell, and Guy Woodward. 2017. "Next-Generation Global Biomonitoring: Large-Scale, Automated Reconstruction of Ecological Networks." *Trends in Ecology & Evolution* 32 (7): 477–87. https://doi.org/10.1016/j.tree.2017.03.001.

Brier, Matthew R, Jewell B Thomas, Anne M Fagan, Jason Hassenstab, David M Holtzman, Tammie L Benzinger, John C Morris, and Beau M Ances. 2014. "Functional Connectivity and Graph Theory in Preclinical Alzheimer's Disease." *Neurobiology of Aging* 35 (4). https://doi.org/10.1016/j.neurobiolaging.2013.10.081.

Brookes, Matthew J., Prejaas K. Tewarie, Benjamin A. E. Hunt, Sian E. Robson, Lauren E. Gascoyne, Elizabeth B. Liddle, Peter F. Liddle, and Peter G. Morris. 2016. "A Multi-Layer Network Approach to MEG Connectivity Analysis." *NeuroImage* 132 (May): 425–38. https://doi.org/10.1016/j.neuroimage.2016.02.045.

Buckner, Randy L., Jessica R. Andrews-Hanna, and Daniel L. Schacter. 2008. "The Brain's Default Network." *Annals of the New York Academy of Sciences* 1124 (1): 1–38. https://doi.org/10.1196/annals.1440.011.

Buckner, Randy L., Abraham Z. Snyder, Benjamin J. Shannon, Gina LaRossa, Rimmon Sachs, Anthony F. Fotenos, Yvette I. Sheline, et al. 2005. "Molecular, Structural, and Functional Characterization of Alzheimer's Disease: Evidence for a Relationship between Default Activity, Amyloid, and Memory." *The Journal of Neuroscience: The Official Journal of the Society for Neuroscience* 25 (34): 7709–17. https://doi.org/10.1523/JNEUROSCI.2177-05.2005.

Buldú, Javier M., and David Papo. 2018. "Can Multilayer Brain Networks Be a Real Step Forward?: Comment on 'Network Science of Biological Systems at Different Scales: A Review' by M. Gosak et Al." *Physics of Life Reviews* 24 (March): 153–55. https://doi.org/10.1016/j.plrev.2017.12.007.

Buldú, Javier M., and Mason A. Porter. 2017. "Frequency-Based Brain Networks: From a Multiplex Framework to a Full Multilayer Description." *Network Neuroscience* 2 (4): 418–41. https://doi.org/10.1162/netn_a_00033.

Bullmore, Ed, Jalal Fadili, Voichita Maxim, Levent Şendur, Brandon Whitcher, John Suckling, Brammer Michael, and Michael Breakspear. 2004. "Wavelets and Functional Magnetic Resonance Imaging of the Human Brain." *NeuroImage*, Mathematics in Brain Imaging, 23 (January): S234–49. https://doi.org/10.1016/j.neuroimage.2004.07.012.

Bullmore, Ed, and Olaf Sporns. 2009. “Complex Brain Networks: Graph Theoretical Analysis of Structural and Functional Systems.” *Nature Reviews. Neuroscience* 10 (3): 186–98. https://doi.org/10.1038/nrn2575.

“B-Value Diffusion.” n.d. Questions and Answers in MRI. Accessed September 30, 2018. http://mriquestions.com/what-is-the-b-value.html.

Cao, Jin, and Keith Worsley. 1999. “The Geometry of Correlation Fields with an Application to Functional Connectivity of the Brain.” *The Annals of Applied Probability* 9 (4): 1021–57.

Carter, Alex R., Gordon L. Shulman, and Maurizio Corbetta. 2012. “Why Use a Connectivity-Based Approach to Study Stroke and Recovery of Function?” *NeuroImage* 62 (4): 2271–80. https://doi.org/10.1016/j.neuroimage.2012.02.070.

Ciftçi, Koray. 2011. “Minimum Spanning Tree Reflects the Alterations of the Default Mode Network during Alzheimer’s Disease.” *Annals of Biomedical Engineering* 39 (5): 1493–1504. https://doi.org/10.1007/s10439-011-0258-9.

Clark, Kristi A., Keith H. Nuechterlein, Robert F. Asarnow, Liberty S. Hamilton, Owen R. Phillips, Nathan S. Hageman, Roger P. Woods, Jeffry R. Alger, Arthur W. Toga, and Katherine L. Narr. 2011. “Mean Diffusivity and Fractional Anisotropy as Indicators of Disease and Genetic Liability to Schizophrenia.” *Journal of Psychiatric Research* 45 (7): 980–88. https://doi.org/10.1016/j.jpsychires.2011.01.006.

Cohen Veterans Bioscience. n.d. *Diffusion Spectrum Imaging (DSI): A Tool for Unraveling Disrupted Structural Connectivity in PTSD?* Accessed September 30, 2018. https://www.youtube.com/watch?v=91eOD37so_0.

Colclough, G. L., M. W. Woolrich, P. K. Tewarie, M. J. Brookes, A. J. Quinn, and S. M. Smith. 2016. “How Reliable Are MEG Resting-State Connectivity Metrics?” *NeuroImage* 138 (September): 284–93. https://doi.org/10.1016/j.neuroimage.2016.05.070.

Cox, Robert W. 1996. “AFNI: Software for Analysis and Visualization of Functional Magnetic Resonance Neuroimages.” *Computers and Biomedical Research* 29 (3): 162–73. https://doi.org/10.1006/cbmr.1996.0014.

Craddock, R. Cameron, Pierre Bellec, and Saad Jbabdi. 2018. “Neuroimage Special Issue on Brain Segmentation and Parcellation - Editorial.” *NeuroImage*, Segmenting the Brain, 170 (April): 1–4. https://doi.org/10.1016/j.neuroimage.2017.11.063.

Craddock, R. Cameron, Saad Jbabdi, Chao-Gan Yan, Joshua T. Vogelstein, F. Xavier Castellanos, Adriana Di Martino, Clare Kelly, Keith Heberlein, Stan Colcombe, and Michael P. Milham. 2013. “Imaging Human Connectomes at the Macroscale.” *Nature Methods* 10 (6): 524–39. https://doi.org/10.1038/nmeth.2482.

Crofts, J. J., M. Forrester, and R. D. O’Dea. 2016. “Structure-Function Clustering in Multiplex Brain Networks.” *EPL (Europhysics Letters)* 116 (1): 18003. https://doi.org/10.1209/0295-5075/116/18003.

Daianu, Madelaine, Neda Jahanshad, Talia M. Nir, Clifford R. Jack, Michael W. Weiner, Matthew Bernstein, and Paul M. Thompson. 2015. “Rich Club Analysis in the Alzheimer’s Disease Connectome Reveals a Relatively Undisturbed Structural Core Network.” *Human Brain Mapping* 36 (8): 3087–3103. https://doi.org/10.1002/hbm.22830.

Daianu, Madelaine, Neda Jahanshad, Talia M. Nir, Arthur W. Toga, Clifford R. Jack, Michael W. Weiner, and for the Alzheimer’s Disease Neuroimaging Initiative Thompson Paul M. 2013. “Breakdown of Brain Connectivity Between Normal Aging and Alzheimer’s Disease: A Structural k-Core Network Analysis.” *Brain Connectivity* 3 (4): 407–22. https://doi.org/10.1089/brain.2012.0137.

De Domenico, Manlio. 2017. “Multilayer Modeling and Analysis of Human Brain Networks.” *GigaScience* 6 (5). https://doi.org/10.1093/gigascience/gix004.

De Domenico, Manlio, Shuntaro Sasai, and Alex Arenas. 2016. “Mapping Multiplex Hubs in Human Functional Brain Networks.” *Frontiers in Neuroscience* 10. https://doi.org/10.3389/fnins.2016.00326.

De Domenico, Manlio, Albert Solé-Ribalta, Emanuele Cozzo, Mikko Kivelä, Yamir Moreno, Mason A. Porter, Sergio Gómez, and Alex Arenas. 2013. “Mathematical Formulation of Multilayer Networks.” *Physical Review X* 3 (4): 041022. https://doi.org/10.1103/PhysRevX.3.041022.

De Vico Fallani, Fabrizio, Vito Latora, and Mario Chavez. 2017. “A Topological Criterion for Filtering Information in Complex Brain Networks.” *PLoS Computational Biology* 13 (1): e1005305. https://doi.org/10.1371/journal.pcbi.1005305.

De Vico Fallani, Fabrizio, Jonas Richiardi, Mario Chavez, and Sophie Achard. 2014. “Graph Analysis of Functional Brain Networks: Practical Issues in Translational Neuroscience.” *Phil. Trans. R. Soc. B* 369 (1653): 20130521. https://doi.org/10.1098/rstb.2013.0521.

Desikan, Rahul S., Florent Ségonne, Bruce Fischl, Brian T. Quinn, Bradford C. Dickerson, Deborah Blacker, Randy L. Buckner, et al. 2006. "An Automated Labeling System for Subdividing the Human Cerebral Cortex on MRI Scans into Gyral Based Regions of Interest." *NeuroImage* 31 (3): 968–80. https://doi.org/10.1016/j.neuroimage.2006.01.021.

Destrieux, CE, E Halgren, AM Dale, B Fischl, and MI Sereno. 1998. "Variability of the Human Brain Studied on the Flattened Cortical Surface." *Soc Neurosci Abstr* 24: 1164.

Destrieux, Christophe, Bruce Fischl, Anders Dale, and Eric Halgren. 2010. "Automatic Parcellation of Human Cortical Gyri and Sulci Using Standard Anatomical Nomenclature." *NeuroImage* 53 (1): 1–15. https://doi.org/10.1016/j.neuroimage.2010.06.010.

Duvernoy, Henri M. 1999. *The Human Brain: Surface, Three-Dimensional Sectional Anatomy with MRI, and Blood Supply*. 2nd ed. Wien: Springer-Verlag. //www.springer.com/la/book/9783709167922.

Eickhoff, Simon B., Bertrand Thirion, Gaël Varoquaux, and Danilo Bzdok. 2015. "Connectivity-Based Parcellation: Critique and Implications." *Human Brain Mapping* 36 (12): 4771–92. https://doi.org/10.1002/hbm.22933.

Estrada, Ernesto, and Naomichi Hatano. 2008. "Communicability in Complex Networks." *Physical Review E* 77 (3): 036111. https://doi.org/10.1103/PhysRevE.77.036111.

Fillard, Pierre, Maxime Descoteaux, Alvina Goh, Sylvain Gouttard, Ben Jeurissen, James Malcolm, Alonso Ramirez-Manzanares, et al. 2011. "Quantitative Evaluation of 10 Tractography Algorithms on a Realistic Diffusion MR Phantom." *NeuroImage* 56 (1): 220–34. https://doi.org/10.1016/j.neuroimage.2011.01.032.

Fornito, Alex, Andrew Zalesky, and Michael Breakspear. 2015. "The Connectomics of Brain Disorders." *Nature Reviews. Neuroscience* 16 (3): 159–72. https://doi.org/10.1038/nrn3901.

Gourévitch, Boris, Régine Le Bouquin-Jeannès, and Gérard Faucon. 2006. "Linear and Nonlinear Causality between Signals: Methods, Examples and Neurophysiological Applications." *Biological Cybernetics* 95 (4): 349–69. https://doi.org/10.1007/s00422-006-0098-0.

Grech, Roberta, Tracey Cassar, Joseph Muscat, Kenneth P. Camilleri, Simon G. Fabri, Michalis Zervakis, Petros Xanthopoulos, Vangelis Sakkalis, and Bart Vanrumste. 2008. "Review on Solving the Inverse Problem in EEG Source Analysis." *Journal of Neuroengineering and Rehabilitation* 5 (November): 25. https://doi.org/10.1186/1743-0003-5-25.

Griffa, Alessandra, Benjamin Ricaud, Kirell Benzi, Xavier Bresson, Alessandro Daducci, Pierre Vandergheynst, Jean-Philippe Thiran, and Patric Hagmann. 2017. "Transient Networks of Spatio-Temporal Connectivity Map Communication Pathways in Brain Functional Systems." *NeuroImage* 155 (July): 490–502. https://doi.org/10.1016/j.neuroimage.2017.04.015.

Guillon, J., Y. Attal, O. Colliot, V. La Corte, B. Dubois, D. Schwartz, M. Chavez, and F. De Vico Fallani. 2017. "Loss of Brain Inter-Frequency Hubs in Alzheimer's Disease." *Scientific Reports* 7 (1): 10879. https://doi.org/10.1038/s41598-017-07846-w.

Haan, W. de, W. M. van der Flier, T. Koene, L. L. Smits, P. Scheltens, and C. J. Stam. 2012. "Disrupted Modular Brain Dynamics Reflect Cognitive Dysfunction in Alzheimer's Disease." *NeuroImage* 59 (4): 3085–93. https://doi.org/10.1016/j.neuroimage.2011.11.055.

Haan, Willem de, Yolande A. L. Pijnenburg, Rob L. M. Strijers, Yolande van der Made, Wiesje M. van der Flier, Philip Scheltens, and Cornelis J. Stam. 2009. "Functional Neural Network Analysis in Frontotemporal Dementia and Alzheimer's Disease Using EEG and Graph Theory." *BMC Neuroscience* 10 (August): 101. https://doi.org/10.1186/1471-2202-10-101.

Hagmann, Patric, Leila Cammoun, Xavier Gigandet, Reto Meuli, Christopher J. Honey, Van J. Wedeen, and Olaf Sporns. 2008. "Mapping the Structural Core of Human Cerebral Cortex." *PLOS Biology* 6 (7): e159. https://doi.org/10.1371/journal.pbio.0060159.

Hagmann, Patric, Maciej Kurant, Xavier Gigandet, Patrick Thiran, Van J. Wedeen, Reto Meuli, and Jean-Philippe Thiran. 2007. "Mapping Human Whole-Brain Structural Networks with Diffusion MRI." *PLOS ONE* 2 (7): e597. https://doi.org/10.1371/journal.pone.0000597.

Heuvel, Martijn P. van den, and Olaf Sporns. 2011. "Rich-Club Organization of the Human Connectome." *Journal of Neuroscience* 31 (44): 15775–86. https://doi.org/10.1523/JNEUROSCI.3539-11.2011.

Hlinkaa, Jaroslav, Milan Paluša, Martin Vejmelkaa, Dante Mantini, and Maurizio Corbetta. 2011. "Functional Connectivity in Resting-State FMRI: Is Linear Correlation Sufficient?" *NeuroImage* 54 (3): 2218–25. https://doi.org/10.1016/j.neuroimage.2010.08.042.

Holme, Petter, and Jari Saramäki. 2012. "Temporal Networks." *Physics Reports*, Temporal Networks, 519 (3): 97–125. https://doi.org/10.1016/j.physrep.2012.03.001.

Huisman, T.A.G.M. 2010. "Diffusion-Weighted and Diffusion Tensor Imaging of the Brain, Made Easy." *Cancer Imaging* 10 (1A): S163–71. https://doi.org/10.1102/1470-7330.2010.9023.

Humphries, M.D, K Gurney, and T.J Prescott. 2006. "The Brainstem Reticular Formation Is a Small-World, Not Scale-Free, Network." *Proceedings of the Royal Society B: Biological Sciences* 273 (1585): 503–11. https://doi.org/10.1098/rspb.2005.3354.

Jalili, Mahdi. 2016. "Functional Brain Networks: Does the Choice of Dependency Estimator and Binarization Method Matter?" *Scientific Reports* 6 (July): 29780. https://doi.org/10.1038/srep29780.

Jones, Derek K. 2010. "Challenges and Limitations of Quantifying Brain Connectivity in Vivo with Diffusion MRI." *Imaging in Medicine* 2 (3): 341–55. https://doi.org/10.2217/iim.10.21.

Kaminski, M. J., and K. J. Blinowska. 1991. "A New Method of the Description of the Information Flow in the Brain Structures." *Biological Cybernetics* 65 (3): 203–10. https://doi.org/10.1007/BF00198091.

Khalsa, Sakh, Stephen D. Mayhew, Magdalena Chechlacz, Manny Bagary, and Andrew P. Bagshaw. 2014. "The Structural and Functional Connectivity of the Posterior Cingulate Cortex: Comparison between Deterministic and Probabilistic Tractography for the Investigation of Structure–Function Relationships." *NeuroImage*, Multimodal Data Fusion, 102 (November): 118–27. https://doi.org/10.1016/j.neuroimage.2013.12.022.

Kivelä, Mikko, Alexandre Arenas, Marc Barthelemy, James P. Gleeson, Yamir Moreno, and Mason A. Porter. 2014. "Multilayer Networks." *Journal of Complex Networks* 2 (3): 203–71. https://doi.org/10.1093/comnet/cnu016.

Lachaux, Jean-Philippe, Eugenio Rodriguez, Jacques Martinerie, and Francisco J. Varela. 1999. "Measuring Phase Synchrony in Brain Signals." *Human Brain Mapping* 8 (4): 194–208. https://doi.org/10.1002/(SICI)1097-0193(1999)8:4<194::AID-HBM4>3.0.CO;2-C.

Latora, V., and M. Marchiori. 2003. "Economic Small-World Behavior in Weighted Networks." *The European Physical Journal B - Condensed Matter and Complex Systems* 32 (2): 249–63. https://doi.org/10.1140/epjb/e2003-00095-5.

Lazar, Mariana. 2010. "Mapping Brain Anatomical Connectivity Using White Matter Tractography." *NMR in Biomedicine* 23 (7): 821–35. https://doi.org/10.1002/nbm.1579.

Li, YaPeng, Yuanyuan Qin, Xi Chen, and Wei Li. 2013. "Exploring the Functional Brain Network of Alzheimer's Disease: Based on the Computational Experiment." *PloS One* 8 (9): e73186. https://doi.org/10.1371/journal.pone.0073186.

Liew, Alan W.-C., and Hong Yan. 2006. "Current Methods in the Automatic Tissue Segmentation of 3D Magnetic Resonance Brain Images." Text. February 2006. https://www.ingentaconnect.com/content/ben/cmir/2006/00000002/00000001/art00008.

Litvak, Vladimir, Jérémie Mattout, Stefan Kiebel, Christophe Phillips, Richard Henson, James Kilner, Gareth Barnes, et al. 2011. "EEG and MEG Data Analysis in SPM8." *Computational Intelligence and Neuroscience* 2011: 852961. https://doi.org/10.1155/2011/852961.

Lopes da Silva, Fernando. 2013. "EEG and MEG: Relevance to Neuroscience." *Neuron* 80 (5): 1112–28. https://doi.org/10.1016/j.neuron.2013.10.017.

Lüsebrink, Falk, Alessandro Sciarra, Hendrik Mattern, Renat Yakupov, and Oliver Speck. 2017. "T_1-Weighted *in Vivo* Human Whole Brain MRI Dataset with an Ultrahigh Isotropic Resolution of 250 Mm." *Scientific Data* 4 (March): 170032. https://doi.org/10.1038/sdata.2017.32.

Maier-Hein, Klaus H., Peter F. Neher, Jean-Christophe Houde, Marc-Alexandre Côté, Eleftherios Garyfallidis, Jidan Zhong, Maxime Chamberland, et al. 2017. "The Challenge of Mapping the Human Connectome Based on Diffusion Tractography." *Nature Communications* 8 (1): 1349. https://doi.org/10.1038/s41467-017-01285-x.

Mandke, Kanad, Jil Meier, Matthew J. Brookes, Reuben D. O'Dea, Piet Van Mieghem, Cornelis J. Stam, Arjan Hillebrand, and Prejaas Tewarie. 2018. "Comparing Multilayer Brain Networks between Groups: Introducing Graph Metrics and Recommendations." *NeuroImage* 166 (February): 371–84. https://doi.org/10.1016/j.neuroimage.2017.11.016.

Mantzaris, Alexander V., Danielle S. Bassett, Nicholas F. Wymbs, Ernesto Estrada, Mason A. Porter, Peter J. Mucha, Scott T. Grafton, and Desmond J. Higham. 2013. "Dynamic Network Centrality Summarizes Learning in the Human Brain." *Journal of Complex Networks* 1 (1): 83–92. https://doi.org/10.1093/comnet/cnt001.

Margulies, Daniel S., A. M. Clare Kelly, Lucina Q. Uddin, Bharat B. Biswal, F. Xavier Castellanos, and Michael P. Milham. 2007. “Mapping the Functional Connectivity of Anterior Cingulate Cortex.” *NeuroImage* 37 (2): 579–88. https://doi.org/10.1016/j.neuroimage.2007.05.019.

Mendrik, Adriënne M., Koen L. Vincken, Hugo J. Kuijf, Marcel Breeuwer, Willem H. Bouvy, Jeroen de Bresser, Amir Alansary, et al. 2015. “MRBrainS Challenge: Online Evaluation Framework for Brain Image Segmentation in 3T MRI Scans.” Research article. Computational Intelligence and Neuroscience. 2015. https://doi.org/10.1155/2015/813696.

Michel, Christoph M., Micah M. Murray, Göran Lantz, Sara Gonzalez, Laurent Spinelli, and Rolando Grave de Peralta. 2004. “EEG Source Imaging.” *Clinical Neurophysiology: Official Journal of the International Federation of Clinical Neurophysiology* 115 (10): 2195–2222. https://doi.org/10.1016/j.clinph.2004.06.001.

Mori, Susumu, Barbara J. Crain, V. P. Chacko, and Peter C. M. Van Zijl. 1999. “Three-Dimensional Tracking of Axonal Projections in the Brain by Magnetic Resonance Imaging.” *Annals of Neurology* 45 (2): 265–69. https://doi.org/10.1002/1531-8249(199902)45:2<265::AID-ANA21>3.0.CO;2-3.

Mormino, Elizabeth C., Andre Smiljic, Amynta O. Hayenga, Susan H. Onami, Michael D. Greicius, Gil D. Rabinovici, Mustafa Janabi, et al. 2011. “Relationships between Beta-Amyloid and Functional Connectivity in Different Components of the Default Mode Network in Aging.” *Cerebral Cortex* 21 (10): 2399–2407. https://doi.org/10.1093/cercor/bhr025.

Mucha, Peter J., Thomas Richardson, Kevin Macon, Mason A. Porter, and Jukka-Pekka Onnela. 2010. “Community Structure in Time-Dependent, Multiscale, and Multiplex Networks.” *Science* 328 (5980): 876–78. https://doi.org/10.1126/science.1184819.

“NeuroImageN - High Angular Resolution Diffusion Imaging (HARDI) Tools.” n.d. Accessed September 30, 2018. https://www.neuroimagen.es/webs/hardi_tools/.

Newman, M. E. J. 2004. “Fast Algorithm for Detecting Community Structure in Networks.” *Physical Review E* 69 (6): 066133. https://doi.org/10.1103/PhysRevE.69.066133.

———. 2006. “Modularity and Community Structure in Networks.” *Proceedings of the National Academy of Sciences* 103 (23): 8577–82. https://doi.org/10.1073/pnas.0601602103.

Nolte, Guido, Ou Bai, Lewis Wheaton, Zoltan Mari, Sherry Vorbach, and Mark Hallett. 2004. “Identifying True Brain Interaction from EEG Data Using the Imaginary Part of Coherency.” *Clinical Neurophysiology* 115 (10): 2292–2307. https://doi.org/10.1016/j.clinph.2004.04.029.

Ogawa, S, T M Lee, A R Kay, and D W Tank. 1990. “Brain Magnetic Resonance Imaging with Contrast Dependent on Blood Oxygenation.” *Proceedings of the National Academy of Sciences of the United States of America* 87 (24): 9868–72.

Oostenveld, Robert, Pascal Fries, Eric Maris, and Jan-Mathijs Schoffelen. 2011. “FieldTrip: Open Source Software for Advanced Analysis of MEG, EEG, and Invasive Electrophysiological Data.” *Computational Intelligence and Neuroscience* 2011: 156869. https://doi.org/10.1155/2011/156869.

Pochon, J. B., R. Levy, P. Fossati, S. Lehericy, J. B. Poline, B. Pillon, D. Le Bihan, and B. Dubois. 2002. “The Neural System That Bridges Reward and Cognition in Humans: An FMRI Study.” *Proceedings of the National Academy of Sciences of the United States of America* 99 (8): 5669–74. https://doi.org/10.1073/pnas.082111099.

Pradal, Christophe, Gaël Varoquaux, and Hans Peter Langtangen. 2012. “Publishing Scientific Software Matters.” *Journal of Computational Science* 4 (5): 311–12. https://doi.org/10.1016/j.jocs.2013.08.001.

Raichle, Marcus E. 2010. “Two Views of Brain Function.” *Trends in Cognitive Sciences* 14 (4): 180–90. https://doi.org/10.1016/j.tics.2010.01.008.

———. 2015. “The Brain’s Default Mode Network.” *Annual Review of Neuroscience* 38 (1): 433–47. https://doi.org/10.1146/annurev-neuro-071013-014030.

Raichle, Marcus E., Ann Mary MacLeod, Abraham Z. Snyder, William J. Powers, Debra A. Gusnard, and Gordon L. Shulman. 2001. “A Default Mode of Brain Function.” *Proceedings of the National Academy of Sciences* 98 (2): 676–82. https://doi.org/10.1073/pnas.98.2.676.

Raichle, Marcus E., and Mark A. Mintun. 2006. “Brain Work and Brain Imaging.” *Annual Review of Neuroscience* 29 (1): 449–76. https://doi.org/10.1146/annurev.neuro.29.051605.112819.

Reus, Marcel A. de, and Martijn P. van den Heuvel. 2013. “The Parcellation-Based Connectome: Limitations and Extensions.” *NeuroImage*, Mapping the Connectome, 80 (October): 397–404. https://doi.org/10.1016/j.neuroimage.2013.03.053.

Rubinov, Mikail, and Olaf Sporns. 2010. “Complex Network Measures of Brain Connectivity: Uses and Interpretations.” *NeuroImage*, Computational Models of the Brain, 52 (3): 1059–69. https://doi.org/10.1016/j.neuroimage.2009.10.003.

Sakkalis, V. 2011. “Review of Advanced Techniques for the Estimation of Brain Connectivity Measured with EEG/MEG.” *Computers in Biology and Medicine*, Special Issue on Techniques for Measuring Brain Connectivity, 41 (12): 1110–17. https://doi.org/10.1016/j.compbiomed.2011.06.020.

Sanz-Arigita, Ernesto J., Menno M. Schoonheim, Jessica S. Damoiseaux, Serge A. R. B. Rombouts, Erik Maris, Frederik Barkhof, Philip Scheltens, and Cornelis J. Stam. 2010. “Loss of ‘Small-World’ Networks in Alzheimer’s Disease: Graph Analysis of FMRI Resting-State Functional Connectivity.” *PLOS ONE* 5 (11): e13788. https://doi.org/10.1371/journal.pone.0013788.

Schnitzler, Alfons, and Joachim Gross. 2005. “Normal and Pathological Oscillatory Communication in the Brain.” *Nature Reviews Neuroscience* 6 (4): 285–96. https://doi.org/10.1038/nrn1650.

Seo, Eun Hyun, Dong Young Lee, Jong-Min Lee, Jun-Sung Park, Bo Kyung Sohn, Dong Soo Lee, Young Min Choe, and Jong Inn Woo. 2013. “Whole-Brain Functional Networks in Cognitively Normal, Mild Cognitive Impairment, and Alzheimer’s Disease.” *PLOS ONE* 8 (1): e53922. https://doi.org/10.1371/journal.pone.0053922.

Seunarine, Kiran K., and Daniel C. Alexander. 2014. “Chapter 6 - Multiple Fibers: Beyond the Diffusion Tensor.” In *Diffusion MRI (Second Edition)*, edited by Heidi Johansen-Berg and Timothy E. J. Behrens, 105–23. San Diego: Academic Press. https://doi.org/10.1016/B978-0-12-396460-1.00006-8.

Shulman, Gordon L., Julie A. Fiez, Maurizio Corbetta, Randy L. Buckner, Francis M. Miezin, Marcus E. Raichle, and Steven E. Petersen. 1997. “Common Blood Flow Changes across Visual Tasks: II. Decreases in Cerebral Cortex.” *Journal of Cognitive Neuroscience* 9 (5): 648–63. https://doi.org/10.1162/jocn.1997.9.5.648.

Simas, Tiago, Mario Chavez, Pablo R. Rodriguez, and Albert Diaz-Guilera. 2015. “An Algebraic Topological Method for Multimodal Brain Networks Comparisons.” *Frontiers in Psychology* 6: 904. https://doi.org/10.3389/fpsyg.2015.00904.

Simpson, Sean L., and Paul J. Laurienti. 2016. “Disentangling Brain Graphs: A Note on the Conflation of Network and Connectivity Analyses.” *Brain Connectivity* 6 (2): 95–98. https://doi.org/10.1089/brain.2015.0361.

Singh, Sanjay P. 2014. “Magnetoencephalography: Basic Principles.” *Annals of Indian Academy of Neurology* 17 (Suppl 1): S107–12. https://doi.org/10.4103/0972-2327.128676.

Stam, C. J., and B. W. van Dijk. 2002. “Synchronization Likelihood: An Unbiased Measure of Generalized Synchronization in Multivariate Data Sets.” *Physica D: Nonlinear Phenomena* 163 (3): 236–51. https://doi.org/10.1016/S0167-2789(01)00386-4.

Stam, C. J., W. de Haan, A. Daffertshofer, B. F. Jones, I. Manshanden, A. M. van Cappellen van Walsum, T. Montez, et al. 2009. “Graph Theoretical Analysis of Magnetoencephalographic Functional Connectivity in Alzheimer’s Disease.” *Brain* 132 (1): 213–24. https://doi.org/10.1093/brain/awn262.

Stam, C. J., B. F. Jones, G. Nolte, M. Breakspear, and Ph Scheltens. 2007. “Small-World Networks and Functional Connectivity in Alzheimer’s Disease.” *Cerebral Cortex* 17 (1): 92–99. https://doi.org/10.1093/cercor/bhj127.

Stam, Cornelis J. 2014. “Modern Network Science of Neurological Disorders.” *Nature Reviews. Neuroscience* 15 (10): 683–95. https://doi.org/10.1038/nrn3801.

Stam, Cornelis J., Guido Nolte, and Andreas Daffertshofer. 2007. “Phase Lag Index: Assessment of Functional Connectivity from Multi Channel EEG and MEG with Diminished Bias from Common Sources.” *Human Brain Mapping* 28 (11): 1178–93. https://doi.org/10.1002/hbm.20346.

Sun, Felice T, Lee M Miller, and Mark D’Esposito. 2004. “Measuring Interregional Functional Connectivity Using Coherence and Partial Coherence Analyses of FMRI Data.” *NeuroImage* 21 (2): 647–58. https://doi.org/10.1016/j.neuroimage.2003.09.056.

Supekar, Kaustubh, Vinod Menon, Daniel Rubin, Mark Musen, and Michael D. Greicius. 2008. “Network Analysis of Intrinsic Functional Brain Connectivity in Alzheimer’s Disease.” *PLoS Comput Biol* 4 (6): e1000100. https://doi.org/10.1371/journal.pcbi.1000100.

Symms, M., H. R. Jäger, K. Schmierer, and T. A. Yousry. 2004. “A Review of Structural Magnetic Resonance Neuroimaging.” *Journal of Neurology, Neurosurgery & Psychiatry* 75 (9): 1235–44. https://doi.org/10.1136/jnnp.2003.032714.

Tadel, François, Sylvain Baillet, John C. Mosher, Dimitrios Pantazis, Richard M. Leahy, François Tadel, Sylvain Baillet, John C. Mosher, Dimitrios Pantazis, and Richard M. Leahy. 2011. “Brainstorm: A User-Friendly Application

for MEG/EEG Analysis, Brainstorm: A User-Friendly Application for MEG/EEG Analysis." *Computational Intelligence and Neuroscience, Computational Intelligence and Neuroscience* 2011, 2011 (April): e879716. https://doi.org/10.1155/2011/879716, 10.1155/2011/879716.

Tewarie, Prejaas, Arjan Hillebrand, Bob W. van Dijk, Cornelis J. Stam, George C. O'Neill, Piet Van Mieghem, Jil M. Meier, Mark W. Woolrich, Peter G. Morris, and Matthew J. Brookes. 2016. "Integrating Cross-Frequency and within Band Functional Networks in Resting-State MEG: A Multi-Layer Network Approach." *NeuroImage* 142 (November): 324–36. https://doi.org/10.1016/j.neuroimage.2016.07.057.

Thirion, Bertrand, Gaël Varoquaux, Elvis Dohmatob, and Jean-Baptiste Poline. 2014. "Which FMRI Clustering Gives Good Brain Parcellations?" *Frontiers in Neuroscience* 8 (July). https://doi.org/10.3389/fnins.2014.00167.

Thompson, P. M., C. Schwartz, R. T. Lin, A. A. Khan, and A. W. Toga. 1996. "Three-Dimensional Statistical Analysis of Sulcal Variability in the Human Brain." *The Journal of Neuroscience: The Official Journal of the Society for Neuroscience* 16 (13): 4261–74.

Tijms, Betty M., Alle Meije Wink, Willem de Haan, Wiesje M. van der Flier, Cornelis J. Stam, Philip Scheltens, and Frederik Barkhof. 2013. "Alzheimer's Disease: Connecting Findings from Graph Theoretical Studies of Brain Networks." *Neurobiology of Aging* 34 (8): 2023–36. https://doi.org/10.1016/j.neurobiolaging.2013.02.020.

Toppi, J., F. De Vico Fallani, G. Vecchiato, A. G. Maglione, F. Cincotti, D. Mattia, S. Salinari, F. Babiloni, and L. Astolfi. 2012. "How the Statistical Validation of Functional Connectivity Patterns Can Prevent Erroneous Definition of Small-World Properties of a Brain Connectivity Network." *Computational and Mathematical Methods in Medicine* 2012: 130985. https://doi.org/10.1155/2012/130985.

Tournier, J. -Donald, Fernando Calamante, David G. Gadian, and Alan Connelly. 2004. "Direct Estimation of the Fiber Orientation Density Function from Diffusion-Weighted MRI Data Using Spherical Deconvolution." *NeuroImage* 23 (3): 1176–85. https://doi.org/10.1016/j.neuroimage.2004.07.037.

Tournier, J.-Donald, Fernando Calamante, and Alan Connelly. 2007. "Robust Determination of the Fibre Orientation Distribution in Diffusion MRI: Non-Negativity Constrained Super-Resolved Spherical Deconvolution." *NeuroImage* 35 (4): 1459–72. https://doi.org/10.1016/j.neuroimage.2007.02.016.

Travers, Jeffrey, and Stanley Milgram. 1969. "An Experimental Study of the Small World Problem." *Sociometry* 32 (4): 425–43. https://doi.org/10.2307/2786545.

Tuch, David S., Timothy G. Reese, Mette R. Wiegell, Nikos Makris, John W. Belliveau, and Van J. Wedeen. 2002. "High Angular Resolution Diffusion Imaging Reveals Intravoxel White Matter Fiber Heterogeneity." *Magnetic Resonance in Medicine* 48 (4): 577–82. https://doi.org/10.1002/mrm.10268.

Tuch, David S., Timothy G. Reese, Mette R. Wiegell, and Van J. Wedeen. 2003. "Diffusion MRI of Complex Neural Architecture." *Neuron* 40 (5): 885–95. https://doi.org/10.1016/S0896-6273(03)00758-X.

Tzourio-Mazoyer, N., B. Landeau, D. Papathanassiou, F. Crivello, O. Etard, N. Delcroix, B. Mazoyer, and M. Joliot. 2002. "Automated Anatomical Labeling of Activations in SPM Using a Macroscopic Anatomical Parcellation of the MNI MRI Single-Subject Brain." *NeuroImage* 15 (1): 273–89. https://doi.org/10.1006/nimg.2001.0978.

Varela, F., J. P. Lachaux, E. Rodriguez, and J. Martinerie. 2001. "The Brainweb: Phase Synchronization and Large-Scale Integration." *Nature Reviews. Neuroscience* 2 (4): 229–39. https://doi.org/10.1038/35067550.

Velmurugan, Jayabal, Sanjib Sinha, and Parthasarathy Satishchandra. 2014. "Magnetoencephalography Recording and Analysis." *Annals of Indian Academy of Neurology* 17 (Suppl 1): S113–19. https://doi.org/10.4103/0972-2327.128678.

Vijayalakshmi, R., D. Nandagopal, N. Dasari, B. Cocks, N. Dahal, and M. Thilaga. 2015. "Minimum Connected Component – A Novel Approach to Detection of Cognitive Load Induced Changes in Functional Brain Networks." *Neurocomputing*, Advances on Biological Rhythmic Pattern Generation: Experiments, Algorithms and Applications, 170 (December): 15–31. https://doi.org/10.1016/j.neucom.2015.03.092.

Vlassenko, Andrei G., S. Neil Vaishnavi, Lars Couture, Dana Sacco, Benjamin J. Shannon, Robert H. Mach, John C. Morris, Marcus E. Raichle, and Mark A. Mintun. 2010. "Spatial Correlation between Brain Aerobic Glycolysis and Amyloid-β (Aβ) Deposition." *Proceedings of the National Academy of Sciences* 107 (41): 17763–67. https://doi.org/10.1073/pnas.1010461107.

Wang, Jinhui, Xinian Zuo, Zhengjia Dai, Mingrui Xia, Zhilian Zhao, Xiaoling Zhao, Jianping Jia, Ying Han, and Yong He. 2013. "Disrupted Functional Brain Connectome in Individuals at Risk for Alzheimer's Disease." *Biological Psychiatry* 73 (5): 472–81. https://doi.org/10.1016/j.biopsych.2012.03.026.

Wang, Yueming, Kang Lin, Yu Qi, Qi Lian, Shaozhe Feng, Zhaohui Wu, and Gang Pan. 2018. "Estimating Brain Connectivity With Varying-Length Time Lags Using a Recurrent Neural Network." *IEEE Transactions on Biomedical Engineering* 65 (9): 1953–63. https://doi.org/10.1109/TBME.2018.2842769.

Ward Jr., Joe H. 1963. "Hierarchical Grouping to Optimize an Objective Function." *Journal of the American Statistical Association* 58 (301): 236–44. https://doi.org/10.1080/01621459.1963.10500845.

Watts, Duncan J., and Steven H. Strogatz. 1998. "Collective Dynamics of 'Small-World' Networks." *Nature* 393 (6684): 440–42. https://doi.org/10.1038/30918.

White, J. G., E. Southgate, J. N. Thomson, and S. Brenner. 1986. "The Structure of the Nervous System of the Nematode Caenorhabditis Elegans." *Philosophical Transactions of the Royal Society of London. Series B, Biological Sciences* 314 (1165): 1–340.

Yo, Ting-Shuo, Alfred Anwander, Maxime Descoteaux, Pierre Fillard, Cyril Poupon, and T. R. Knösche. 2009. "Quantifying Brain Connectivity: A Comparative Tractography Study." In *Medical Image Computing and Computer-Assisted Intervention – MICCAI 2009*, edited by Guang-Zhong Yang, David Hawkes, Daniel Rueckert, Alison Noble, and Chris Taylor, 886–93. Lecture Notes in Computer Science. Springer Berlin Heidelberg.

Yu, Meichen, Marjolein M. A. Engels, Arjan Hillebrand, Elisabeth C. W. van Straaten, Alida A. Gouw, Charlotte Teunissen, Wiesje M. van der Flier, Philip Scheltens, and Cornelis J. Stam. 2017. "Selective Impairment of Hippocampus and Posterior Hub Areas in Alzheimer's Disease: An MEG-Based Multiplex Network Study." *Brain* 140 (5): 1466–85. https://doi.org/10.1093/brain/awx050.

Yu, Meichen, Marjolein M. A. Engels, Arjan Hillebrand, Van Straaten, Elisabeth C. W, Alida A. Gouw, Charlotte Teunissen, et al. 2017. "Selective Impairment of Hippocampus and Posterior Hub Areas in Alzheimer's Disease: An MEG-Based Multiplex Network Study." *Brain* 140 (5): 1466–85. https://doi.org/10.1093/brain/awx050.

Zalesky, Andrew, Alex Fornito, and Ed Bullmore. 2012. "On the Use of Correlation as a Measure of Network Connectivity." *NeuroImage* 60 (4): 2096–2106. https://doi.org/10.1016/j.neuroimage.2012.02.001.

Zhao, Xiaohu, Yong Liu, Xiangbin Wang, Bing Liu, Qian Xi, Qihao Guo, Hong Jiang, Tianzi Jiang, and Peijun Wang. 2012. "Disrupted Small-World Brain Networks in Moderate Alzheimer's Disease: A Resting-State FMRI Study." *PLOS ONE* 7 (3): e33540. https://doi.org/10.1371/journal.pone.0033540.

Zilles, K., A. Schleicher, C. Langemann, K. Amunts, P. Morosan, N. Palomero-Gallagher, T. Schormann, et al. 1997. "Quantitative Analysis of Sulci in the Human Cerebral Cortex: Development, Regional Heterogeneity, Gender Difference, Asymmetry, Intersubject Variability and Cortical Architecture." *Human Brain Mapping* 5 (4): 218–21. https://doi.org/10.1002/(SICI)1097-0193(1997)5:4<218::AID-HBM2>3.0.CO;2-6.